Functional Diversity of Fibroblast Growth Factor Homologous Factor Family of Proteins

by

Katarzyna Dover

A dissertation submitted to the Graduate Faculty in Biology in partial fulfillment of the requirements for the degree of Doctor of Philosophy, The City University of New York

2010

Approval Page

This manuscript has been read and accepted for the Graduate Faculty in Biology in satisfaction of the dissertation requirements for the degree of Doctor of Philosophy.

Date	Chair of Examining Committee Dr. Mitchell Goldfarb, Hunter College
Date	Executive Officer Dr. Laurel A. Eckhardt
	Committee Member Dr. Richard Chappell, Hunter College
	Committee Member Dr. Carmen Melendez-Vasquez, Hunter College
	Committee Member Dr. Robert Kass, Columbia University
	Committee Member Dr. Trine Krogh-Madson, Weill-Cornell Medical Center

Supervising Committee

The City University of New York

Abstract

Functional Diversity of Fibroblast Growth Factor Homologous Factor Family of Proteins

by

Katarzyna Dover

Thesis Advisor: Dr. Mitchell Goldfarb

FHFs resemble other fibroblast growth factors on a basis of amino acid composition and crystal structure but evolved to carry on distinct, FGF unrelated functions. To date, FHFs have been implicated most clearly in modulation of voltage gated sodium channels (VGSCs).

FHFs are the classical example of an increase in gene diversity through the alternative promoter usage and splicing. Hence, the multiplicity of isoforms makes this family of proteins an interesting yet, challenging research topic. Different isoforms of FHFs have distinct sub-cellular localizations and differently modulate voltage gated sodium channels. By influencing critical parameters of channel physiology, including voltage dependence of channel steady-state inactivation, recovery from inactivation and current density, the FHF family of proteins has emerged as important regulators of cellular excitability.

The role of different FHF isoforms in modulation of VGSCs and their influence on cellular excitability is the main topic of this thesis. Performed experiments aimed to: (i) establish a channel-binding surface, common to all FHFs, (ii) categorize major FHF isoforms into functional groups based on the ability to modulate sodium channel Nav1.6, (iii) elucidate the mechanism involved in A-type FHF induced long-term, use-dependent channel inactivation, and (iv) determine potential differential localization of A-type FHFs in the brain and in subcellular compartments of cerebellar, hippocampal and sensory neurons.

Acknowledgements

There are people who pass through our lives, however briefly, that change us forever. Their influence is profound and helps shape our future. My mentor, Dr. Mitchell Goldfarb, is such a person.

Dr. Goldfarb is an extraordinary mentor who does not believe in second hand learning. He takes the time to train his students in person. Opting for the bench rather than the comfort of his office, he genuinely enjoys performing experiments with his students. His ideas are brilliant and his enthusiasm contagious. Dr. Goldfarb's depth of knowledge, expertise and wisdom, gained throughout the years of experience, is readily shared. There are also other qualities like curiosity, passion for learning, optimism, and the openness to new ideas that keep the endeavor fresh and exciting.

I am honored and grateful for meeting Dr. Goldfarb on my path of professional development, and the path of life.

Thank you for your time, patience and commitment to my success. Thank you for recognizing my potential and granting me space and time to grow. Thank you for the wonderful research project and extensive training, for in depth discussions and helpful advice, for steering me in the right direction and keeping me out of trouble. I will always cherish the memories of working together and the time spent in your lab. Simply put, I could not have become who I am without you!

I would like to thank Dr. Richard Chappell, for his sincere interest in my professional development and progress here at Hunter. I am grateful for his kindness, support, and the

willingness to adjust his schedule to make my exams possible. I could always count on Dr. Chappell, and knowing that he is a member of my committee has been comforting.

Dr. Carmen Melendez-Vasquez has always been supportive and encouraging. She has been kind and generous with her time and lab resources. She provided essential training on the culture of myelinated DRG neurons and her expertise was always valued and appreciated. Thank You.

I am grateful to Dr. Trine Krogh-Madson from Weill-Cornell Medical Center for expressing interest in our research. Thank you for accepting the invitation to serve on this committee on such short notice. Your time, expertise and commitment are well appreciated.

My sincere gratitude to Dr. Robert Kass, Chair of Pharmacology at Columbia University, for his interest in our research and service on this committee. Dr. Kass provided us with the expression vector for sodium channel Nav 1.5, which allowed us to demonstrate the function of Long Term Inactivating Particle. Thank you for providing access to your expertise and resources, for your time and service on this committee.

It is a great honor to have such distinguished external committee members, and such accomplished members here at Hunter. I hope you have found this time as well spent and valuable as I have. I look forward to learning more about your endeavors.
Thank you all, in advance, for your future support and valuable relationships!

I would also like to thank Dr. Michael Urbanski for helpful discussions, good advice and training and Annie Yum for excellent care of laboratory animals.

Special thanks to my husband Terence Dover:

It is easy to get lost in the abstract thought. You were always there to catch me and bring me back to reality. Being an artist yourself, you saw the beauty in the art of science. Being so close to me you also witnessed the struggle, the disappointment, the countless hours spent on the quest to discover. You always listened. As much as you could, you tried to understand, and never complained. I am very sorry for cancelled dates, abrupt changes in plans, for a messy house and no dinner on the table. I was on a mission and you were there to make sure I would survive.
It is not a Grammy I am about to get, but in the category of the best supportive husband you won me again and again.

Thank you all!

Sincerely,

Kasia Dover

Table of Contents

List of Figures

Pictures:

Manuscript Figures, referred to in Chapter V:

Figures included in Chapters III, IV, VI:

List of Tables

Manuscript Tables, Chapter V:

Abbreviations:

AA	Amino Acid
AIS	Axon initial segment
BDNF	Brain-derived neurotrophic factor
BSA	Bovine albumin serum
BSS	Hank's Balanced Saline Solution
DMEM	Dulbecco's modified Eagle's medium
DRG	Dorsal root ganglion
ECL	Enhanced chemiluminescence
FBS	Fetal Bovine Serum
FGF	Fibroblast growth factor
FHF	Fibroblast growth factor homologous factor
GFP	Green fluorescent protein
HEK293	Human embryonic kidney cell line
HEPES	4-(2-Hydroxyethyl)piperazine-1-ethanesulfonic acid
HRP	Horseradish Peroxidase
IB2	Islet brain 2 protein
k	slope value
KO	gene knockout
MAPK	Mitogen activated protein kinase
Neuro2A	Neuroblastoma cell line
NF	Neurofilament
PBS	Phosphate buffered saline
PCR	Polymerase chain reaction
PKA	Protein kinase A
PKC	Protein kinase C
PMSF	Phenylmethylsulfonyl fluoride
PVDF	Polyvinylidine Fluoride
RT	Room temperature
SDS-PAGE	Sodium dodecylsulfate polyacrylamide gel elecrtophoresis

TLB Tritin lysis buffer

TTX Tetrodotoxin

TTX-R/ TTX^{r} Tetrodotoxin resistant

VGSCs Voltage gated sodium channels

WT Wild-type

CHAPTER I

Introduction

1.1 FHFs- members of FGF family of proteins

Fibroblast growth factors homologous factors (FHFs) belong to a large family of fibroblast growth factors (FGFs) with which they share high degree of sequence and structural homology (Smallwood et al., 1996, Coulier et al., 1997, Verdier et al., 1997).

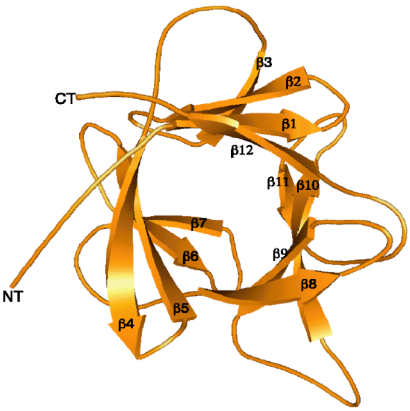

Picture 1. Ribbon representation of the crystal structure of FHF1B (Olsen et al., 2003)

The core region, common to all FHF/FGFs consists of 120-130 amino acids which adopt β-trefoil fold consisting of three sets of four, antiparallel β-strands (Olsen et al., 2003). Despite many similarities, FHFs do not share the same biochemical and functional characteristics with other members of FGF family. What sets them apart is FHF's inability to bind and signal through FGF receptors and to be excreted extracellularly. The first feature can be linked to two surface residues; Arg 52 and Val 95 which are characteristic for FHFs and are not found in FGFs, and to the carboxyl-terminal extension unique to FHFs (Goetz et al., 2009). It has been shown (Olsen et al., 2003) that mutations of the corresponding core residues in FGF1 to Arg and Val diminished capacity of that FGF to bind to FGF receptors. As mentioned before, FHFs lack recognizable secretory sequence and therefore remain intracellular. It has been speculated (Smallwood et al 1996; Florkiewicz et al., 1998) that similar to FGF1 and 2 family members who also lack secretory sequence, FHFs can be released from the cell via a mechanism independent of the ER-Golgi system during cell

injury and function as growth factors. To date, there are no reports in literature that would support this hypothesis. Instead more and more data accumulate demonstrating that FHFs have evolved to carry out diverse, growth factor unrelated functions.

1.2 FHF isoform diversity

One of the hallmarks of the FHF protein family is isoform diversity. There are four FHF genes: FHF1, 2, 3, 4 located on chromosomes 3, X, 17, 13 respectively, which encode multiple FHF proteins (Munoz-Sanjaun et al., 1999 and 2000). Each FHF gene has two or more transcription initiation sites and give rise to messenger RNAs with a distinct first exon spliced to common exons II-V (Goldfarb, 2005). Protein products of the same FHF gene are identical in the core region and C-terminus but vary in the length of the N-terminal extension. The differences can be small e.g. seven amino acids difference between FHF2U and FHF2V or as significant as ~60 amino acid residues as in FHF1A vs. FHF1B. FHFs reported by Munoz-Sanjuan et al., 2000 account for three FHF1 isoforms, nine FHF2 isoforms, two FHF3 and two FHF4 isoforms.

Interestingly, the sequence alignment of all FHFs revealed higher degree of homology among A and B isoforms of different genes than between A and B isoform of the same

Picture 2. Sequence Alignment of N-terminal extensions of A and B Isoforms of FHFs

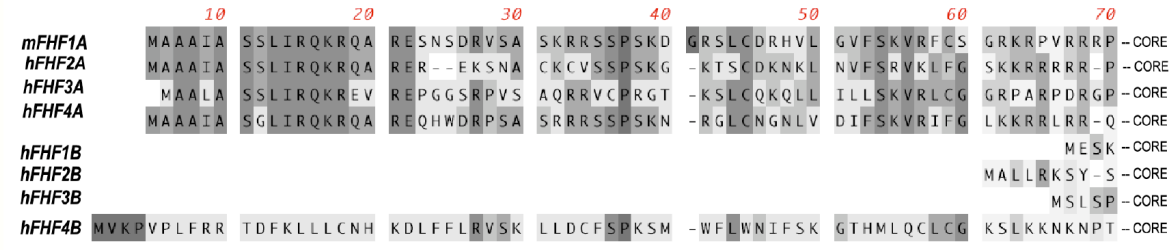

gene. The length and amino acid composition of N-terminal extensions of FHFs may hold

the answer to the question of differential localization and ability to modulate voltage gated sodium channels. It has been reported by Smallwood et al., 1996 and Wang et al., 2000 that A type FHFs have bipartite nuclear localization signal (NLS) composed of two clusters of 3 to 4 basic residues separated by a 10 amino acid spacer. When transfected to human embryonic kidney cells (HEK293), A type FHFs preferentially accumulate at the nucleus and B type at the cytoplasm. The subcellular localization of FHFs changes when studied in neuronal cells due to the association of FHFs with voltage gated sodium channels and possibly other neuronal specific factors. The distribution of the FHFs in the neuronal compartments also depends on the length and the amino acid composition of the N-terminal extension. For example, FHF1A and FHF1B expressed in cerebeller granule neurons show preferential accumulation of A but not B isoform at axon initial segments (AIS) (Goldfarb et al., 2007). A similar pattern was observed in the hippocampal neurons transfected with FHFs 1A, 2A, 1B, 2B (Huang and Goldfarb, unpublished data). Another FHF that co-localizes with AIS of hippocampal and cerebellar granule neurons is FHF4B, the only B type FHF with extended N-terminus (Wittmack et al., 2004; Lou et al., 2005; Goetz et al., 2008). In the myelinated dorsal root ganglion neurons (DRGs) FHF1A positive signal was detected at the first three nodes following the soma and gradually declined within three subsequent heminodes. FHF1B did not co-localize to these compartments but rather was found at the distal nodes of Ranvier (Taweri and Goldfarb, unpublished data). Similar observations for FHF2B were reported by Wittmack et al., 2004 and Rush et al., 2006. Since A and B isoforms differently modulate sodium channel physiology, our working hypothesis is: *FHF4B and A type FHFs associate with voltage*

gated sodium channels at AIS to optimize action potential generation and B type FHFs located at distal nodes optimize action potential propagation.

1.3 The role of FHFs in the development and mature nervous system

In the effort to elucidate the biological role of FHF family of proteins, several studies have been undertaken. *In situ* hybridization conducted in mouse and chicken (Hartung et al., 1997; Munoz-Sanjaun et al., 1999 and 2000) revealed prominent but not exclusive FHFs expression in developing and mature neurons of the central and peripheral nervous system. To a lesser extent, FHFs were also found in developing heart, embryonic olfactory epithelium, connective tissues and embryonic limb mesenchyme. Based on these findings, FHFs were suspected to serve in the development of the nervous system and other tissues.

More recently, two intracellular FHF binding partners were identified through yeast-two hybrid screens with FHF2 (Schoorlemmer and Goldfarb, 2001) and FHF1B (Liu et al., 2001). One such a target was MAPK scaffold protein islet brain-2 (IB2). FHF-IB2 interaction has been investigated in FHF1 overexpression system in NIH3T3 and PC12 cells and FHF-IB2 complexes were isolated from rat brain homogenates. In both cases, results showed a high specificity of the FHF-IB2 interaction, e.g. FHF formed precipitable complexes with IB2, but not with closely related IB1 protein. Also the attempts to bind IB2 to FGF1 were proven unsuccessful. The sites of FHF interaction with IB2 were mapped to β4-β5 loop and β9-strand housing Arg52 and Val95 (Olsen et al., 2003) and FHF binding domain on IB2 was narrowed to 250 residues unique to this protein. Although it has been proposed (Schoorlemmer and Goldfarb et al., 2001 and

2002) that FHFs may function as cofactors facilitating recruitment of the MAP kinases such as p38 to the IB2 scaffold allowing p38 to be phosphorylated, the role of FHF-IB2-MAP kinase complexes in the nervous system is still unknown.

Another protein that associated with FHF1B in yeast two-hybrid screen was voltage gated sodium channel Nav1.9 (Liu et al., 2001). Since then, several other FHFs were found not only to bind to multiple voltage gated sodium channels, but also to influence their physiology. FHF1B interacts with cardiac sodium channel Nav1.5 and induces a hyperpolarizing shift in steady-state inactivation (Liu et al., 2003). FHF2B associates with sodium channel Nav1.6 and selectively co-localizes at nodes of Ranvier of DRG neurons. The co-expression of FHF2B and Nav1.6 in DRG-derived cell lineND7/23 significantly increased peak current amplitude and caused a 4 mV depolarizing shift in the voltage-dependence of fast inactivation (Wittmack et al., 2004). Similar effects, but of a much higher magnitude (20 mV depolarizing shift) were reported by Rush et al., 2006 in the study involving FHF2A. Lastly, FHF4 have been shown to interact with Nav1.5 and Nav1.1, endogenous channels in neuroblastoma cells and cultured hippocampal neurons. Depending on the isoform and a cell line in which it was studied, FHF4 decreased or increased current density (Lou et al., 2005). These examples substantiate *FHFs as modulators of sodium channel physiology*, affecting multiple parameters such as a voltage dependence of channel inactivation, time constants of fast and slow inactivation, recovery from fast and slow inactivation and sodium current density.

One of the objectives of my research concerned the molecular mechanisms underling modulation of voltage gated sodium channels by A-type FHFs. Therefore, further discussion of the topic requires an overview of sodium channel physiology.

1.4 Voltage Gated Sodium Channels- short overview

Voltage gated sodium channels are expressed in all excitable cells in which they underlie the generation and propagation of action potential (Goldin et al., 2001 and 2003; Catterall et al., 2000 and 2005). Sodium channels are integral membrane proteins composed of a pore forming α-subunit often associated with one or two β subunits. To date, nine α (Nav1.1-1.9) and four beta (β_{1-4}) subunits have been identified. The typical sodium channel α-subunit is made of a single polypeptide (approximately 2000 a.a. long) organized into four domains (DI - DIV), each containing six membrane-spanning regions designated S1-S6. The α-subunit alone is sufficient for functional channel expression but without auxiliary β subunits its properties are often altered (Catterall et al., 2000; Burbridge et al., 2002). Sodium channel beta subunits are known to regulate channel expression and voltage dependence of channel gating (Chen and Isom et al., 2004). In addition, they form links to the intracellular cytoskeleton and extracellular matrix (Isom et al., 2001). The narrow entry to the pore is lined with P-loops, which partially re-enter the plasma membrane between segments S5 and S6. This region contains a selectivity filter and is responsible for sodium ion specificity. The inner portion of the channel is formed by combined S5 and S6 segments of all four domains. On the cytoplasmic side of the pore, domains I-IV are linked by intracellular loops. The loop connecting DIII and DIV contains the fast inactivation gate, which contains the hydrophobic cluster

isoleucine-phenylealanine-methionine (IFM particle). The IFM particle interacts with its docking site on the inner face of the channel pore during inactivation. Substitutions of IFM residues with Q result in non-inactivating channels (West et al., 1992; Eaholtz et al., 1994 and 1998). All channels end at the cytoplasmic side of the plasma membrane with C-tail, which is an essential for both channel activation and inactivation (Montegazza et al., 2001; Motoike et al., 2004).

Although the crystal structure of VGSCs has yet to be resolved, molecular models have been constructed based on sequence homology to the structurally solved bacterial potassium channel (Cronin et al., 2003) and rat brain voltage-gated potassium channel Kv1.2 (O'Reilly et al., 2006). It is believed that, similar to potassium, sodium channels respond to membrane depolarization by outward movement of the positively charged voltage sensing particles located in S4 segments of each of four domains. The displacement of voltage sensors triggers conformational changes leading to rearrangement of pore forming S6 segments and result in a pore widening (Pathak et al., 2005 and 2007; Posson et al., 2008). Within 1-2 milliseconds of opening, channels transition to a non-conductive, inactivation state, which is a consequence of the blocking of the intracellular face of the pore with an IFM particle, an integral part of the inactivation gate. Only under condition of sufficient membrane depolarization can the conductive open state be reached. For weaker depolarizations, channels transition through a series of closed states and usually inactivate without ever being open. The process of channel inactivation from the closed states is referred to a steady-state inactivation.

1.5 Fast versus slow inactivation of VGSCs

In addition to fast inactivation, which develops within milliseconds of channel activation, prolonged depolarization lasting seconds (delivered in a single phase or multiple, brief depolarization cycles) causes sodium channels to undergo a process called slow inactivation. Slow inactivation was first described by Rudy et al., 1978 and since then has been reported by many groups. Whereas the fast inactivation mechanism of channels is relatively well understood, the mechanism of slow inactivation still awaits clarification. Several regions of the channel have been implicated in development of the slow inactivated state. One of them is a p-region, located at the outer vestibule of the channel's pore. As demonstrated by Balser et al., 1996 and Vilin et al., 1999, the transposition of p-loops from cardiac channel Nav1.5 to skeletal muscle channel Nav1.4 conferred slow inactivation properties characteristic for cardiac channel isoform. In another study, Tomaselli et al. (1995) reported that W402C substitution in outer vestibule of Nav1.4 eliminates slow inactivation. Different outer vestibule substitutions in Nav1.4 (K1237S or K1237E) resulted in development of an even longer lasting inactivation state, referred to as ultra-slow inactivation (Todt et al., 1999). Interestingly, equivalent charge preserving mutations lysine to arginine (K1237R) did not have such an effect. The time constant for entry and exit from ultra-slow inactivation was estimated at 100 s. In addition to the p-loops lining the outer vestibule, other regions of the channel's pore have been reported to contribute to slow inactivation. These include the S4 voltage sensors, which confer the voltage dependence of slow-inactivation (Kontis and Goldin, 1997; Ruben et al., 1990); β subunits, which control pore movement (Vilin et al., 1999) and reported by McCullum et al., 2003 and Groome et al., 2003 and 2007 charged residues

located near the IFM particle in the domain III-IV linker. Authors of these studies demonstrated that charge reversal (EE to RR) and charge neutralization (EE to QQ), but not charge replacement (EE to DD) mutations at positions 1314 and 1315 of the DIII-DIV linker stabilized steady-state fast inactivation and significantly decreased probability of slow inactivation. This could explain the interdependence between fast and slow inactivation and the fact that enzymatic removal of fast inactivation gate or molecular ablation due to mutation IFM to QQQ increases probability of slow inactivation. Based on those observations, an emerging physical model of slow inactivation has been proposed (McCullum et al., 2003). During prolonged depolarization lasting several seconds, S4 voltage sensors undergo secondary transitions leading to the collapse of the permeation pathway. The recovery from this state is long, measured on the time scale of seconds. The successful docking of the IFM particle and charge/allosteric interactions of surrounding residues with the docking site, stabilizes the channel's conformation, which is less favorable for occurrence of those secondary transitions. In recent years, several other residues located within the S6 transmembrane region were reported to have an effect on slow inactivation. O'Reilly et al. (2001) demonstrated that valine to lysine substitution at position 787 (V787K) of rat sodium channel Nav1.4 enhanced slow inactivation and accelerated the rate of entry to that process by two orders of magnitude (30 msec vs. 3 sec). By contrast, valine to cysteine substitution (V787C) had an opposite effect. Entry into slow inactivated state was slower t ~5sec and less voltage-dependent. Similar effect was observed and reported by Chancey et al., 2007 for cardiac channel Nav1.5. Valine to lysine or glutamine substitutions at the corresponding 930 position (V930K, V930Q), rendered naturally slow inactivation resistant cardiac channels,

susceptible to slow inactivation. Based on these data the emerging trend is: Fast inactivation stabilizing mutations decrease probability for slow inactivation while fast inactivation disrupting mutations increase it. The removal of positive charges in the outer vestibule region and addition of positive charges in the transmembrane S6 segment, promote and prolong slow inactivation.

Fast and slow channel inactivation are two functionally distinct processes. Whereas fast inactivation limits sodium ion conduction within duration of a single action potential, the effects of slow inactivation can be seen within a train of action potentials. The entry of channels into slow inactivated state limit channels availability for conduction. This in turn elevates action potential threshold, limits duration of bursts, and results in suppression of membrane excitability. Because of these properties slow inactivation has been proposed to regulate neuronal firing patterns, synaptic integration and backpropagation. Disruptions of either form of inactivation has been implicated in many human diseases. Fast inactivation altering mutations in cardiac channel Nav1.5 cause long QT syndrom (Wang et al., 1996), mutations in skeletal muscle channel Nav1.4 underlie hypercalemic periodic paralysis (McClatchey et al., 1992), and mutations in Nav1.1 isoform cause epilepsy (Rhodes et al., 2004). Alterations in slow inactivation are associated with myotonias and paralysis, which can be aggravated by cold or exercise (Ruff et al., 1994, Cannon et al., 2006, Fournier et al., 2006, Carle et al., 2009).

In the Chapter V of this thesis, we report that, under condition of high frequency stimulation, A-type FHFs limit availability of sodium channels through an inactivation process lasting up to 2 sec. Because of the fast (milliseconds) onset and use-dependent

requirement, the newly described phenomenon does not fit the criteria for either fast or slow inactivation. To distinguish A-type FHF related reduction in channels availability, we propose to refer to this process as long-term, use dependent inactivation.

1.6 How do FHFs modulate voltage gated sodium channels?

Although the structural mechanism underlying modulation of VGSCs by FHFs is unknown, certain aspects of the FHF-sodium channel interaction are well established. First, in order to exert any modulatory effect, FHFs have to associate with the channels (Goetz et al., 2009, Liu et al., 2003). FHF binding domain has been mapped to the proximal region of C-terminal tail of the pore forming α-subunits of the channels Nav1.9 (Liu et al., 2001), Nav1.5 (Liu et al., 2003) and Nav1.6 (Wittmack et al., 2004; Rush et al., 2006). Liu et al. (2003) stressed the importance of highly conserved, acidic residues within the binding domain and report that aspartic acid to glycine substitution (D1790G) in a channel binding domain of Nav1.5 was sufficient to disrupt FHF-channel interaction and its ability to modulate the mutant channel. The recent advances in solving a crystal structure of FHF2B (Goetz et al., 2009) allowed for identification of key amino acid residues located on the surface of FHF2B critical for binding to the C-tail of the Nav1.6 and endogenous channels of

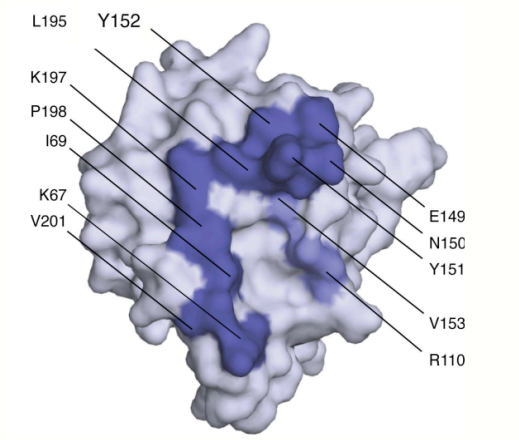

Picture 3. Molecular surface representation of FHF2B (Goetz et al., 2009). VGSC binding interface is highlighted in dark blue.

Neuro2A cells. FHF2B bearing mutations in those residues were unable to bind sodium channels or induce a depolarizing shift in voltage dependence of channel inactivation.

Second, FHFs do not modulate voltage dependence of channel activation, but have an effect on channel inactivation (Liu et al., 2001 and 2003; Lou et al., 2005; Rush et al., 2006; Goldfarb at al., 2007). Moreover, the reports by Rush et al., 2006 and our data presented in Chapters III and VI demonstrate that, long isoforms of FHFs induce a stronger depolarizing shift in voltage dependence of channel inactivation than short B isoforms, and only A type FHFs are capable of eliciting a use-dependent channel inactivation. The lack of the effect on channel activation suggests that FHFs do not interfere with upward movement of S4 voltage sensors but rather affect other regions of the channel. The potential candidates are: the inactivation loop housing the IFM particle, the cytoplasmic face of the channel forming a docking site, or the C-tail to which FHFs are bound.

1.7 FHFs as regulators of cellular excitability

The most direct evidence for FHFs involvement in regulation of cellular excitability comes from the FHF gene knockout and loss of function studies. In mice, targeted disruption of FHF4 gene results in the development of behavioral abnormalities classified as ataxia, paroxysmal dyskinesia, muscle weakness and learning deficits (Wang et al., 2002; Wozniak et al., 2007). Similarly, in humans, loss of function mutation in FHF4 gene have been linked to the genetically inherited syndrome, spinocerebellar ataxia (van Swieten et al., 2003; Dalski et al., 2005). Due to the overlapping expression and functional redundancy between some FHF isoforms, a single knockout of FHF1 did not

yield new behavioral phenotypes (Goldfarb et al., 2007). Beside the slight changes in the muscle strength, $FHF1^{-/-}$ mice appeared normal. Strikingly, FHF4 and FHF1 double knockout mice exhibited accentuated $FHF4^{-/-}$ deficits plus development of new phenotypes. Severe ataxia was accompanied by muscle atrophy and $FHF1^{-/-}FHF4^{-/-}$ mice suffered from hyperexcitability. The electrophysiology recordings performed on cerebellar granule neurons slices demonstrated impaired excitability of $FHF4^{-/-}$ and $FHF1^{-/-}FHF4^{-/-}$ neurons. Upon stimulation, wild type granular neurons produced trains of action potential spikes, $FHF4^{-/-}$ cells fired only few times and $FHF1^{-/-}FHF4^{-/-}$ could generate single action potential spike. Also the voltage threshold for action potential generation was elevated in single and double knockout neurons. This comprehensive study, for the first time, provided direct evidence for the role of FHFs in action potential generation. Since FHFs co-localize with voltage gated sodium channels at other subcellular compartments e.g. nodes of Ranvier, we can hypothesize that they might control action potential propagation and other voltage channel related processes.

GOALS

The experiments described in this thesis aimed to:

1. Analyze the FHF binding surface necessary for interaction with the C-terminal end of VGSCs (Chapter III).
2. Categorize all major FHF isoforms on a basis of their ability to modulate key parameters of channel's physiology (Chapter IV).
3. Investigate long-term, use-dependent inactivation induced by A-type FHFs (Chapter V). (i) Determine which amino acid residues are responsible for this effect. (ii) Study the relationship between fast and long-term, use-dependent inactivation. (iii) Propose a molecular model of channel inactivation by A-type FHFs. (iv) Demonstrate that short, synthetic peptide corresponding to first 20 amino residues of A-type FHFs alone is sufficient to induce long-term channel inactivation.
4. Study the differential localization of A-type FHFs in the wild-type mouse brain and neuronal compartments of dorsal root ganglion (DRG), hippocampal and cerebellar granule neurons (Chapter VI).

CHAPTER II

Methods and Reagents

2.1 Mammalian cell lines

Neuroblastoma (Neuro2A) cell line was maintained in Dulbecco's modified Eagle's medium (DMEM) supplemented with 10% fetal bovine serum, 4 mM L-glutamine, 100 U/ ml penicillin and 100 µg/ ml streptomycin and incubated at 37°C in a humidified incubator gassed with 95% air and 5% CO2. Neuro2A cell line stably expressing tetrodotoxin resistant version of sodium channel Nav1.6 was maintained under similar conditions with addition of 1mg/ml G418 (Clontech).

2.2 Cerebellar granule neuron cell culture

Cerebellar granule neuron cultures were prepared from postnatal day nine (P9) wild-type mice. Animals were anesthetized with isofluorene and euthanized by decapitation. Cerebella were dissected and meningis removed in cold BSS solution (Hank's Balanced Saline Solution buffered with HEPES pH 7.0 and supplemented with 4 mM L-glutamine, 100 U/ ml penicillin, and 100 µg/ ml streptomycin). Tissues were minced with the scalpel in the presence of 2ng/ml BDNF and digested for 10 min at RT in BSS solution containing 1% Trypsin and 1mg/ml DNaseI. Trypsinization reaction was ended by switching the trypsin solution to horse serum media containing 5% horse serum in high glucose Dulbecco's Modified Eagle Media (DMEM) supplemented with 4 mM L-glutamine, 100 U/ ml penicillin, 100 µg/ ml streptomycin and 1 mg/ml DNaseI. Cells were mechanically dissociated by trituration with sequentially reduced size fire polished

Pasteur pipettes and pelleted by centrifugation at 1krpm for 5 min at 4°C. Cells were washed with reduced DNaseI horse serum media, pelleted, and resuspended in DNase free growth media (5% fetal bovine serum, DMEM plus supplements). Cells were plated at low density (1 cerebellum per 8, 12 mm glass coverslips) or at medium density (1 cerebellum per well or filter in 6 well dish format). All surfaces were coated with poly-D-lysine. Cells were maintained in a humidified incubator gassed with 95% air and 5% CO2 in growth media additionally supplemented with 5 ng/ml BDNF. A half media replacement took place every 2 or 3 days and at days in vitro 2 and 5 cells were treated with 10 uM fluorodeoxyuridine and 10 uM uridine to inhibit the growth of dividing cells. Cells grown on coverslips were maintained for two weeks and cells grown in dishes or on filters were maintained for three weeks.

2.3 Hippcampal neuron cell culture

Primary Hippocampal neurons were prepared from embryonic day18 rat hippocampi. Briefly, dissected tissues were digested for 20 min at 37°C and 5 min at RT with papain in BSS medium (Hank's Balanced Saline Solution supplemented with HEPES Buffer solution, 100U/ml penicillin, and 100ug/ml streptomycin) and mechanically dissociated by trituration with original and reduced-bore Pasteur pipette. Dissociated cells were plated at low density on 12 mm glass coverslips coated with poly-L-Lysine and maintained in MEM with Earle's salts, 10% heat inactivated horse serum, 1% fetal bovine serum, 0.4% glucose, 2mM L-glutamine, 100U/ml penicillin, 100 ug/ml streptomycin, 1mM Sodium Pyruvate. After 4h incubation, coverslips were positioned cell-side down on a wax drop spacers and cultured in Neurobasal medium supplemented

with 2% B27, 100U/ml penicillin, 100 ug/ml streptomycin and 2mM L-glutamine. Every three days a growth media were partially replaced with conditioning media. Cytosine arabinoside and deoxycytidine were added to a final concentration 2μM to prevent culture overgrowth by glia cells. Cultures were maintained at 37°C in a humidified incubator gassed with 95% air and 5% CO2. After two weeks cells were fixed and processed for immunofluorescence.

2.4 Plasmids

2.4.1 Assembly of Nav1.6 cDNA in pCEFL expression vector

A full-length coding sequence of Nav1.6 was amplified from mouse brain RNA using RT-PCR and four sets of primers. Resulting four cDNA fragments (1.2 kbp, 1.6 kbp, 1.4 kbp and 1.7 kbp) were digested with restriction enzymes HindIII/Xho, Xho/BglII, SfiI/XbaI, XbaI/NotI (New England Laboratories) and assembled in pCEFL expression vector through four cycles of molecular cloning. After each ligation step plasmids were transformed by electroporation to ElectroMAX DH10B E. coli (Invitrogen). The success of each cloning cycle was verified by enzymatic digest and DNA sequencing.

2.4.2 Molecular cloning of Nav1.6 cDNA to a vector pCMV-IRES-neo3

A full length coding sequence of Nav1.6 was shuttled from pCEFL-Nav1.6 vector to bicistronic vector pCMV-IRESneo3 (Clontech) through EcoRV/NotI site. Excision of the Nav1.6 cDNA involved HindIII restriction digest, Klenow reaction to blunt HindIII ends, NotI digest. Both DNA fragments were gel purified before ligation.

2.4.3 Site directed mutagenesis to confer TTX resistance of sodium channel Nav1.6

A tetrodotoxin resistant (TTX^r) version of sodium channel Nav1.6 was produced by tyrosine-362 to serine (Y362S) substitution. A Quick Change mutagenesis Kit and protocol (Stratagene) was employed with two mutagenic primers and pCMV-Nav1.6-IRESneo3 as a template.

2.4.4 Site directed mutagenesis to construct TTX resistant Nav1.6 sodium channel with impaired fast inactivation gate

IFM particle of TTX resistant Nav1.6 was mutated to IQM in Quick Change mutagenesis (Stratagene) PCR reaction with two sets of mutagenic primers and pCMV-Nav1.6TTX^r-IRESneo3 as a template.

2.4.5 Site directed mutagenesis to construct TTX resistant Nav1.6 sodium channel with impaired docking site

A highly conserved alanine (A1317) in S4/S5 linker in Domain III of TTX resistant Nav1.6 was mutated to glutamine (Q) in Quick Change mutagenesis (Stratagene) PCR reaction with two sets of mutagenic primers and pCMV-Nav1.6TTX^r-IRESneo3 as a template.

2.4.6 Plasmids for FHFs- GFP fusion proteins

Plasmids: pFHF1A-GFP, pFHF1B-GFP, pFHF2A-GFP, pFHF2B-GFP, pFHF4B-GFP were already available in the Goldfarb's lab. FHF4A-IRES-ZsGreen expression vector was constructed. Briefly, exon 1A of FHF4A was amplified by PCR from mouse

genomic DNA, purified and digested with enzymes BglII and MluI. A coding sequence of FHF4B was amplified by PCR from plasmid pFHF4B-GFP, purified and digested with enzymes MluI and SacII. Both fragments were cloned into expression vectors pIRES-ZsGreen through BglII/SacII sites. Assembled coding sequence of FHF4A was confirmed by DNA sequencing.

A prokaryotic expression plasmid for an N-terminally truncated mutant FHF2A protein, pFHF2A ^{octamutant} was provided by Drs. Regina Goetz and Moosa Mohammadi (NYU Medical Center). This DNA was used to construct eukaryotic vector pFHF2B^{octamutant}-GFP through PCR and cloning (M. Goldfarb). The embedded FHF2B mutations were: K14F, I16R, Y98N, Y99H, L142R, K144M, P145S, and V148S.

2.4.7 Molecular cloning of FHF isoforms to an expression vector pIRES-ZsGreen

The coding sequences for FHF1A, FHF1B, FHF2A, FHF2B, FHF4B were shuttled from pEGFP expression vectors to pIRES-ZsGreen bicistronic vector (Clontech) by NcoI digest, ligation of NcoI-EcoRI adaptors, and cloning to pIRES-ZsGreen vector through EcoRI site. The correct orientation of the cloned fragments was verified by DNA sequencing.

2.4.8 Site directed mutagenesis to construct FHF plasmids used in inactivation particle studies

FHF2A mutants: 5Q, 7Q, I5A and LI/AA were constructed by the site directed mutagenesis using pFHF2A-IRES-ZsGreen as a PCR template and two sets of mutagenic primers. The correct clones were verified by sequencing. An additional round of site directed mutagenesis was employed to generate FHF2A 12Q construct. This time the

plasmid pFHF2A-7Q-IRES-ZsGreen served as PCR template. The mutagenic primers were the same as those used in construction of 5Q expression vector. The mutated residues in 5Q mutant were R11Q, K13Q, R14Q, R17Q, R19Q and in 7Q mutant K55Q, K56Q, R57Q, R58Q, R59Q, R60Q, R61Q, in LI/AA mutant L9A, I10A. 12Q mutant had combined 5Q and 7Q mutations.

2.5 Transfections

2.5.1 Stable transfection to establish Neuro2A Nav1.6$_{TTX}^{r}$ cell line

Neuro2A cell line stably expressing tetrodotoxin resistant version of channel Nav1.6 were established using calcium phosphate method. Neuro2A cells grown on 10 cm dishes were co-transfected with 10 ug of plasmid pCMV-Nav1.6 $_{TTX}^{r}$ -IRESneo3 and 10 ug of mouse genomic DNA. 24 hours post-transfection cells were split and growth media supplemented with 1 mg/ml G418. A G418 resistant clones were harvested after 14 days using cloning cylinders (Belco) and expanded. Clones were screened by electrophysiology recordings in the presence of 1 mM TTX to confirm the presence of tetrodotoxin resistant sodium currents. In events resulting in selection of mixed population clones, further sub-cloning was performed. Only physiologically uniforme clones were saved and cultured.

2.5.2 Transient transfections

For electrophysiology profiling of FHF isoforms Neuro2A or Neuro2A Nav1.6$_{TTX}^{r}$ cells were transfected with pFHFs-IRES-ZsGreen constructs using Lipofectamine 2000 (Invitrogen) reagents and protocol. Briefly, cells grown to 50% confluensy on 12-well

dishes were treated with a mixture of 2 µl of Lipofectamine, 3 µg of plasmid and maintained in 0.8 ml serum free culture media. After 4 h of transfection cells are re-fed with DMEM plus supplements (10% fetal bovine serum, 4 mM L-glutamine, 100 U/ ml penicillin and 100 µg/ ml streptomycin), allowed to recover for 1h, trypsinized and re-plated at low density on poly-D-lysine coated glass cover slips. The recordings from highly fluorescent cells were performed 48 to 72h after transfection in the presence or absence of 100 µM tetrodotoxin.

2.5.3 Transient co-transfections

To demonstrate FHF2A induced long-term inactivation of cardiac channel Nav1.5, Neuro2A cells were co-transfected with human Nav1.5 cDNA in pCDNA3.1 expression vector and pmFHF2A-IRES-ZsGreen or IRES-ZsGreen empty vector (control).

To investigate the relationship between fast and long-term inactivation of sodium channel Nav1.6, Neuro2A cells were co-transfected with pCMV-Nav1.6$_{TTX}^{r}$-(F1478Q)-neo or pCMV-Nav1.6$_{TTX}^{r}$-(A1371Q)-neo and pmFHF2A-IRES-ZsGreen or IRES-ZsGreen empty vector (control). All co-transfections were performed using Lipofectamine 2000 (Invitrogen) protocol and reagents, as described previously in *Transient transfection* method section. FHF and channel expressing plasmids were mixed in 1: 5 ratio before adding to the incubation mix.

2.6 Peptides

Short, synthetic peptides corresponding to amino acid residues 2-12, 11-21 and 2-21 of FHF2A were purchased from Invitrogen. Peptides were acetylated at the N-terminus, purified by HPLC, and analyzed by mass spectroscopy.

2.7 Cell and brain lysates

Triton lysis buffer containing 20 mM Tris-HCl pH 7.4, 137 mM NaCl, 2 mM EDTA, 25 mM B-glycerophosphate, 2 mM Na pyrophosphate, 1 mM Na orthovanadate, 10% glycerol, 1% Triton X-100, 1mM PMSF, 10 μg/ml leupeptin, 10 μg/ml aproteinin was used in all cell and brain lysates preparations and as a dilution medium in all immuno-precipitation reactions. The procedures involving the use of TLB were handled at 4°C.

2.8 Co-immunoprecipitations

2.8.1 Co-immunoprecipitation of sodium channel Nav1.6 with FHF2B and its octamutant derivative

HEK293T cells were grown in 10 cm dishes in Dulbecco's media with supplements for 24h to reach 80% confluency. After re-feeding with serum free media, cells were co-transfected using Lipofectamine 2000 (Invitrogen) method with plasmids expressing a full-length murine sodium channel Nav1.6 and GFP fusion proteins: FHF2B or $FHF2B^{octamutant}$. Following 48 hours incubation, cells were washed in lysis buffer without detergent, lysed in a triton lysis buffer and immunoprecipitated with rabbit anti-GFP polyclonal antibodies (Fitzgerald Laboratories) crosslinked to a Sepharose beads (Pierce). After washing, bound proteins were released to 4x Laemmlli sample buffer in 15 min

incubation at 37°C without β-mercaptoethanol. Both, immumoprecipitates and total protein lysates were resolved on 7.5% and 12% SDS polyacrylamide gel and transferred to polyvinylidene fluoride membranes. For detection of Nav1.6 or FHF fusion proteins a mouse monoclonal anti-PAN sodium channel antibody (Sigma) or anti-GFP antibody (Invitrogen) were used; followed by donkey anti-mouse IgG HRP-conjugated antibody (Jackson Laboratories). The signal was detected using ECL chemiluminescent system (GE).

2.8.2 Co-immunoprecipitation of sodium channels with A-typeFHFs

Cortical and cerebellar brain lysates were prepared from the wild-type and FHF1, FHF4 double knockout mice in triton lysis buffer. Briefly, animals were anesthetized with isofluorine, decapitated and whole brains removed. Cerebella were dissected from the rest of the brain and both preparations were processed separately. Tissues were homogenized in triton lysis buffer and protein concentration was measured by Bradford assay with thioglobuline as a protein standard. Preps were diluted with triton lysis buffer until final concentration fell below 4 mg/ml. Lysates were span at 14krpm for 10 min at 4°C to pellet the nuclei and insoluble material. Final protein concentration was established as before by Bradford assay.

2.9 Mouse brain and DRG cryosections

Whole brains and lumbar DRGs with attached motor and sensory neurons were dissected from wild-type 2-3 months old mice. Tissue preps were fixed in 4% paraformaldehyde, 4% sucrose in phosphate buffered saline (PBS), cryoprotected in 25% sucrose PBS and

embedded in O.C.T. compound (Tissue-Tek, Sakura). 20 μm sagittal sections were cut on cryostat (BRIGHT Instrument Company LTD.) pre-chilled to -17°C and collected on gelatin-coated slides.

2.10 Antibodies

Primary antibodies utilized in A-type FHFs localization studies were: mouse monoclonal anti- A-type FHF (mIgG2b) (1:50, NeuroMab), mouse monoclonal anti-PAN sodium channel (mIgG1) (1:1000, Sigma), polyclonal rabbit anti-MAP2 (1:2000, Millipore) or chicken anti- NFB (chIgY) (1;1000, Covance). For fluorescent detection these antibodies are coupled with corresponding secondary antibodies: goat anti-mouse IgG(H+L)-Alexa Fluor 488 (1:100, Invitrogen), goat anti-mouse IgG1-Alexa Fluor 594 (1:100, Invitrogen), goat anti-rabbit-Alexa Fluor 594 (1:00, Invitrogen) or donkey anti-chicken IgY-Cy5 (1:100, Jackson Immunoresearch). The cell nuclei were stained with TO-PRO iodide (1:1000, Invitrogen).

2.11 Immunocytochemistry/Immunohistochemistry

Rat hippocampal neurons (DIV12) and mouse cerebellar granule neurons (DIV14) were fixed on coverslips in 4% paraformaldehyde, 4% sucrose in phosphate buffered saline (PBS) on ice for 10 min. Mouse whole brain sagittal cryosections and DRG cryosections were additionally post fixed in the same solution for 5 min prior to immunostaining. All samples were washed with PBS, permabilized with 0.5% Triton X-100 in PBS for 10 min at RT and pre-blocked with 10% FBS, 0.2% Triton X-100 in PBS for 1 hr at RT. Two rounds of primary/secondary antibody incubations were applied since anti –A type FHF

and anti- PAN sodium channel antibody were raised in the same host. First primary antibody incubation was carried out overnight at 4^{o}C, followed by the wash and 2h, RT incubation with first secondary antibody. After the wash, second primary antibody was applied for 2h at RT, followed by the wash and 2h, RT second secondary antibody incubation. In control experiments the second primary antibody was omitted. Used antibodies were diluted in PBS containing 2.5% FBS, 0.2%Triton X-100. Each wash consisted of 3, 10 min RT incubations with 0.2% Triton X-100 PBS. Last two 10 min washes were done with TO-PRO iodide in PBS and PBS. Cells containing coverslips were inverted and mounted on the glass slides, and glass slides containing cryosections were enclosed by the coverslips. A hardening Vectashield (Vecror Laboratories) was used as a mounting medium. Digital images were taken on Leica confocal microscope and assembled by PhotoShop.

2.12 Axonal preps

Distal axon preps were prepared from three weeks old, medium density cerebellar granule cultures grown on filter membranes (Millicell Cell Culture Inserts, Millipore). Filter specifications (3 μm pore diameter) allowed for maintaining of the cell bodies on the top portion of the filter and distal axons on the bottom of the filter. Cells were washed in cold lysis buffer (20 mM Tris-HCl pH 7.4, 137 mM NaCl, 2 mM EDTA, 25 mM B-glycerophosphate, 2 mM Na pyrophosphate, 1 mM Na orthovanadate, 10% glycerol, 1mM PMSF, 10 μg/ml leupeptin, 10 μg/ml aproteinin). Distal axons were harvested from the bottoms of the filters using a cell scraper. Collected material was pelleted and lysed in1% Triton lysis buffer on ice for 10 min with occasional vortexing. Lysate was span

down to remove insoluble material. Because of the limited amount of the material, protein concentration was not determined.

Proximal and distal axon preps were prepared from three weeks old, medium density cerebellar granule cultures grown in 5 wells on 6 well dishes. Cells were washed with cold lysis buffer and mechanically displaced with the cell scraper. To separate cell somas from the proximal and distal axons cells were titurated with reduced bore Pasteur pipettes and centrifuged at low speed. Undissociated cellular material was removed by two cycles of centrifugation at 300 rpm for 10 min. Cell somas were pelleted by two cycles of centrifugation at 1krpm for 15 min. Axon containing supernatant was transferred to a new tube. The separated fractions were monitored microscopically. Separated cell and axon fractions were pelleted, resuspended in 1% triton lysis buffer, lysed on ice for 10 min, vortexed, and precleared. Total protein concentration was determined by Bradford assay. Both types of axonal preps were analysed by Western Blot and probed for sodium channel and A-type FHF signal with mouse, monoclonal anit-PAN sodium channel antibody (Sigma, 1ug/ml) and mouse monoclonal anti-A-type FHF tissue culture supernatant (NeuroMab, 1: 500) followed by goat anti-mouse HRP conjugated antibody (Jackson, 1: 5000).

2.13 Western Blot

Sodium channels and FHFs were resolved on 7.5% and 12% SDS-polyacrylamide gels (SDS-PAGE). Electrophoresis was carried out overnight at 75V in running buffer (0.1% SDS, 10 mM β-mercaptoethanol in Tris-Glycine). Separated proteins were transferred to polyvinylidene difluoride membranes (PVDF, Immobilion-P, Millipore) in 5h, 800mA or

overnight, 200mA transfer in the presence of 20% Methanol in Tris-Glycine buffer maintained at 11°C. Blots were rinsed with Tris Buffered Saline (TBS) and blocked with 5% non-fat milk (Nestle) in TBS for 1h at RT. Primary antibodies incubations were curried out in 2.5% Bovine Serum Albumine (BSA) in TBST(0.1% Tween 20 in TBS) overnight at 4°C or for 2h at RT. Secondary antibody incubations were performed in a same buffer for 1-1.5h at RT. After primary and secondary antibody incubations blots were washed three times for 10 min with TBST at RT. An additional two 5 min TBST and two 5 min TBS washes were applied before chemmiluminescence detection with ECL reagents (GE or Roche). Developed blots were exposed to Kodak X-OMAT film (Carestream Health). The apparent molecular weight of proteins was estimated by comparison to the migration pattern of the pre-stained molecular weight standards Dual Color or Kaleidoscope Precision Plus Protein Standards (Bio-Rad).

2.14 Whole-cell voltage clamp recordings

Whole-cell voltage clamp recordings were performed on Neuro2A cell lines: Neuro2A or Neuro2ANav1.6TTX^r and their derivatives expressing one of the FHFs: FHF1A, FHF1B, FHF2A, FHF2B, FHF4A, or FHF4B. For studying long-term inactivation of the cardiac channel by the long-term inactivating particle, Neuro2A cells were transfected with Nav1.5 expression vector. Transfected cells were plated at low density on coverslips and used 48-72h post transfection. FHF expressing cells were identified by green fluorescence.

Recordings were obtained at RT using Axopatch 200B amplifier, Digidata 1322 digital/ analog interface, and pCLAMP9 software (Molecular Devices Inc.). Borosilicate glass pipettes with resistance 1-2 MΩ were pulled using Micropipette Puller (Shutter

Instruments). Extracellular recording solutions contained: 120 mM NaCl, 26 mM $NaHCO_3$, 3 mM KCl, 10 mM glucose, 4 mM $MgCl_2$, 2 mM $CaCl_2$, 0.2 mM $CdCl_2$, 3 mM myoinositol, 2mM Na pyruvate. For analyses of Neuro2A cells expressing Nav1.6TTXr and Nav1.5 channels, 1 mM TTX was added to fully block endogenous TTX sensitive currents. The intracellular pipette solution contained: 104 mM CsF, 50 mM tetraethylamine chloride, 10 mM HEPES pH7.2, 5 mM glucose, 2 mM $MgCl_2$, 10 mM EGTA, 2 mM ATP, and 0.2 mM GTP. Recordings were initiated following seal formation >5 GΩ , cell break-in, and at least 5 min waiting period (to allow for cellular dialysis). In cases were FHF2A (2-21) peptide or anti-A type FHF Abs were used, the waiting period was extended to 10 and 30 min, respectively. Signals were filtered at 5 kHz and digitized at 10 or 20 kHz. The electrotonic capacitative and leak currents in voltage clamp pCLAMP protocols were subtracted during data acquisition using the pre-sweep hyperpolarizing P/N method in the software; access resistance (<5 MΩ) was not compensated. Following protocols were implemented:

To analyze ***voltage dependence of channel activation (Protocol 1.)***, cells were held at -90 mV holding potential for 5 ms and stepped to test voltages in a range (-50 mV to 25 mV). Cells were held at test voltages for 30 ms to allow for channels activation followed by fast inactivation and then returned to -90 mV holding potential to allow for recovery from the inactivation. Starting from -50 mV test potential the voltage of each subsequent sweep was increased by 5mV. The obtained peak current (I_{peak}) was plotted against test voltage (V_m). The percentage of open channels was computed from the linear portion of the curve and plotted versus V_m. The data points were fitted to the Boltzmann distribution

curve from which two values were obtained: the voltage at which 50% of channels are activated referred to $V_{1/2}$ of activation and a slope factor k.

To analyze ***voltage dependence of channel fast inactivation (Protocol 2.)***, cells were held for 5 ms at -110 mV holding potential and then subjected to the preconditioning test voltages in the range of (-110 mV to -20 mV). The duration of preconditioning steps was 60 ms and the voltage of each subsequent preconditioning sweep increased by 5 mV. The preconditioning steps were followed by a depolarization step to 0 mV for 20 ms. Since at 0 mV all channels are open, pairing this step with the preconditioning step allow for measuring the fraction of channels available for activation/inactivation. Each test sweep ended with repolarization at -90 mV during which channels recover from inactivation. The peak currents were converted to the percentage of channels available and plotted versus preconditioning voltage V_m. The data points were fitted to the Boltzmann distribution curve from which $V_{1/2}$ of the inactivation and k slope value can be read.

To analyze ***voltage dependence of long-term, use -dependent inactivation (Protocol 3.)*** a two-pulse protocol was employed. Cells were held at -90 mV holding potential and subjected to test voltages in a range of (-90 mv to +50 mV). The duration of the first pulse was 15 ms and the voltage of each subsequent sweep was increased by 5 mV. Following 40 ms fast recovery time at -90 mV, cells were subjected to a second pulse of depolarization to 0 mV for 10 ms. During 40 ms recovery time channels recovered from fast inactivation and the second depolarization revealed fraction of channels available (i.e., not subject to slow inactivation). The peak currents were converted to the percentage of channels available and

plotted versus first pulse voltage V_m. The data points were fitted to the Boltzmann distribution curve from which $V_{1/2}$ of slow, use-dependent inactivation and k slope value can be obtained.

The ***recovery from the fast inactivation (Protocol 4.)*** was analyzed by two-pulse protocol. Each pulse consisted of 6 ms depolarization step from -90 mV to 0 mV, separated by variable time interval. The recovery time changed with each subsequent sweep from 0.5 ms to 20 ms in 0.5 ms increments. All sweeps ended with the extended periods of recovery time at -90 mV. The second peak current for each sweep was expressed as a percentage of maximal channel recovery and plotted versus recovery time. Obtained τ value reflects the time at which 63% of channels recovered from inactivation.

The ***accumulation of use-dependent inactivation (Protocol 5.)*** was measured using four pulse protocol. Cells were held at -90 mV holding potential and subjected to four test depolarizations from –90 mV to 0 mV. Test pulses were separated by 40 ms recovery time at –90 mV, during which channels were allowed to recover from fast inactivation. Additionally, 4 s at –90 mV command was run at the end of each sweep to allow for channels recovery from slow, use-dependent inactivation. The duration of test depolarizations in the first sweep was 2 ms and each subsequent sweep was extended by 2 ms intervals. The longest pulse depolarization time was 16 ms. The second, third and fourth peak current of each sweep were expressed as a percentage of the first maximal peak current and plotted versus depolarization number.

Boltzmann equation: $f(Vtest) = [1 + e(V1/2 – Vtest)/k] -1 + C$.

Protocol 1. Voltage dependence of channel activation.

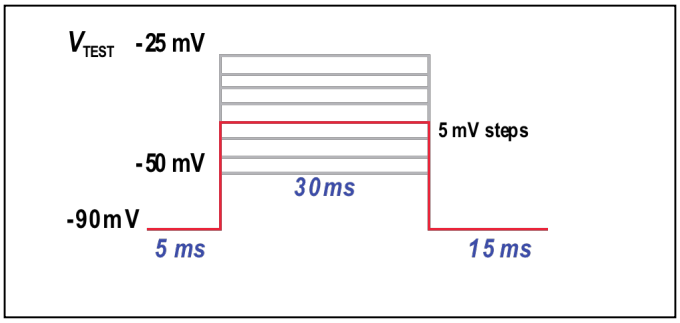

Protocol 2. Voltage dependence of channel steady-state fast inactivation.

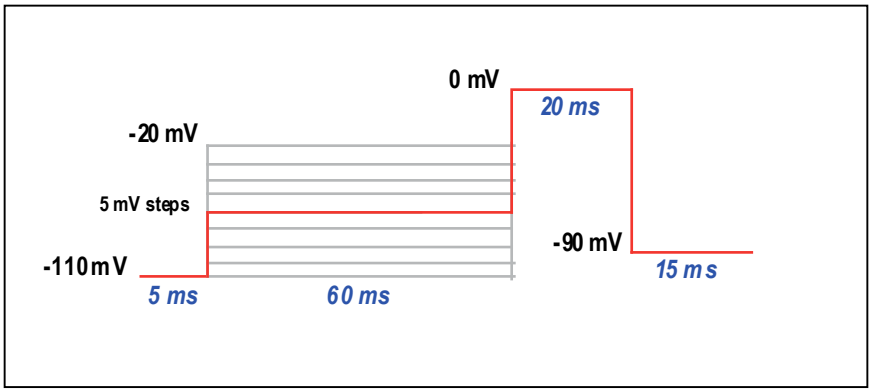

Protocol 3. Voltage dependence of channel long-term, use-dependent inactivation.

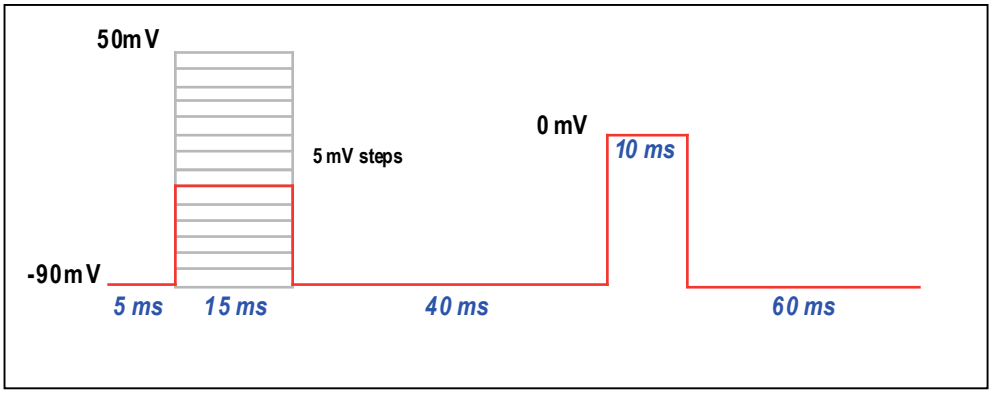

Protocol 4. Recovery from fast inactivation.

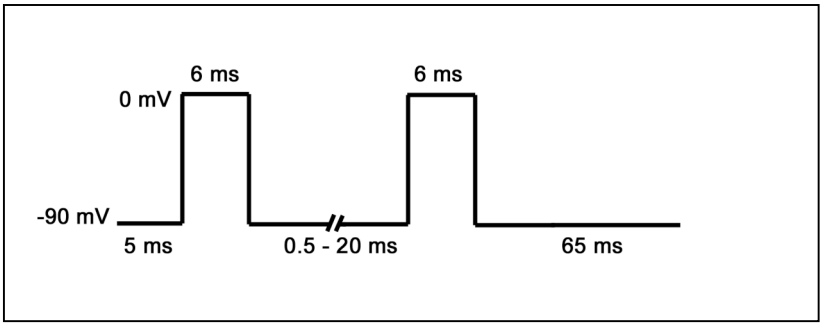

Protocol 5. Accumulation of long-term, use dependent inactivation.

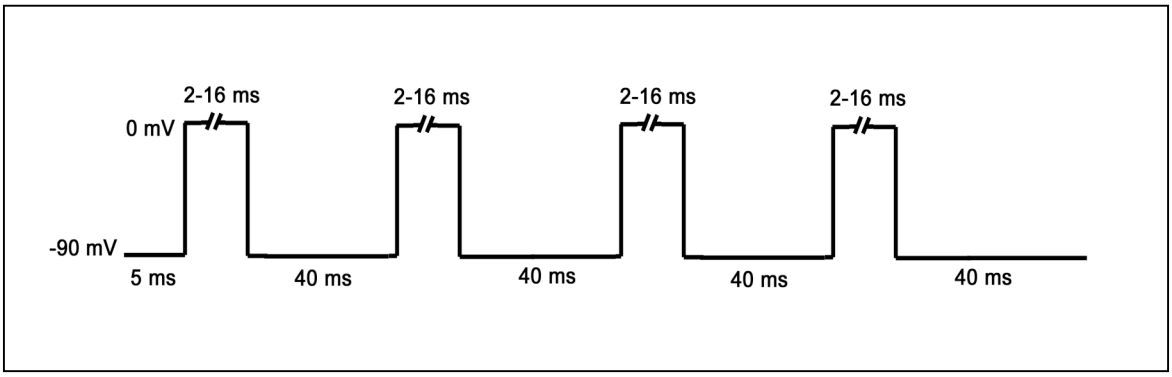

NOTE: The diagrams are not to scale and the time indicated reflects the duration for which data points were collected.

CHAPTER III

Determination of the channel-binding surface, common to all FHFs

This part of the research was done in collaboration with Dr. Moosa Mohammadi and Dr. Regina Goetz from Department of Pharmacology and Skirball Institute of Biomolecular Medicine, New York University School of Medicine

3.1 Introduction

A successful mapping of the channel-binding surface, common to all FHFs, became possible following the discovery of the crystal structure of FHF2A by Goetz and co-workers. Unlike it's predecessor, FHF1B, which crystallized as a monomer, FHF2A formed crystallographic dimers revealing important structural differences, further distinguishing FHFs from FGF family of proteins, as well as sites of protein –protein interaction. It was hypothesized, that the molecular surface of FHF2A involved in dimer formation in vitro, may be responsible for the interaction with the C-terminal end of VGSCs in vivo.

To test this hypothesis, structure guided point mutations were introduced into a core of FHF2A and FHF1B. The mutated residues corresponded to the amino acids: K67F, I69R, Y151N, Y152H, L195R, K197M, P198S, V201S of FHF2A and fulfilled three basic rules. Mutated residues were involved in dimer formation, were conserved among all FHFs, and were substituted with corresponding residues found on FGFs. FHF2A and FHF1B and their mutated variants (single, double, triple, quadruple and octamutamts) were tested by analytical size exclusion chromatography and surface

plasmon resonance for ability to bind to C-terminal ends of sodium channels Nav1.5, Nav1.6, and Nav1.9. It was established that the long N-terminal extension characteristic for all A-type FHFs is not necessary for channel binding, since all tested A and B FHF isoforms interacted with the carboxyterminal end of sodium channels, forming high affinity complexes at 1:1 stoichiometric ratio. On the contrary, the core substitutions lower the affinity of channel interaction for both tested FHFs in the mutation dependent manner. Since studied residues are conserved among all FHFs, Goetz and co-workers proposed, that newly identified surface represents a universal channel binding site, common to all FHFs.

The experiments performed in our lab further substentiate in vitro findings and demonstrate that identified channel binding surface on FHFs is necessary for interaction with sodium channels in vivo, FHF localization at AIS and modulation of channel inactivation.

My contribution to the project has consisted of performing co-immuno-precipitation and electrophysiology experiments using wild-type and octamutant FHFs.

3.2 Results

3.2.1 Channel binding surface, common to all FHFs is necessary for the interaction with sodium channel Nav1.6 in vivo

To demonstrate that channel-binding surface identified through biophysical assays in vitro is necessary for channel binding in vivo, FHF2B or its octamutant counterpart were co-expressed with sodium channel Nav1.6 in HEK293T cells and studied by immunoprecipitation. HEK293T was a cell line of choice since, as reported by Shirihata

et al., 2006, these cells do not express endogenous sodium channels or FHFs. The Lipofectamine method was used for co-transfections and both FHFs were expressed as GFP fusion proteins. Following 48h of incubation, transfected cells were lysed and co-immunoprecipitated with anti-GFP antibodies cross-linked to a Sepharose beads. The eluted material was further analyzed by Western Blot with anti-PAN sodium channel antibodies to detect Nav1.6 and anti-GFP antibodies to visualize FHF-GFP fusion proteins. The results presented in Figure 3.1 clearly demonstrate that eight point mutations introduced into channel binding surface of FHF2B completely abolished its ability to form precipitable complexes with sodium channel Nav1.6, even under conditions where more FHF2B^{octamutant}-GFP containing lysate was used. The result stresses the importance of the newly identified FHF molecular surface for channel binding in vivo.

3.2.2 Channel binding surface on FHFs 2A and 2B is necessary for the modulation of the sodium channels endogenously expressed in Neuro2A cells

Whole-cell voltage clamp recordings were performed using Neuro2A cells transiently transfected with wild-type or octamutant versions of FHF2A and FHF2B. As a measure of precaution, all tested FHFs were expressed as GFP untagged proteins from bicistronic vectors. The level of protein expression was monitored by green fluorescence and only healthy, highly fluorescent cells were considered for recordings. Since Neuro2A cells express endogenous sodium channels Nav1.1, Nav1.2, Nav1.7, the modulatory effect of the wild-type or mutant FHFs 2A and 2B on those channels could be assessed. The voltage dependence of sodium channel inactivation was measured by whole- cell voltage

clamp using solutions specific to detection of sodium currents. A more detailed description of electrophysiology protocols and techniques used in this experiment can be found in the Chapter II, Electrophysiology Methods section. The results summarized in Figure 3.2 show that both tested wild-type FHFs induce a depolarizing shift in the voltage dependence of channel inactivation with FHF2A having more profound effect over FHF2B (21 mV vs. 8.3 mV shift, respectively). Introduced mutations into channel binding surface of FHF2A or FHF2B resulted in inability of this FHFs to shift the voltage dependence of channel inactivation. Presented data demonstrate that FHFs can only function as channel modulators when bound to the C-terminal end of sodium channels.

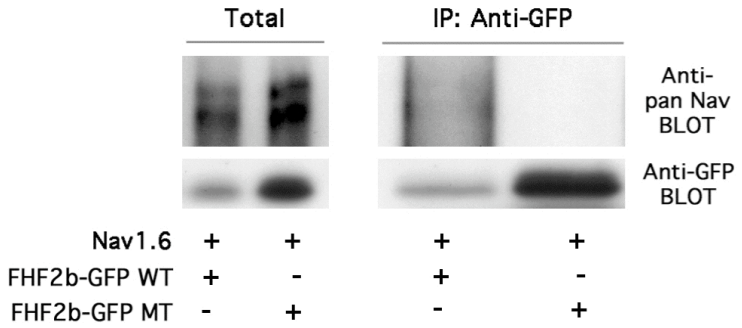

Figure 3.1 Channel binding surface on FHF2B is necessary for the interaction with sodium channel Nav1.6 in vivo.

Co-immunoprecipitation of sodium channel Nav1.6 with wild-type and mutant FHF2B. HEK293T cells were co-transfected with plasmids expressing full length sodium channel Nav1.6 and wild-type FHF2B-GFP or its mutated derivative FHF2B^{octamutant}-GFP. The mutated residues in FHF2B octamutant were: K14F, I16R, Y98N, Y99H, L142M, P145S, V148S. Cell lysates were immunoprecitipated with anti GFP antibodies and analyzed for the ability to co-capture Nav1.6. The immunoprecipitated protein complexes (right panel) and total protein cell extracts (left panel) were examined by immunobloting with anti pan sodium channel antibody to detect Nav1.6 and anti GFP antibody to detect wild-type and mutant FHFs. As illustrated in the last column of the right panel FHF2B octamutant does not form precipitable complexes with Nav1.6.

A Neuro2A Endogenous channel Inactivation

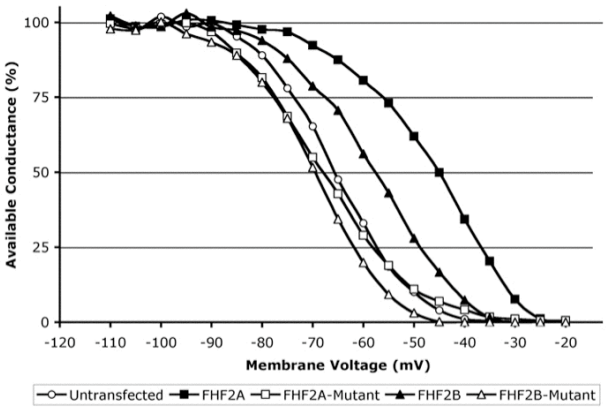

B

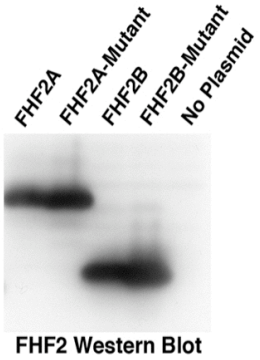

C Summary of electrophysiology data

Plasmid	V1/2 Inactiv (mV)	k Inactiv (mV)	# Cells	T-Test (P)
None	-65.7 +/- 6.5	-6.0 +/- 1.3	15	
FHF2A	***-44.7 +/- 7.8***	-7.7 +/- 1.5	16	$< 4 \times 10^{-9}$
FHF2A-Mutant	-68.1 +/- 7.5	-5.5 +/- 5.0	12	
FHF2B	***-57.4 +/- 5.4***	-8.5 +/- 1.5	8	$< 4 \times 10^{-3}$
FHF2B-Mutant	-70.4 +/- 8.5	-5.5 +/- 0.8	10	

Figure 3.2 Channel binding surface on FHFs 2A and 2B is necessary for the modulation of the sodium channels endogenously expressed in Neuro2A cells.

Neuro2A cells untransfected or transfected with ether FHF2A, FHF2A octamutant, FHF2B or FHF2B octamutant were analyzed for voltage dependence of steady-state fast inactivation. The whole-cell voltage clamp recordings were performed under conditions specified in "Electrophysiology methods". Panel A) Voltage dependence of fast inactivation of endogenous Neuro2A sodium channels modulated by tested FHFs. Current traces recorded for each condition were normalized and fitted to Boltzmann distribution curves. Obtained $V_{1/2}$ of inactivation, (k) slope values along with indication

of number of cells analyzed and T-test parameters are summarized in Panel C). Note the values of $V_{1/2}$ of inactivation recorded for FHF2A and FHF2B octamutant are no longer shifted to the right as seen with wild-type FHF2A and FHF2B but rather resemble $V_{1/2}$ of inactivation of untransfected Neuro2A cells. Panel B) Western-Blot analysis of Neuro2A cells used in electrophysiology recordings (control for FHF protein expression). Positive FHF detection in all cells transfected with FHF-GFP bicistronic vectors and lack of FHF signal in untransfected sample. The differences in molecular weight between A and B FHF isoforms are reflected in the differential migration of corresponding bands on 12.5% PA gel during SDS-PAGE.

3.3 Discussion

Efforts to map a channel-binding surface on FHFs have been undertaken previously. Liu et al., 2003 reported identification of the segment encompassing first 41N-terminally located residues on FHF1B required for binding to sodium channel Nav1.5. The experimental approach employed in the study consisted of the overexpression of subsequently truncated versions of GFP tagged FHF1B in HEK system followed by the pull down assay with GST tagged polypeptide mimicking C-terminus of Nav1.5. The removal of the first 5 a.a. residues had no effect on channel binding while subsequent deletions (a.a. 1-41) greatly diminished and (a.a.1-76, 1-142, 1-181) completely abolished interaction with Nav1.5. Based on these results authors concluded that first 41 a.a. residues of FHF1B are essential for Nav1.5 channel binding. Surprisingly, the authors of the study were not concerned that performed deletions were affecting structural core of the FHF1B and were substantial e.g. a.a. residues 1-41 form 3 out of total 12 β-sheets. The deletion of such a large portion of the protein can lead to misfolding and disruption of functional domains, including the channel binding domain, located elsewhere. Second, to demonstrate that 1-41 region is essential for Nav1.5 binding, other large cluster of a.a. residues should be deleted while preserving 1-41 region. If under those conditions association with Nav1.5 was maintained one could consider 1-41 region involved in channel binding. In another study Lou et al., 2005 tested A and B isoforms of FHF4 and its N-terminally truncated version for ability to bind sodium channels Nav1.5 and Nav1.1. The authors concluded that N-terminal extension of FHF4 is necessary for binding to Nav1.5 but not to Nav1.1. Since FHF4 is not expressed in the cardiac tissue the first result can lead to misinterpretations. On the other hand, the

maintenance of the interaction of N-terminally truncated FHF4 with Nav1.1 further suggests, that channel binding domain is not defined by N-terminal end of FHFs but rather resides in the other region of the protein.

The experimental approach and the study outcome reported by Goetz et al., 2009 differs from Liu's and Lou's in many respects. The concept to explore a channel-binding surface on FHFs was derived from the careful examination of the crystal structure of FHF2A, not by the study of the linear representation of amino acid sequences of FHFs 1 and 4. The authors took precautions to avoid disruption of overall protein structure. The introduced point mutations were distributed among different structural elements, which come together to form the molecular surface of FHFs, rather than being confined to one particular element. Also the amino acid residues under investigation were substituted with the corresponding residues found in FGFs and in theory should not interfere with B-trefoil fold of FHFs.

Several lines of evidence corroborate the universal nature of the channel-binding surface, common to all FHFs. First, the residues involved are conserved among all FHFs and are located within the FHF homology core. Second, different FHFs can bind to the same or different sodium channels regardless of the type or isoform. For example, Wittmack et al., 2004 and Rush et al., 2006 show that FHF2A and FHF2B can interact with sodium channel Nav1.6. Our experimental data presented in Chapter V further extends that group for FHF1A, FHF1B, FHF4A and FHF4B. But it is also known that, for example, FHF1B can bind to Nav1.9, Nav1.5 and endogenous channels expressed in hippocampal, cerebellar and DRG neurons.

The data obtained from my co-immunoprecipitation experiment of FHF2B and FHF2B octamutant with sodium channel Nav1.6 are in agreement with previous findings of Goetz and co-workers. The results clearly demonstrate that mutated residues are necessary for channel binding in vivo as shown by the inability of FHF2B octamutant to form precipitable complexes with sodium channel Nav1.6. The electrophysiology data, further demonstrate that channel binding is necessary for proper function of FHFs as channel modulators (since untethered FHF2B and FHF2A failed to induce a depolarizing shift in voltage dependence of channel inactivation). Together with the localization studies performed by Laezza, my data extends the validity of in vitro biophysical assays and allows for structure to function transition.

CHAPTER IV

Electrophysiology of FHF isoforms

4.1 Introduction

FHFs influence various parameters of sodium channel's physiology including voltage dependence of channel inactivation, time of the recovery from the inactivation, and current density. A pairwise comparison of FHF2A with FHF2B (Wittmack et al., 2004, Rush et al., 2006) and FHF4A with FHF4B (Lou et al., 2005, Laezza et al., 2009) revealed that the type and the magnitude of the modulatory effect tightly correlates with the length and amino acid composition of N-terminal extensions present on different FHFs. The authors of these studies also warned that the cellular background and the type of sodium channel under investigation greatly contribute to the final outcome of whole-cell voltage clamp recordings. In the past, different FHF isoforms were evaluated in variety of cell lines (Xenopus oocytes, HEK293, ND27/23, Neuro2A, hippocampal and cerebellar granule neurons) expressing different assortments of sodium channels. Therefore, their modulatory effects cannot be reliably compared.

Protein sequence alignment of N-terminal extensions of major isoforms of FHFs has unveiled a high degree of homology among long, N-terminal extensions of A-type FHFs and among the short, N-termini of B-type FHFs, with the long FHF4B being the only exception of the rule. We hypothesized that, *regardless of the gene from which they were transcribed, FHFs sharing N-terminal homology modulate channels in a similar way.* If proven correct, the results of this study will suggest functional redundancy among FHF family of proteins and explain why double FHF gene knockouts were necessary to produce FHF deficient phenotypes (Goldfarb et al., 2007, X. Huang, PhD Thesis 2009). By using FHF sequence alignment and supported

functional studies, one can start mapping functional domains within N-termini of FHFs responsible for each particular modulatory effect.

The experimental approach employed in this study consisted of evaluating major FHF isoforms (FHF1A, FHF2A, FHF4A, FHF1B, FHF2B, FHF4B) for their abilities to modulate a tetrodotoxin (TTX)-resistant variant of Nav1.6 stably expressed in Neuro2A cells. Neuro2A was the cell line of choice for several reasons. First, Neuro2A cells exhibit neuron-like characteristics. They express multiple sodium channel α subunits Nav1.2, 1.3, 1.4, 1.7) and two β subunits (β_1 and β_3) (Lou et al., 2005). All endogenous channels are TTX sensitive and can be inhibited by addition of the TTX to an extracellular bath solution. Second, Neuro2A cells are easy to culture, transfect and patch during whole-cell voltage clamp recordings. Third, this cell line was used previously (Lou et al., 2005) for studying the effect of FHF4A and FHF4B on endogenous Neuro2A channels and our data could be cross-referenced. The choice of the sodium channel was guided by the fact that Nav1.6 is abundantly expressed at axon initial segments of mature cerebellar, hippocampal and Purkinje neurons (Schaller et all., 1995, Caldwell et al., 2000, Levin et al., 2006); Nav1.6 was found to be a major channel isoform expressed at nodes of Ranvier in both central and peripheral nervous system (Caldwell et al., 2000, Boiko et al., 2001) and different FHF isoforms were reported to localize to those regions (Wittmack et al., 2004, Rush et al., 2006, Goldfarb et al., 2007, Laezza et al., 2009).

Initially, the unmodified Neuro2A cell system was utilized to examine the effect of FHFs on endogenous, TTX-sensitive channels. Following the establishment of the stable Neuro2A cell line expressing tetrodotoxin resistant derivative of the sodium channel Nav1.6 (Figure 4.1, and 4.2), the evaluation of FHFs was repeated. This time the electrophysiology recordings were performed in the presence of TTX and the obtained results reflected the modulatory effect of

FHFs on Nav1.6. The whole-cell voltage clamp recordings were carried out as described in detail in Chapter II, Electrophysiology Method section. Implemented protocols aimed to measure voltage dependence of channel activation, inactivation and time of recovery from fast inactivation.

4.2 Results

4.2.1 Voltage dependence of activation of sodium channel Nav1.6 is not affected by different isoforms of FHF.

The voltage dependence of channel activation was studied in the Neuro2A cell line stably expressing $Nav1.6^{TTXr}$ in the presence of TTX. Whole-cell voltage clamp recordings were performed on healthy, highly fluorescent cells co-expressing one of the FHFs (FHF1A, FHF1B, FHF2A, FHF2B, FHF4A, FHF4B) from GFP bicistronic vectors (Figure 4.2) The following activation protocol was employed. Cells were held at -90 mV holding potential and depolarized for 30 ms to test voltages in a range (-50 mV to +25 mV) in 5 mV increments and subsequently returned to -90 mV holding potential. During each of the depolarization cycles sodium channels were activated, fast inactivated and allowed to recover from inactivation at -90 mV holding potential. Recorded sodium current traces were analyzed (for more details please refer to Chapter II, Electrophysiology Methods, Protocol 1) and $v_{1/2}$ of activation and k slope factors were obtained for each tested FHF. As summarized in Table 4.1, the $v_{1/2}$ of the activation recorded in the absence and presence of FHFs was in -35 mV to -40 mV range. None of the tested FHFs had a statistically significant modulatory effect on voltage dependence of activation of sodium channel Nav1.6, as reflected by relatively high p values.

4.2.2 A-type FHFs and FHF4B have stronger modulatory effect on voltage dependence of channel inactivation than short B-type FHFs.

Voltage dependence of channel inactivation was studied in Neuro2A cell line expressing endogenous sodium channels and in a Neuro2A derivative stably expressing $Nav1.6^{TTXr}$ in the presence of TTX. Whole-cell voltage clamp recordings were conducted using the inactivation

protocol. Cells held at -110 mV holding potential, were subjected to preconditioning potentials in a range of (-110 mV to -20 mV) for 60 ms and additionally depolarized to 0 mV test potential for 20 ms. At the end of each test depolarization cells were returned to -110 mV holding potential. The idea behind the inactivation protocol is as follows: During the preconditioning depolarization a fraction of channels undergo inactivation and become unavailable for activation during 0 mV testing potential. Since this process is voltage dependent, by plotting the percentage of available channels versus preconditioning voltage, the voltage dependence of inactivation can be established. (For more information please refer to Chapter II, Electrophysiology methods). The value of $v_{1/2}$ of inactivation recorded for sodium channel Nav1.6 in the absence of FHFs equaled -79.1 +/- 3.7 mV. FHFs having long terminal extensions such as FHF1A, FHF2A, FHF4A, FHF4B induced large, depolarizing shifts in voltage dependence of inactivation (12.7 mV, 12.8 mV, 15.8 mV, 16.8 mV, respectively). FHF having short N-terminus had either no effect in the case of FHF1B or induced much smaller depolarizing shift (7.6 mV, the value recorded for FHF2B). A similar pattern emerged from the evaluation of the panel of FHFs on endogenous Neuro2A channels (Figure 4.6). The $v_{1/2}$ of inactivation in the absence of FHFs was -65.7 +/- 6.5 mV. FHF1A, FHF2A, FHF4A and FHF4B positively shifted voltage of inactivation by 20.3 mV, 21 mV, 17.7 mV, respectively. Again, FHF1B had no effect and FHF2B induced 8.3 mV depolarizing shift.

4.2.3 A-type FHFs induce long-term inactivation of sodium channel Nav1.6 and endogenous channels expressed in Neuro2A cells.

Initially, the panel of FHFs including FHF1A, FHF1B, FHF2A, FHF2B, FHF4B was assayed for ability to long-term inactivate sodium channels endogenously expressed in Neuro2A cells

(Figure 4.7, A) The protocol employed in this study consisted of two cycles of depolarization to 0 mV for 6 ms from the holding potential -90 mV separated by variable intervals (0.5 msec to 20 msec) of recovery at -90 mV. During the first cycle of depolarization sodium channels undergo activation and inactivation. The variable times of recovery followed by second depolarization allow for calculation of the percentage of channels recovered. By comparing the percentage of channels recovered at the same time interval the effect of FHFs on channels recovery can be assessed. The data presented in the Figure 4.7, A shows, that in the absence of FHFs or in the presence of FHF1B, FHF2B, FHF4B, within 20 ms of recovery time over 90% of endogenous Neuro2A channels fully recouped from the first cycle of depolarization. In contrast, in the presence of FHF1A or FHF2A only 70% of channels recovered. The remaining 30% of channels had undergone long-term inactivation. Similar results were obtained from analysis of A and B type of FHFs on $Nav1.6^{TTXr}$ (Figure 4.7, B). The voltage clamp protocol was modified to consist of several depolarization cycles 16 msec in duration separated by 40 msec recovery periods at – 90 mV. Obtained data are summarized in Figure 4.7. Again only A-type FHFs induced long-term inactivation of sodium channel $Nav1.6TTX^{r}$.

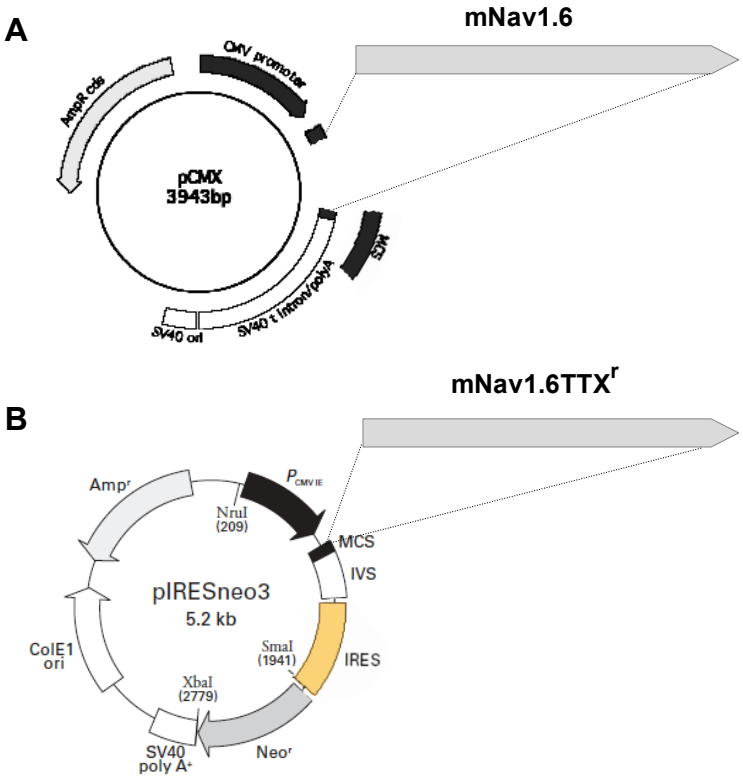

Figure 4.1. Expression vectors for studying sodium channel Nav1.6 in neuronal (Neuro2A) and non-neuronal (HEK) cell lines.

A full-length coding sequence of mouse sodium channel Nav1.6 was assembled from four cDNA fragments and subsequently shuttled to pCMX and pIRESneo3 (Clontech) vectors. TTX resistance of Nav1.6 in pCMV-Nav1.6-IRESneo3 was conferred mutating tyrosine at position 362 to serine (Y362S). Panel A) Schematic representation of pCMX-Nav1.6 expression vector used for stable and transient transfections to HEK293/293T cells.

Panel B) Schematic representation of bicistronic expression vector pCMV-Nav1.6$_{TTX}^{r}$-IRESneo3 used to establish Neuro2A cell line stably expressing TTX-resistant Nav1.6.

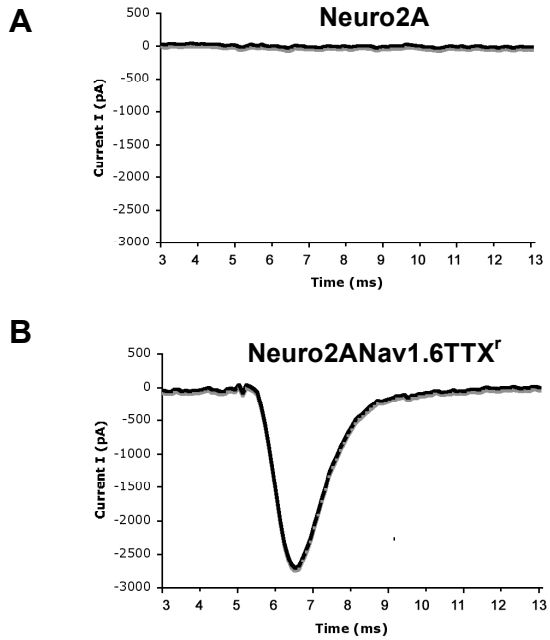

Figure 4.2 Neuro2A cells stably expressing Nav1.6TTX^r produce tetrodotoxin resistant currents.

Neuro2A cells and the derivative stably expressing TTX-resistant Nav1.6 were analyzed by whole-cell voltage clamprecording in the presence of potassium and calcium channels inhibitors and 1uM TTX. Cells were held at -90mV test potential for 5 ms and stepped to –20 mV to induce transient sodium current. Panel A) Lack of TTX-resistant currents in untransfected N2A. Panel B) Representative traces of TTX-resistant sodium currents recorded from Neuro2A cells stably expressing Nav1.6TTX^r. Conclusion: *TTX-resistant currents found in modified Neuroblastoma cell line originate from successful, stable transfection of Neuro2A cells with Nav1.6TTX^r.*

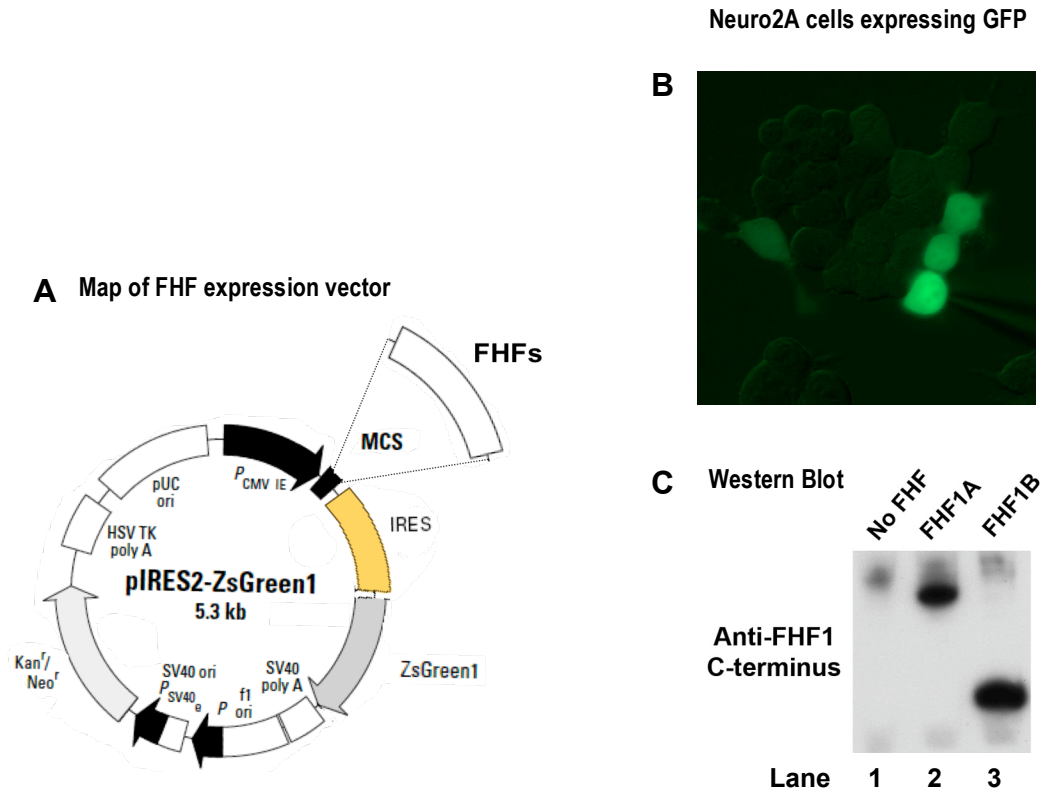

Figure 4.3 Untagged FHFs and green fluorescence protein (GFP) are co-expressed in Neuro2A cells from bicistronic vectors.

All FHFs used in electrophysiology recordings were transcribed from GFP bicistronic vectors. DNAs encoding FHF1A, FHF2A, FHF4A, FHF1B, FHF2B, FHF4B were cloned into MCS of pIRES-ZsGreen1vector (Clontech). Neuro2A cells transfected with this type of constructs expressed untagged FHFs and the level of FHF's expression correlated with the level of green fluorescence. Panel A) Schematic representation of the FHF expression vector used in all electrophysiology experiments. Panel B) Neuro2A cells in culture expressing GFP (picture taken 48h after Lipofectamine2000 transfection). Panel C) Western Blot analysis of lysates prepared from Neuro2A cells transfected with empty bicistronic vector (lane 1) or vectors encoding FHF1A or FHF1B (lane 2 and lane 3, respectively).

Nav1.6 ACTIVATION				
Plasmid	$V_{1/2}$ activation (mV)	k (mV)	# Cells	T-test (P)
None	- 35.0 +/- 3.3	6.1 +/- 0.6	7	---
FHF1A	- 40.0 +/- 3.9	4.0 +/- 3.9	5	0.05
FHF1B	- 38.3 +/- 1.3	4.7 +/- 0.6	4	0.05
FHF2A	- 39.1 +/- 7.0	4.1 +/- 0.9	7	0.12
FHF2B	- 36.6 +/- 3.1	4.8 +/- 0.4	6	0.39
FHF4A	- 37.6 +/- 4.6	4.8 +/- 1.1	5	0.32
FHF4B	- 36.1 +/- 3.7	5.0 +/- 1.0	6	0.59

Figure 4.4 FHFs have no effect on voltage dependence of activation of sodium channel Nav1.6TTX^r.

The voltage dependence of channel activation was studied in Neuro2A cell line stably expressing tetrodotoxin resistant version of sodium channel Nav1.6 in the presence of tetrodotoxin. Whole-cell voltage clamp recordings were performed on healthy, highly fluorescent cells co-expressing one of the FHFs (FHF1A, FHF1B, FHF2A, FHF2B, FHF4A, FHF4B) from GFP bicistronic vectors. The measure voltage dependence of steady-state activation cells were held at -90 mV holding potential and depolarized for 30 ms to test voltages in a range (-50 mV to +25 mV) in 5 mV increments and subsequently returned to -90 mV holding potential. Recorded sodium current traces were analyzed (for more details please refer to Chapter II, Electrophysiology Methods, Protocol 1). $v_{1/2}$ of activation and k slope factors were obtained for each tested FHF. As summarized in Figure 4.4, the $v_{1/2}$ of the activation recorded in the absence and presence of FHFs was in -35 mV to -40 mV range. None of the tested FHFs had a statistically significant modulatory effect on voltage dependence of activation of sodium channel Nav1.6, as reflected by relatively high p values.

A

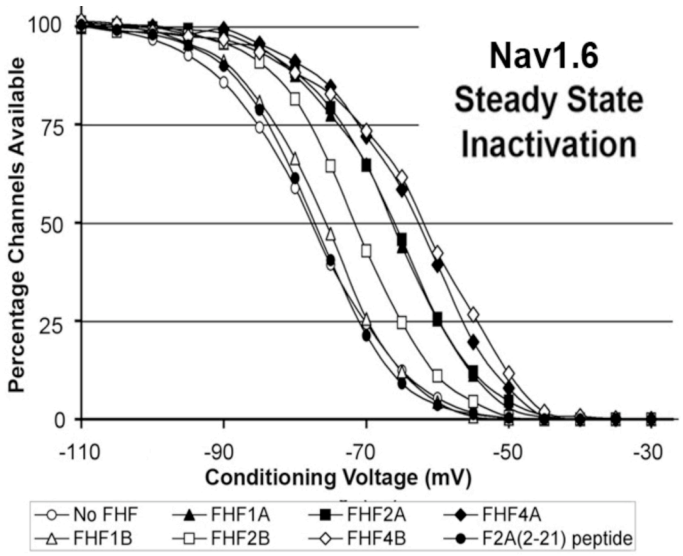

B **Summary of Electrophysiology data**

Nav1.6 STEADY- STATE INACTIVATION				
Plasmid	**$V_{1/2}$ inactivation (mV)**	**k (mV)**	**# Cells**	**T-test (P)**
None	- 79.1 +/- 3.7	-5.5 +/- 0.5	8	---
FHF1A	**- 66.4 +/- 2.8**	-5.0 +/- 0.2	5	**3(exp)-5**
FHF1B	- 78.0 +/- 2.6	-5.6 +/- 0.3	5	0.12
FHF2A	**- 66.3 +/- 4.3**	-5.6 +/- 0.3	8	**2(exp)-5**
FHF2B	**- 71.5 +/- 2.2**	-5.5 +/- 0.5	8	**3(exp)-4**
FHF4A	**- 63.3 +/- 3.3**	-6.1 +/- 0.8	5	**2(exp)-5**
FHF4B	**-62.3 +/- 4.3**	-6.8 +/- 1.4	8	**1(exp)-6**

Figure 4.5 A-type FHFs and FHF4B exert stronger depolarizing shift in voltage dependence of steady-state fast inactivation of sodium channel Nav1.6TTX^r than small B-type FHFs.

Voltage dependence of channel inactivation was studied in Neuro2A cell line stably expressing tetrodotoxin resistant version of sodium channel Nav1.6 in the presence of tetrodotoxin. Whole-cell voltage clamp recordings were conducted using inactivation protocol. Cells held at -110 mV holding potential, were subjected to preconditioning potentials in a range of (-110 mV to -20 mV) for 60 ms and additionally depolarized to 0 mV test potential for 20 ms. At the end of each

test depolarization cells were returned to -110 mV holding potential. Recorded peak currents were plotted versus preconditioning voltage and fitted to the Boltzmann distribution curve. The value of $v_{1/2}$ of steady-state inactivation and k (slope value) were obtained for each tested FHF and presented in a table format. Panel A) Availability curves for sodium channel Nav1.6TTX^r in the absence and presence of different FHFs. Panel B) Summary of the electrophysiology data. Obtained results show that FHFs with long terminal extensions: FHF1A, FHF2A, FHF4A, FHF4B induce large, depolarizing shifts in voltage dependence of channel inactivation (12.7 mV, 12.8 mV, 15.8 mV, 16.8 mV, respectively) whereas FHFs having short N-termini, have no effect (as in the case of FHF1B) or induce much smaller depolarizing shift (7.6 mV, the value recorded for FHF2B).

A **Neuro2A Endogenous Channel Inactivation**

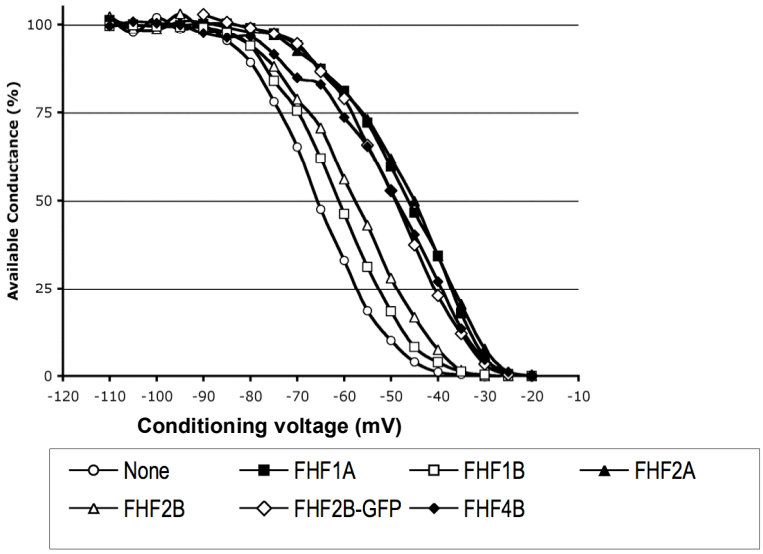

B **Summary of Electrophysiology data**

Endogenous Neuro2A channels STEADY- STATE INACTIVATION				
Plasmid	**$V_{1/2}$ inactivation (mV)**	**k (mV)**	**# Cells**	**T-test (P)**
None	- 65.7 +/- 6.5	-6.0 +/- 1.3	15	---
FHF1A	**- 45.3 +/- 8.1**	-7.7 +/- 1.6	12	**5(exp)-7**
FHF1B	- 61.2 +/- 7.0	-6.6 +/- 0.4	10	0.1
FHF2A	**- 44.7 +/- 7.8**	-7.7 +/- 1.5	16	**4(exp)-9**
FHF2B	**- 57.4 +/- 5.4**	-8.5 +/- 1.5	8	**4(exp)-3**
FHF2B-GFP	**- 48.9 +/- 3.6**	-8.6 +/- 1.6	8	**4(exp)-8**
FHF4B	**-48.0 +/- 7.3**	-9.5 +/- 1.4	10	**8(exp)-6**

Figure 4.6 A-type FHFs and FHF4B induce large depolarizing shift in voltage dependence of steady-state fast inactivation of sodium channels endogenous to Neuro2A cells.

Voltage dependence of channel inactivation was studied in unmodified Neuro2A cell line expressing endogenous, tetrodotoxin sensitive sodium channels: Nav1.2, Nav1.3, Nav1.4 and Nav1.7. Whole-cell voltage clamp recordings were conducted using inactivation protocol. Cells held at -110 mV holding potential, were subjected to preconditioning potentials in a range of (-110 mV to -20 mV) for 60 ms and additionally depolarized to 0 mV test potential for 20 ms. At

the end of each test depolarization cells were returned to -110 mV holding potential. Recorded peak currents were plotted versus preconditioning voltage and fitted to the Boltzmann distribution curve. The value of $v_{1/2}$ of steady-state inactivation and k (slope value) were obtained for each tested FHF and presented in a table format. Panel A) Availability curves for sodium channels in the absence and presence of different FHFs. Panel B) Summary of the electrophysiology data. Obtained results, reproduced data obtained for sodium channel Nav1.6TTX^r and show strong modulatory capabilities of A-type FHFs and FHF4B.

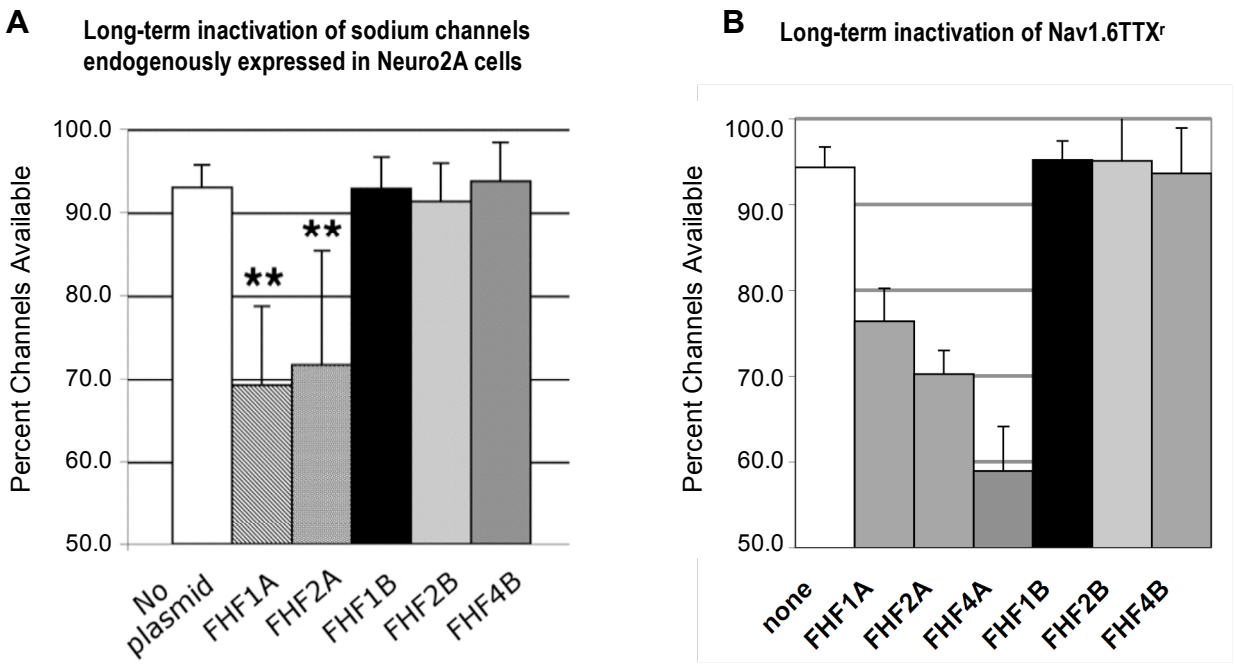

Figure 4.7 A-type FHFs induce long-term, use-dependent inactivation of sodium channel Nav1.6TTX^r and sodium channels endogenously expressed in Neuro2A cells

Panel A) Major isoforms of FHFs were tested for ability to induce long-term, use-dependent inactivation of tetrodotoxin sensitive sodium channels: Nav1.1, Nav1.2, Nav1.3, Nav1.7 (endogenously expressed in Neuro2A cells). Whole-cell, voltage clamp recordings were performed with solutions designed to isolate sodium currents, in the absence of tetrodotoxin. FHF-transfected and untransfected Neuro2A cells were subjected to two 6 ms depolarizations (0 mV) separated by a 20 ms –90mV recovery phase. Presented data, expressed as the percentage of endogenous channels available in second depolarization in comparison to the first demonstrates, that A-type FHFs induce long-term inactivation, while B-type FHFs do not; **, $P < .04$.

Panel B) In analogous experiment, different isoforms of FHF were tested for ability to long-term inactivate sodium channel Nav1.6 expressed in Neuro2A cells as a tetrodotoxin resistant variant. Whole-cell voltage clamp recordings were carried out as before except two modifications. 100

μm TTX was added to the extracellular solution and the recovery time between depolarizations was extended to 40 ms. Obtained results show that from the pool of tested FHFs, only A-type FHFs induce long-term, use dependent inactivation of sodium channel Nav1.6 TTX^r.

4.3 Discussion

The experiments described in this chapter were motivated by the need to evaluate all major FHF isoforms for ability to influence key parameters of sodium channel physiology in a uniform system. We were able to demonstrate that all tested FHFs modulated sodium channel Nav1.6 or endogenous channels expressed in Neuro2A cells in an isoform-specific manner. Based on our test, FHF isoforms could be categorized into three functional groups: A-type FHFs, having long N-terminal extensions, comprising FHF1A, FHF2A, FHF3A, FHF4A, characterized by a strong depolarizing shift in voltage dependence of inactivation, and ability to induce a long-term, use-dependent inactivation. B-type FHFs, having short N-termini, encompassing FHF1B and FHF2B, characterized by small depolarizing shift in voltage dependence of inactivation, and the lack of long-term, use-dependent inactivation. We also report that the long FHF4B is the only member of the third functional group exerting a strong depolarizing shift in voltage dependence of inactivation without inducing long-term, use-dependent inactivation. In a sense, FHF4B represents a mixture of A-type and B-type functional characteristics.

The presented survey marks an important initial step toward defining functional domains within N-terminal ends of FHFs. Through deletion and substitution mutagenesis studies, it should be possible to identify the amino acid residues necessary for each observed modulatory effect as well as domains responsible for differential localization of FHFs at various cellular compartments.

CHAPTER V

Long-term, use-dependent channel inactivation by A-type FHFs

The objective of this chapter is to summarize and highlight major discoveries published in the paper titled "Long-term Inactivation Particle for Voltage-Gated Sodium Channels" by Katarzyna Dover, Sergio Solinas, Egidio D'Angelo, and Mitchell Goldfarb. My contribution to the published work consisted of (i) preparation of the plasmid constructs used for the expression of the sodium channel $Nav1.6^{TTXr}$, its mutated variants, and all tested FHFs, (ii) establishment of Neuro2A cell line stably expressing $Nav1.6^{TTXr}$, (iii) performance of whole-cell voltage-clamp recordings, the results of which appear in Figure 1 panels A to F, Figure 2 panels A to H, Figure 3 panels A to E, Figure 6 panel A, and corresponding tables. I would like to acknowledge the involvement of my mentor Dr. Goldfarb, who provided training, oversight and often personally helped with the experiments. The printout of the published paper composed by Dr. Goldfarb is attached at the end of this chapter. As commented by the reviewing editor of The Journal of Physiology "This is an elegant demonstration of the molecular mechanisms governing a form of long-term inactivation of voltage-gated Na channels. It is extensively documented and beautifully illustrated."

5.1 Summary

One of the key findings reported in the previous chapter was that all A-type FHFs induce long-term inactivation of sodium channel Nav1.6 and several channels endogenously expressed in Neuro2A cells. Here, by employing a combination of mutagenesis and whole-cell voltage clamp recordings we continued to elucidate the process of long-term inactivation by A-type

FHFs. To simplify the experimental setup we decided to work exclusively with FHF2A, a representative member of A-type FHFs and with Nav1.6 stably expressed as TTX-resistant variant in Neuro2A cells.

As shown in panels A and B of Figure 1, upon application of two cycles of depolarization spaced by 5-20 ms recovery time, in the absence of FHF2A, the majority of Nav1.6 channels recovered within 10-20 ms. By contrast, in the presence of FHF2A under the same experimental conditions, only 70% of channels recovered within a comparable time frame. The remaining 30% of channels entered a nonconductive state, which we refer to as long-term inactivation. The first question addressed, was: How long does it take for Nav1.6 channels to recover from long-term inactivation in the presence of FHF2A? By further extending the recovery period between two depolarization cycles we determined (panel D Figure1) that 2s are required for the vast majority channels to recover. The time constant for recovery from long-term inactivation (τ) was established and shown to be 300-400 ms. Because of the rapid onset and intermediate recovery time, this described process differs from classical fast or slow inactivation. Recorded long-term inactivation is a direct consequence of the interaction of sodium channel Nav1.6 with FHF2A. Without FHF2A, long-term inactivation cannot be observed.

Another feature of the A-type FHF induced long-term inactivation is use dependence. As presented in panel C of Figure1, with each additional cycle of depolarization more and more channels accumulated into a non-conductive state. The 40 ms recovery intervals following each depolarization cycle were sufficient for Nav1.6 channels to recover from the fast but not from a long-term inactivation. In the panel C of Figure 2 we also demonstrated, that extending the time of each depolarization from 2-16 ms had little effect on the accumulation of channels into a long-term inactivated state. Based on these findings we suspect, that under a condition of high

frequency stimulation, use dependence of long -term inactivation may limit the repetitive firing of neurons expressing A-type FHFs.

The relationship between the fast and the long-term inactivation was studied extensively. The voltage dependence of the steady-state, fast inactivation and the long-term inactivation were established (panel A Figure 2) showing significant differences in $v_{1/2}$ values (-66.3 mV vs. -46.7 mV, respectively). The interpretation of these results lead to the formulation of the hypothesis, which states: *Fast and long-term inactivation are two competing channel states. At lower voltages, fast inactivation is a predominant form of channel inactivation, while additional voltage driven channel transitions are necessary for long-term inactivation to occur.* To test this hypothesis Neuro2A cells co-expressing sodium channel Nav1.6 and FHF2A were subjected to two pulse recovery protocols. The first depolarization was held at -55 mV or 0 mV, followed by 2-16 ms recovery interval at -90 mV. The percentage of the available channels was calculated from the current response to the second depolarization held at 0 mV. As predicted, any inactivation that took place during -55 mV depolarization was a fast inactivation, since virtually all channels were able to recover within 16 ms. In contrast, the inactivation at 0 mV represented a mixture of the fast and the long-term inactivation, since during 16 ms only a fraction of channels recovered. Because voltage gated sodium channels respond to the changes in membrane potential by their conformational rearrangements, we concluded: Lower voltage driven channel transitions favor fast inactivation. With rising voltage, channel's conformation changes in favor of long-term inactivation.

In another experiment the competitive nature of the fast and the long-term inactivation was assessed. By introducing phenylalanine to glycine point mutation in the position 1478 of channel's intrinsic IFM particle, we were able to generate a fast inactivation deficient Nav1.6

channels (West et al., 1992). As depicted in panel E of Figure 2, in the absence of FHF2A, once activated, mutated channels remained conductive for the entire duration of the activating protocol. The introduction of FHF2A into the experimental system not only rescued the inactivation process (panel F Figure 2) but also eliminated the use-dependent effect, characteristic for the long-term inactivation (panel F Figure 2 lower part). The result confirms our predictions that without a competition from the fast inactivation particle, all observed inactivation will be long-term inactivation. Nav1.6 (F1478Q) channels will inactivate at higher voltages resulting in wider sodium current traces, and most importantly, long-term inactivation will be maximal following a single depolarization cycle (lower panel F, panel G of Figure 2).

As reported previously (panel C of Figure 2) the magnitude of the FHF2A induced long-term inactivation on wild-type Nav1.6 channels depends on the number of the depolarization cycles, and not as much on the duration of each individual cycle. In panel H of Figure 2, we provide further evidence that fast inactivation limits entry into FHF2A-induced long-term inactivation. Nav1.6 (A1371G) displays leaky fast inactivation, due to instable docking of the fast inactivation particle onto the channel inner pore (Smith and Goldin et 1997). As shown in panel H of Figure 2, Nav1.6 (A1371G) undergo greater FHF-induced long-term inactivation as a depolarization cycle is lengthened. We suspect that the dissociation of weakly docked IFM fast inactivation particle continuously renders channels susceptible to long-term inactivation.

Several lines of evidence strongly suggested the existence of the long-term inactivation particle located within the N-terminal extension of all A-type FHFs. The results from profiling major FHF isoforms for ability to modulate sodium channels revealed that only A-type FHFs can long-term inactivate Nav1.6 and several other channels endogenously expressed in Neuro2A cells. B-type FHFs having short N-terminal ends or FHF4B having long, but unrelated N-

terminus could not exert a long-term inactivation effect. Since both A-type FHFs and FHF4B induce ~15-20 mV depolarizing shift in voltage dependence of channels inactivation, it was deduced and later experimentally confirmed (panel B and C of Figure 3), that the functional domain affecting voltage dependence of steady-state inactivation is separate from the functional domain responsible for long-term inactivation. The search for a long-term inactivation particle began with careful examination of the protein sequence alignment of N-terminal extensions of all A-type FHFs and the decision to mutate two clusters of positively charged amino acid residues, located in the proximal and distal regions of N-terminal extension of FHF2A (panel A of Figure 3). Whole-cell voltage clamp recordings performed on Neuro2A cells co-expressing $Nav1.6^{TTXr}$ and each of the tested FHF2A mutants (FHF2A-5Q, FHF2A-7Q, FHF2A-I5A and FHF2A-LI/AA) allowed for assigning the functional domain to a region spanning residues 1-18 of FHF2A. As shown in panel B of Figure 3, leucine and isolucine at positions 9 and 10 as well as adjacent cluster of basic residues rich in lysines and arginines were critical for domain's function. Having established the region within N-terminal extension of A-type FHFs necessary for long-term inactivation of sodium channel Nav1.6 we began to explore whether the N-terminus of FHF2A alone could act as a long-term inactivation particle sufficient for channel's inactivation. Although such short fragments lacked the FHF core and could not be concentrated near channel's pore through interaction with the C-terminal end of the channel (panel B Figure 3), we predicted, that the lack of tethering could be compensated by a sufficiently high concentration of the peptide, delivered to the cell through the patch pipette. By applying standard recovery and accumulation protocols, we were able to demonstrate that, just like full length FHF2A, a 20 residue synthetic peptide corresponding to FHF2A (2-21) induced long-term inactivation of sodium channel Nav1.6 (panel A Figure 4). Long-term inactivation was cycle-

dependent (panel B Figure 4), but maximal long-term inactivation occurred in a single depolarization cycle when assayed on the fast inactivation-defective Nav1.6 (F1478) channel (panel C Figure 4). It was also established that 1 mM peptide concentration was optimal for accumulation of sodium channels Nav1.6 and Nav1.5 into long-term inactivation state (panel D and E Figure 4).

The effect of the long-term inactivation particle on cellular excitability was demonstrated by voltage clamp and current clamp recordings performed on cultured cerebellar granule neurons. As shown in panels A and B of Figure 5, cerebellar granule neurons cultured for 16 days had well established sodium and potassium currents and upon current injection were able to fire repetitive trains of action potentials. The delivery of the particle mimicking peptide FHF2A (2-21) through the patch pipette had no effect on outward movement of potassium ions, but induced accumulating long-term inactivation of sodium channels (panel C Figure 5). When assayed by current clamp recording, FHF2A (2-21) peptide inhibited repetitive firing of cerebellar granule neurons (panel D Figure 5). In another experiment the relationship between the peptide concentration, sodium channels availability and the number of generated action potential spikes was assayed. The data summarized in the panel E of Figure 5 shows that with increasing peptide concentration, the amount of available channels diminished and the number of evoked action potential spikes decreased. The presented results substantiate the role of long-term inactivation particle in regulation of neuronal excitability and points at the particle's therapeutic potential in treatment of disorders of hyperexcitability.

Based on the outcome of our experiments, we decided to extend, a previously described by Raman and Bean 12 states kinetic model for voltage gated sodium channels, by including additional long-term inactivated channel states: L3, L4, L5 and L6. A new, 16 state model,

reflects sodium channel transitions in the presence of A-type FHFs (panel B Figure 6). Long-term inactivated channel states were also incorporated into the existing computer model of cerebellar granule neuron (D'Angelo et al., 2001, Diwakar et al., 2009). As presented in panels D, E and F of Figure 6 by assigning the appropriate rate constants for each transitional state (panel C Figure 6), our empirical data were faithfully replicated in the computer simulations using voltage clamp and current clamp protocols.

To summarize, we proposed a molecular model of voltage gated sodium channel inactivation by A-type FHFs (panel A Figure 6). According to the model, at the closed channel state, both, fast and long-term inactivation particles are exposed to the cytoplasm. At the lower voltage driven channel transitions, fast inactivation is a predominant way of inactivating channels. During this process, the IFM particle gains access to the channel's docking site and terminates the sodium ion conduction. With rising voltage, the cytoplasmic face of the pore widens, and fast and long-term inactivation particles begin to compete for ability to inactivate. A-type FHF tethered to the C-terminal end of the channel delivers a long-term inactivation particle but it has not been resolved, whether the particle directly interacts with the channel's docking site or acts through a different mechanism. It is clear though, that once fast inactivated, channels become unavailable for long-term inactivation, and therefore several depolarization cycles are necessary to accumulate channels into the long-term inactivated state. In the future, the proposed model will be further tested. One of the planned experiments aims at introducing substitutions into the inner vestibule of the sodium channel $Nav1.6^{TTXr}$ and screening for channel mutants with impaired long-term inactivation.

The search for the biological function of A-type FHFs will be continued. In the next chapter I will explore a localization of A-type FHFs in the mouse brain and in cellular compartments of DRG, hippocampal and cerebellar granule neurons.

5.2 "Long-term Inactivation Particle for Voltage-Gated Sodium Channels" by Katarzyna Dover, Sergio Solinas, Egidio D'Angelo, and Mitchell Goldfarb – Manuscript in press at Journal of Physiology (London).

Long-Term Inactivation Particle for Voltage-Gated Sodium Channels

Katarzyna Dover[1,2], Sergio Solinas[3], Egidio D'Angelo[3], and Mitchell Goldfarb[1,4]

[1] Department of Biological Sciences, Hunter College of City University, 695 Park Avenue,

New York, NY 10065, USA

[2] Graduate Program in Biology, City University of New York

[3] Department of Physiology, University of Pavia, via Forlanini 6, Pavia, Italy

[4] Correspondence to: Mitchell Goldfarb, Hunter College of City University, Department of Biological Sciences, Room HN834, 695 Park Avenue, New York, NY 10065, Email: goldfarb@genectr.hunter.cuny.edu

Abstract

Action potential generation is governed by the opening, inactivation, and recovery of voltage-gated sodium channels. A channel's voltage-sensing and pore-forming alpha subunit bears an intrinsic fast inactivation particle that mediates both onset of inactivation upon membrane depolarization and rapid recovery upon repolarization. We describe here a novel inactivation particle housed within an accessory channel subunit (A-type FHF protein) that mediates rapid-onset, long-term inactivation of several sodium channels. The channel-intrinsic and tethered FHF-derived particles, both situated at the cytoplasmic face of the plasma membrane, compete for induction of inactivation, causing channels to progressively accumulate into the long-term refractory state during multiple cycles of membrane depolarization. Intracellular injection of a short peptide corresponding to the FHF particle can reproduce channel long-term inactivation in a dose-dependent manner and can inhibit repetitive firing of cerebellar granule neurons. We discuss potential structural mechanisms of long-term inactivation and potential roles of A-type FHFs in the modulation of action potential generation and conduction.

Introduction

Voltage-gated sodium channels carry the inward flow of sodium ions driving generation of action potentials in excitable cells. Rising membrane potential leads to sodium channel opening and also induces fast inactivation, which facilitates membrane repolarization and fast channel recovery. The inactivation/recovery cycle of sodium channels permits repetitive firing in muscle and nerve cells. A membrane-embedded sodium channel alpha subunit harbors the channel's ion selectivity pore, the voltage-gated activation mechanism, and the fast inactivation gating particle residing in a short cytoplasmic loop (West *et al.*, 1992; Eaholtz *et al.*, 1994; Caterall, 2000). Other mechanisms of channel inactivation have been described. Upon membrane depolarization, a rapid open channel block can be conferred on neuronal sodium channel $Na_v1.6$ by certain associated channel beta subunits, and unblocking upon repolarization accounts for the transient resurgent current of this channel in certain cells (Raman & Bean, 1997, 2001; Grieco *et al.*, 2005). A quite distinct mode of inactivation, so-called slow inactivation, requires a far longer period of membrane depolarization to induce, and recovery from slow inactivation may take on the order of seconds or minutes. Slow inactivation is thought to reflect conformational changes to the external portion of the alpha subunit pore (Ulbricht, 2005).

Sodium channel fast inactivation is modulated by alpha subunit interaction with a family of cytoplasmic proteins termed fibroblast growth factor homologous factors (FHFs) (Smallwood *et al.*, 1996; Hartung *et al.*, 1997; Wang *et al.*, 2000; Goldfarb, 2005). Several FHFs have been shown to delay channel inactivation by raising the voltage at which inactivation occurs (Liu *et al.*, 2003; Wittmack *et al.*, 2004; Lou *et al.*, 2005; Rush *et al.*, 2006; Goldfarb *et al.*, 2007). FHF modulation of sodium channel fast inactivation enhances the excitability of cerebellar granule and Purkinje neurons, lowering the voltage threshold for action potential onset and allowing for

repetitive firing upon depolarizing current injection (Goldfarb *et al.*, 2007; Shakkottai *et al.*, 2009).

Two FHFs, FHF2A and FHF4A, have also been shown to induce a distinct mode of long-term inactivation of $Na_v1.6$ (Rush *et al.*, 2006; Laezza *et al.*, 2009). In this paper, we report that all A-type FHFs exert rapid onset long-term inactivation on $Na_v1.6$ and other sodium channels. A-type FHFs accomplish long-term inactivation by providing an independent, N-terminally situated cytoplasmic gating particle that competes with the channel's intrinsic inactivation particle for blockade of the channel upon membrane depolarization. We further show that injection of a synthetic peptide corresponding to the A-type FHF particle reproduces long-term sodium channel inactivation and concomitantly acts to oppose sustained firing of excitable cells.

Methods

Plasmids. Murine $Na_v1.6$ cDNA was amplified in segments by reverse transcription-PCR from mouse brain RNA and cloned into bicistronic vector pIRESneo3 (Clontech). The cDNA insert was sequenced in entirety, and the plasmid-bearing E. coli was cultured at 25°C with 50 μg/ml ampicillin to avoid selection for deletions in the plasmid. Point mutations were introduced using complementary mutagenic primers and PfuTurbo DNA polymerase (Stratagene). TTX resistance was introduced by Y371S substitution, as shown previously (Rush *et al.*, 2006). Further substitutions into $Na_v1.6^{TTXr}$ included F1478Q in the DIII/DIV inactivation loop (West *et al.*, 1992; Eaholtz *et al.*, 1994; Caterall, 2000) or A1317Q in the loop's docking site (Smith & Goldin, 1997). All FHF cDNAs were cloned into bicistronic vector pIRES2-ZsGreen1 (Clontech) to enable expression of untagged FHFs along with fluorescent protein. FHF2A

mutations I5A, LL/IA (L9A/I10A), 5Q (K13Q/R14Q/R17Q/R19Q/K21Q), and 7Q (K55Q/K56Q/R57Q/R58Q/R59Q/R60Q/R61Q) were generated using complementary mutagenic primers. The 8xMT octamutant version of FHF2A cDNA (Goetz *et al.*, 2009) was shuttled into pIRES2-ZsGreen1. Human $Na_v1.5$ cDNA in the pCDNA3.1 expression vector was the generous gift of R. Kass.

Cells. Neuro2A (N2A) cells and the sodium channels they express were described elsewhere (Lou *et al.*, 2005). N2A cells were transfected with $pNa_v1.6^{TTX^r}$-IRESneo3 by the calcium phosphate method, selected with 1.4 mg/ml G418, and colonies maintained in 1 mg/ml G418 and screened electrophysiologically in the presence of TTX (see below) to obtain cells stably expressing $Na_v1.6^{TTX^r}$. Cerebellar granule neurons were prepared from P9 mouse pups and cultured for 16 days, as previously described (Goldfarb *et al.*, 2007), with the procedure modified to include 5 ng/ml brain-derived neurotrophic factor (BDNF) in the culture medium. As predicted from earlier studies (Courtney *et al.*, 1997; Tucker & Fadool, 2002), BDNF enhanced viability and expression of potassium channels, allowing the neurons to generate action potentials with strong afterhyperpolarizations necessary for repetitive firing. Mice used for preparation of neuronal cultures were housed and treated in compliance with Hunter College's Institutional Animal Care and Use Committee (IACUC).

Peptides. Peptides were custom synthesized and purified commercially (Invitrogen Corp.). All peptides were N-terminally acetylated and corresponded to FHF2A residues 2-21, 2-12, and 11-21, purified by HPLC, and identity confirmed by mass spectroscopy.

Antibodies. An N-terminally acetylated synthetic peptide corresponding to FHF2A residues 2-21 with additional GlyGlyCys at C-terminus was directionally coupled via the sulfhydryl group to carrier and used as immunogen in rabbits. Antisera were precleared of antibodies against the

coupling moiety by taking flow-through from affinity column bearing an unrelated peptide, and specific antibodies were then purified on agarose bearing the coupled immunizing peptide. Rabbit antibodies against the C-termini of either FHF2 or FHF1 were described previously (Schoorlemmer & Goldfarb, 2001; Wittmack *et al.*, 2004).

Transient DNA transfections. FHF bicistronic vectors were transiently expressed in N2A or N2A- $Na_v1.6^{TTXr}$ cells. Semiconfluent cultures on 12-multiwell dishes were treated with a mixture of 2 μl Lipofectamine 2000 (Invitrogen) and 3 μg plasmid in 0.8 ml medium for 4 hrs, then refed with fresh medium. For immunoblotting experiments, cells were maintained another two days before lysate preparation. For electrophysiology, cells were trypsinized, plated at lower density onto polylysine-coated borosilicate coverslips, and maintained for two to three days, and green fluorescent cells were selected for recordings. For electrophysiological analyses of $Na_v1.5$ and mutant forms of $Na_v1.6^{TTXr}$, N2A cells were cotransfected with 2.5 μg channel-expressing plasmid and 0.5 μg pIRES-ZsGreen plasmid with or without FHF cDNA inserts.

Immunoblotting. Immunoblotting was used to compare expression levels for different FHF vectors. Culture layers were directly lysed in cracking buffer (6M urea – 2% SDS – 125 mM Tris pH 7 – bromophenol blue) and equal portions of lysates from parallel transfected wells were electrophoresed through 12% polyacrylamide SDS gels. After transfer to PVDF membranes and blocking in 5% dehydrated milk, blots were incubated overnight with antibodies (0.5 μg/ml) and subsequently with peroxidase-conjugated anti-rabbit IgG secondary antibodies, and detection performed by enhanced chemiluminescence. This analysis demonstrated that all FHF2 expression vectors gave comparable levels of expression (Fig. 3D), and that both FHF1A and FHF1B vectors gave comparable expression (Supplemental Fig. 1). Following immunoblot

detection with antibodies against FHF2 C-terminus, antibodies were stripped using guanidine-containing solution at 50^{o}C, and the filter was reblocked and probed with rabbit antibodies against the N-terminus of FHF2A.

Electrophysiological analysis of sodium channels in Neuro2A cells

General setup and methods. All recordings were performed on cells grown on coverslips. For analysis of sodium currents in transiently transfected N2A and derivative cell lines, the recording chamber was filled with carbogen-bubbled extracellular solution: 120 mM NaCl – 26 mM $NaHCO_3$ – 3 mM KCl – 10 mM glucose – 4 mM $MgCl_2$ – 2 mM $CaCl_2$ – 0.2 mM $CdCl_2$ – 3 mM myoinositol – 2 mM Na pyruvate (pH 7.2). For analyses on $Na_v1.5$ and $Na_v1.6^{TTX^r}$, 1 mM TTX was added to fully block currents from endogenous sodium channels (Supplemental Fig. 2). The intracellular pipette solution for recording sodium currents contained 104 mM CsF – 50 mM tetraethylamine chloride – 10 mM HEPES pH 7.2 – 5 mM glucose – 2 mM $MgCl_2$ – 10 mM EGTA – 2 mM ATP – 0.2 mM GTP, with pipettes pulled to give electrical resistance of 1-2 MΩ. In some experiments, pipette solution was supplemented with peptides or antibodies. Voltage and current commands and recordings utilized an Axopatch 200B amplifier, Digidata 1322 digital/analog interface, and pCLAMP9 software (Molecular Devices Inc.). After obtaining a pipette/cell seal of >5GΩ on green fluorescent cells, whole cell access was obtained by brief gentle suction. Recordings were initiated at least five minutes after break-in to allow cellular dialysis and dissipation of junctional potential between pipette and cytoplasm. In N2A cells, recordings with peptides in pipettes were initiated at least ten minutes after break-in, while recordings with antibodies in pipettes were generally initiated at least 30 minutes after break-in to allow for macromolecule diffusion into cells. Signals were filtered at 5 kHz and digitized at

10 or 20 kHz. Passive properties of recorded cells (membrane capacitance, leak resistance, and series/access resistance) were calculated from current responses to a voltage-clamped step depolarization from –90 mV to –80 mV (see Suppl. Table 6). For measurements of evoked sodium currents, electrotonic capacitative and leak currents in voltage clamp pCLAMP protocols were subtracted during data acquisition using the pre-sweep hyperpolarizing P/N method in the software; series resistance (3.5 +/- 0.9 MΩ) was not compensated. For each accessed cell, a full set of command/record protocols (see below) were attempted, although loss of access sometimes occurred prior to set completion.

2-pulse protocol for sodium channel recovery. For $Na_v1.6^{TTX^r}$, mutant derivatives, and N2A endogenous channels, the 40-sweep protocol used –90 mV holding command preceding two 16 msec 0 mV pulses separated by a variable length –90 mV interpulse recovery phase (0.5-20 msec). For $Na_v1.5$, the interpulse and holding command voltages used was –130 mV and depolarization pulses were to –30 mV. Fraction channels recovered for each sweep equaled $I_{Na\text{-}peak}(2)/ I_{Na\text{-}peak}(1)$.

4-pulse protocol for accumulation of sodium channel long-term inactivation. For $Na_v1.6^{TTX^r}$, mutant derivatives, and N2A endogenous channels, the 8-sweep protocol used –90 mV holding command, four 0 mV pulses of varying duration (2-16 msec), and 40 msec –90 mV interpulse recovery phases. For $Na_v1.5$, the interpulse and holding command voltages used was –130 mV and depolarization pulses were to –30 mV. Fraction of channels recovered 40 msec after n depolarization cycle equaled $I_{Na\text{-}peak}(n+1)/ I_{Na\text{-}peak}(1)$.

Recovery from long-term inactivation. For $Na_v1.6^{TTXr}$ and mutant derivatives, the 20-sweep protocol used –90 mV hold, three 10 msec 0 mV pulses with 20 msec interpulse recoveries, followed by a variable –90 mV recovery phase of 20 + 100(n-1) msec and a final 0 mV pulse. In each of the n sweeps, the first three pulses allowed for accumulation into long-term inactivation, and channel recovery calculated as $I_{Na\text{-}peak}(4)/ I_{Na\text{-}peak}(1)$; sweep 1 recovery time was defined as t=0, thereby filtering out most fast-recovering channels. Values for recovered channels in all sweeps were then fitted to the exponential recovery equation: $\text{Recovered}(t) = 1 - A_{fast}(e^{-t/Tau_{fast}}) - A_{slow}(e^{-t/Tau_{slow}}) - C$. At least 70% of total sodium conductance was associated with slow recovering channels.

For $Na_v1.5$, several 2-pulse depolarization protocols were run with variable –130 mV recovery phases spanning from 1-400 msec. Percent recovered channels for all time points were fitted to equation: $\text{Recovered}(t) = 1 - A_{fast}(e^{-t/Tau_{fast}}) - A_{slow}(e^{-t/Tau_{slow}}) - C$. In presence of FHF2A or F2A(2-21) peptide, 15-20% of channels displayed slow recovery.

Voltage dependence of channel steady-state inactivation. The 21-sweep protocol used –110 mV holding command, a 60 msec variable test voltage step [-110 + 5(n-1) mV], followed by a 0 mV pulse. For each of n sweeps, peak sodium current accompanying the 0 mV pulse was measured, and the fraction of channels available (not inactivated) at test voltage equaled $I_{Na\text{-}peak}(V_{test})/ I_{Na\text{-}peak}(-110mV)$. To obtain $V_{1/2}$ and k values for inactivation, data were fitted to Boltzmann equation: $f(V_{test}) = [1 + e^{(V_{1/2} - V_{test})/k}]^{-1} + C$.

Voltage dependence of channel long-term inactivation. The 19-sweep protocol used –90 mV holding command, a 16 msec variable test voltage [-90 + 5(n-1) mV] step, a 40 msec –90 mV recovery phase, followed by a 0 mV pulse. For each of n sweeps, peak sodium current accompanying the 0 mV pulse was measured, and the fraction of channels available (not long-term inactivated) at test voltage equaled $I_{Na\text{-}peak}(V_{test})/ I_{Na\text{-}peak}(-90mV)$. Data were fitted to Boltzmann equation shown above.

Voltage dependent inhibition of channel long-term inactivation. The protocol assays for the ability of a variable test voltage to prevent subsequent 0 mV depolarization from inducing $Na_v1.6$ long-term inactivation. The 19-sweep protocol used –90 mV holding command, a 60 msec variable test voltage [-90 + 5(n-1) mV] step, a 16 msec 0 mV step, a 40 msec –90 mV recovery phase, followed by a second 0 mV pulse.

Voltage dependence of channel activation. The 17-sweep protocol used –90 mV holding command and a 30 msec variable test voltage [-60 + 5(n-1) mV], and the peak sodium current induced by each test voltage measured. $I_{Na\text{-}peak}$ was plotted against test voltage, and maximum sodium conductance computed from the ohmic linear portion of the plot (-5 to 20 mV). The fraction of activated channels at different test voltages was fitted to the Boltzmann equation shown above.

Electrophysiological analysis of cultured cerebellar granule neurons. For analysis of activated currents and excitability of cerebellar granule neurons, cells were placed in carbogen-bubbled physiological extracellular solution (120 mM NaCl – 26 mM $NaHCO_3$ – 3 mM KCl – 1.2 mM KH_2PO_4 – 3 mM glucose – 3 mM myoinositol – 2 mM Na pyruvate – 2 mM $CaCl_2$ – 1.2 mM $MgSO_4$) and accessed with patch pipettes filled with 126 mM K gluconate – 4 mM NaCl – 5

mM HEPES – 15 mM glucose – 1 mM 1.2 mM $MgSO_4$ – 3 mM ATP – 0.1 mM GTP – 0.15 mM BAPTA – 0.05 mM $CaCl_2$ (buffered with KOH to pH 7.2) and pulled to have electrical resistance of 10-12 MΩ, as previously described (Goldfarb *et al.*, 2007). Pipette solution was sometimes supplemented with F2A(2-21) peptide. Small diameter neurons that predominate the cultures were whole cell patched, and their identity as mature granule cells confirmed by small membrane capacitance (3-6 pF), high input resistance (~1 GΩ) and large inward (sodium) and outward (potassium) currents (>800 pA each). Passive properties of recorded cells (membrane capacitance, leak resistance, and series/access resistance) were calculated from current responses to a voltage-clamped step from –60 mV to –70 mV (see Suppl. Table 6). Each neuron was then voltage-clamped at –90 mV, and subjected to four 16 msec depolarizations at 0 mV separated by 40 msec recovery phases at –90 mV in order to record magnitude of induced currents and potential accumulation of long-term inactivation. The neuron was then switched to current clamp, sufficient current was manually injected to adjust membrane holding potential to –80 mV, and the cell subjected to a multisweep protocol with 800 msec current injections of variable magnitude. Injected current was varied among sweeps from below spiking threshold to above maximal spiking frequency in order to determine the maximum spike frequency of the neuron. Commanded and recorded voltages were adjusted by –10 mV to offset error caused by pipette/bath liquid junctional potential (Goldfarb *et al.*, 2007).

Statistical analysis of electrophysiological data. Parameter values recorded from a cohort of comparable cells were expressed as mean +/- standard deviation. Significance of differences in parameter values between cohorts was tested by 2-tailed unpaired Student t test.

Computer modeling of sodium channel long-term inactivation. Model building and simulations were conducted on the NEURON software platform. A new 16-state sodium channel Markov model is shown in Figure 6B. This model is a revision of the 13-state model of Raman and Bean (Raman & Bean, 2001), which accommodates closed states C1 to C5, open state O, fast inactivation states I1 to I6, and open-blocked state OB responsible for resurgent current. The new model deletes state OB (since channels in N2A cells lack resurgent current) and adds long-term inactivation states L3 to L6 (L1 and L2 are omitted, as they are predicted to have virtually zero percent occupancy at any voltage or time). To model a sodium channel subject to long-term inactivation (comparable to association with FHF2A), kinetic parameters were set as follows: α = 353.91*exp(v/13.99) mV/ms; β = 1.272*exp(-v/13.99) mV/ms; n_1 = 5.422; n_2 = 3.279; n_3 = 1.83; n_4 = 0.738; γ = 150 ms^{-1}; δ = 40 ms^{-1}; C_{on} = 0.025 ms^{-1}; O_{on} = 0.75 ms^{-1}; a = $(O_{on} / C_{on})^{0.25}$; C_{off} = 0.5 ms^{-1}; O_{off} = 0.002 ms^{-1}; b = $(O_{off} / C_{off})^{0.25}$; L_{on} = 0.001 ms^{-1}; L_{off} = 0.15 ms^{-1}; c = 20; d = 0.075. Of particular importance in setting parameter values, rate of transition from open (O) to long-term inactivated (L6) state ($L_{on}*c^2$ = 0.4 ms^{-1}) was set to approximately half the rate of transition from O to fast-inactivated state I6 (O_{on} = 0.75 ms^{-1}), thereby driving one-third of channels into long-term inactivation following steep depolarization. This revised sodium channel model will be publicly available at ModelDB (http://senselab.med.yale.edu/modeldb). For neuronal excitability simulations, the previously described multicompartment model of the cerebellar granule cell (Diwakar *et al.*, 2009) was modified by concentrating sodium channels into the hillock and axon initial segment, consistent with immunofluorescence data (Diwakar *et al.*, 2009). Modeled sodium channels in the wild-

type cell lack long-term inactivation (L_{on} = 0), while F2A(2-21) peptide injection was simulated by enabling long-term inactivation (L_{on} = 0.001 ms^{-1}). Somatic membrane voltage was monitored during simulation of 12 pA current injection for 200 msec. These granule cell simulations also added back the resurgent sodium current component generated by O $\leftrightarrow$ OB, with $k_{(O \rightarrow OB)}$ = 1.75 ms^{-1} and $k_{(OB \rightarrow O)}$ = 0.0201*exp(-v/25)mV/ms, as previously described (Diwakar *et al.*, 2009).

Results

A-type FHFs induce long-term inactivation of several sodium channels

FHF modulation of sodium channel physiology was studied by whole cell voltage clamp in Neuro2A (N2A) cells stably expressing an engineered tetrodotoxin (TTX)-resistant variant of $Na_v1.6$ (Rush *et al.*, 2006) and transiently transfected with a bicstronic vector to express both a specific FHF and green fluorescent protein. The use of a common cell line to study all FHFs allowed for reliable functional comparisons across the FHF family, and the bicistronic vector obviated the need for FHF protein modifications that could potentially affect channel modulation. A two-pulse depolarization protocol was used to monitor the recovery of channels from inactivation in fluorescent cells. In the absence of FHF, virtually all channels recovered from fast inactivation within 20 msec (Fig. 1A), whereas FHF2A drove approximately one-third of the channels into a longer-term inactivation state (Fig. 1B). Repetitive 16 msec depolarization cycles separated by 40 msec recovery periods resulted in accumulation of channels in the long-term inactivated state (Fig. 1C and Table 1). Such long-term inactivated channels exhibited slow recovery with time constants of 371 msec at –90 mV and 153 msec at –110 mV (Fig. 1D and Table 1).

FHFs are encoded by four genes, each giving rise to multiple isoforms differing in their N-terminal sequences through alternative promoter usage and splicing (Goldfarb, 2005). Among six FHFs (1A, 1B, 2A, 2B, 4A, 4B) assayed for modulation of $Na_v1.6$, only the three A-type FHFs induced accumulating long-term inactivation (Fig. 1E and Table 1). The observed variability in the accumulation of long-term inactivation induced by A-type FHFs may be explained in part by different rates of recovery (Table 1). All FHFs were also tested for modulation of voltage-dependent steady-state inactivation of $Na_v1.6$. FHF1A, FHF2A, FHF4A,

and FHF4B each induced 13-16 mV depolarizing shifts in the $V_{1/2}$ of inactivation (Fig. 1F and Table 1), while FHF2B induced a lesser shift and FHF1B had no demonstrable effect. These data show that induction of long-term inactivation and shift in steady-state inactivation are not tightly correlated across the spectrum of tested FHFs.

The ability of A-type FHFs to induce long-term inactivation extends to other sodium channels in addition to $Na_v1.6$. N2A cells were transiently transfected with expression vectors for the cardiac channel $Na_v1.5$ (naturally TTX-resistant) and a GFP expression vector with or without FHF2A. In the presence of FHF2A, $Na_v1.5$ channels in fluorescent cells assayed in presence of TTX experienced accumulating long-term inactivation (Suppl. Table 1). Additional assays were conducted in the absence of TTX to analyze the behavior of endogenous sodium channels in N2A cells, which express $Na_v1.1$, $Na_v1.2$, $Na_v1.3$, and $Na_v1.7$, but not $Na_v1.6$. (Lou *et al.*, 2005). Both FHF1A and FHF2A induced robust accumulating long-term inactivation of this endogenous mixture of channels as well (Suppl. Table 1).

FHF-induced long-term inactivation and intrinsic fast inactivation are mutually exclusive channel states

Several lines of experiments described here defined long-term inactivation as an FHF-induced channel state distinct from fast inactivation. To determine the voltage dependence of long-term inactivation, cells expressing $Na_v1.6$ and FHF2A were clamped at different test voltages for 16 msec, returned to –90 mV for 40 msec to allow for fast channel recovery, and depolarized to 0 mV to assess available channels. $V_{1/2}$ for long-term channel inactivation (-46.7 mV) was far more positive than $V_{1/2}$ for steady-state inactivation (-66.3 mV), though still

negative to $V_{1/2}$ for activation (-39.1 mV) (Fig. 2A and Table 1). This result suggested that at more negative voltages, most steady-state inactivation would represent fast inactivation. To test this prediction, the recovery of $Na_v1.6$ from inactivation in a representative cell expressing FHF2A was monitored after depolarization to either 0 mV or –55 mV. While approximately one-third of channels depolarized to 0 mV had undergone long-term inactivation, ninety percent of channels recovered rapidly following inactivation at –55 mV (Fig. 2B). In another experiment, the time dependence for onset of long-term inactivation was assessed by varying the duration of each depolarization cycle through the range of 2-16 msec. The degree of long-term inactivation was found to be near maximal after only 2 msec depolarization per cycle (Fig. 2C). Accumulation of channels into long-term inactivation was more determined by the number of depolarization cycles than by the duration of depolarization.

The above data showed that FHF2A-dependent long-term inactivation occurs only at greater voltage-driven channel transitions than are needed for fast inactivation, and further showed that the fraction of channels driven into long-term inactivation is restricted by a rapid process. A series of experiments were conducted to further test the hypothesis that fast inactivation blocks channel entry into the long-term inactivated state. First, $Na_v1.6$ channels were preferentially driven into fast inactivation and tested for whether they were protected against long-term inactivation upon subsequent steep depolarization. As shown in the inset of Fig. 2D, cells expressing $Na_v1.6$ and FHF2A were clamped to variable test voltages for 60 msec, followed by two 16 msec depolarizations to 0 mV separated by a 40 msec recovery period at –90 mV. The current induced in the first 0 mV depolarization reported degree of steady state inactivation, while the second 0 mV depolarization reported degree of long-term inactivation (Fig. 2D). Test voltages in the range of –50 to –60 mV, which drove 60-90% of the channels

into steady state inactivation, also partially protected against subsequent 0 mV-induced long-term inactivation (Fig. 2D). We suspect that the inability to fully block long-term inactivation with this protocol reflects some overlap in the voltage ranges of Boltzmann curves for voltage dependence of fast and long-term inactivation (Fig. 2A), thereby preventing selection of a test voltage that exclusively and efficiently induces fast inactivation. More depolarizing test voltages (-40 to –45 mV) failed to inhibit long-term inactivation (Fig. 2D), as these voltages were themselves capable of inducing the long-term inactivated state (Fig. 2A).

In a second experiment, long-term inactivation was assayed in mutant channels with impaired fast inactivation. For several sodium channel isoforms, a phenylalanine residue in the so-called IFM particle within the DIII/DIV cytoplasmic loop is essential for fast inactivation (West *et al.*, 1992). The corresponding F1478Q substitution engineered into $Na_v1.6^{TTX^r}$ successfully suppressed channel fast inactivation at any test voltage in transfected N2A cells (Fig. 2E). In the presence of FHF2A, inactivation of $Na_v1.6_{(F1478Q)}$ was restored, with most channels driven into long-term inactivation by a single 16 msec depolarization cycle (Fig. 2F,G and Suppl. Table 2). FHF1A could also induce robust long-term inactivation of $Na_v1.6_{(F1478Q)}$ (Fig. 2G, Suppl. Table 2). Because $Na_v1.6_{(F1478Q)}$ is defective for fast inactivation, the voltage dependence of FHF2A-induced $Na_v1.6_{(F1478Q)}$ steady state inactivation was depolarized near to the value of $V_{1/2}$ for long-term inactivation (Suppl. Table 2).

As an alternative to disruption of the IFM particle, a mutation was engineered in the docking site within the channel pore for this particle. As predicted from prior studies on $Na_v1.2$ (Smith & Goldin, 1997), the corresponding A1317Q mutation in $Na_v1.6^{TTX^r}$ rendered fast

inactivation leaky, yielding far greater persistent current attributable to unstable docking of the IFM particle (Fig. 2H inset). Whereas 2 msec depolarization cycles induced FHF2A-dependent $Nav1.6_{(A1317Q)}$ of magnitude similar to wild-type channel (Fig. 2D and 2H), the extent of $Nav1.6_{(A1317Q)}$ long-term inactivation increased substantially as the duration of depolarization cycles were lengthened (Fig. 2H). This finding suggests that fast-inactivated $Nav1.6_{(A1317Q)}$ channels remained sensitive to long-term inactivation in an ongoing manner as its weakly bound IFM particle dissociated.

The above experiments demonstrate that sodium channel fast inactivation and long-term inactivation are distinct channel states, and that channel fast inactivation inhibits entry into long-term inactivation.

Long-term inactivation requires FHF2A channel-binding and N-terminal cytoplasmic effector domains

To better understand the molecular mechanism of sodium channel long-term inactivation, mutant versions of FHF2A were tested for their ability to modulate $Na_v1.6$. The 62-66 residue N-terminal extensions of FHF1A, 2A, and 4A share substantial sequence similarity, including 94% identity for residues 1-18 and a cluster of basic residues close to the FHF core (Fig. 3A). FHF2A variants bearing mutations in the N-terminal regions or in core residues known to be necessary for association with channel carboxy-terminal tails (Goetz *et al.*, 2009) were assayed for their ability to induce $Na_v1.6$ long-term inactivation. While mutation of seven consecutive core-proximal basic residues to glutamines (7Q mutant) (Fig. 3A) did not interfere with induction of long-term inactivation, mutations near the N-terminus had significant effects (Fig.

3B). FHF2A mutants bearing five lysine/arginine-to-glutamine substitutions between residues 13-21 (5Q mutant) or bearing two alanine substitutions at leucine-9 and isoleucine-10 (LI/AA mutant) (Fig. 3A) were defective for induction of long-term inactivation (Fig. 3B, Suppl. Table 3), while their ability to induce a depolarizing shift in $V_{1/2}$ steady-state (fast) inactivation remained intact (Fig. 3C, Suppl. Table 3). FHF2A(I5A) (Fig. 3B) retained competence to induce long-term inactivation, albeit to a somewhat reduced extent and with a faster rate of recovery (Fig. 3C, Suppl. Table 3). The core octamutant version of FHF2A(8xMT) (Goetz *et al.*, 2009) was incapable of modulating fast inactivation or of inducing long-term inactivation (Fig. 3B, Suppl. Table 3). This survey demonstrated that long-term inactivation requires the channel-tethering domain in the FHF core and an N-terminal effector domain.

If the N-terminal effector region of channel-bound FHF2A is freely exposed to the cytoplasm, an antibody to the effector epitope would be predicted to block long-term inactivation without blocking FHF modulation of fast inactivation. An N-terminal acetylated peptide corresponding to residues 2-21 of FHF2A was used as immunogen to raise polyclonal antibodies, and the specificity of the affinity-purified antibodies was tested by immunoblotting. Whereas previously described antibodies against the FHF2 C-terminus (Wittmack *et al.*, 2004) recognize FHF2B, FHF2A, and all FHF2A mutant proteins (Fig. 3D, top panel), the FHF2A N-terminal antibodies only recognized FHF2A and its 5Q, 7Q, and 8xMT derivatives efficiently and detected FHF2A mutants I5A and LI/AA poorly (Fig. 3D, lower panel). These N-terminal antibodies were delivered into cells expressing $Na_V1.6$ and FHF2A by diffusion from the patch pipette. Shortly after attaining whole cell access, sodium channels could still undergo long-term inactivation (Fig. 3E, left panel). After a 30 min period to allow diffusion of antibody into cells, long-term inactivation was virtually abolished (Fig. 3E, right panel and Suppl. Table 3). FHF2A

antibody perfusion did not affect the depolarizing shift in steady-state fast inactivation induced by FHF2A (Suppl. Table 3), demonstrating the specificity of the antibody's effect. As a further test of specificity, long-term inactivation induced by FHF2A(I5A) was not strongly inhibited by antibody, reflecting poorer recognition of the mutant FHF by the antibodies (Fig. 3D and Suppl. Table 3).

FHF2A residues 2-21 constitute a long-term inactivation particle

Long-term inactivation of sodium channels requires tethering and effector domains of FHF2A. We considered the possibility that the N-terminal effector region of an A-type FHF in the form of a synthetic peptide may be sufficient to induce long-term inactivation. We also speculated that the requirement for channel tethering could be obviated by high peptide concentration. Peptides were synthesized corresponding to residues 2-12, 11-21, or 2-21 of FHF2A. Peptides were N-terminally acetylated and Met-1 was omitted due to predicted posttranslational cleavage of FHF2A's N-terminal methionine in vivo (Frottin *et al.*, 2006). When 1 mM F2A(2-21) peptide was added to patch pipettes for diffusion-driven delivery into cells, long-term inactivation of $Na_v1.6$ was evident within five minutes of cell break-in (Fig. 4A and Table 1).

By several criteria, the properties of long-term inactivation induced by pipette injection were very similar to those induced by expression of full-length FHF2A protein. In presence of peptide, channels displayed a $V_{1/2}$ = - 42.7 mV for long-term inactivation, accumulated into the long-term inactivated state following multiple cycles of depolarization, and recovered from long-term inactivation with a time constant of 323 msec at –90 mV (Fig. 4B and Table 1). Additionally, this peptide could drive most inactivation-defective $Na_v1.6_{(F1478Q)}$ channels into long-term inactivation with a single 16 msec depolarization cycle (Figs. 2G, 4C and Suppl. Table

2), analogous to full-length FHF2A. F2A(2-21) peptide acted in a dose-dependent manner, and the shorter peptides lacking either the basic residue cluster or the hydrophobic N-terminus lacked significant activity at 1 mM concentrations (Fig. 4D and Suppl. Table 4). Together with the FHF mutagenesis data (Fig. 3B), these findings show that the N-terminal region of FHF2A is a necessary and sufficient long-term channel inactivation gating particle. Additionally, F2A(2-21) peptide did not shift the voltage dependence of steady-state fast inactivation (Fig. 1F and Table 1), consistent with FHF2A mutagenesis data showing that the N-terminal region is not required for modulation of fast inactivation (Fig. 3C).

F2A(2-21) peptide was also tested for its ability to induce long-term inactivation of cardiac channel $Na_v1.5$. Indeed, at 1mM concentration, the peptide induced accumulating long-term inactivation of $Na_v1.5$ to an extent indistinguishable from that driven by expression of FHF2A protein (Fig. 4E and Suppl. Table 1).

F2A(2-21) peptide-mediated long-term inactivation of sodium channels blocks repetitive neuronal firing

Sustained high-frequency neuronal firing requires efficient fast recovery of sodium channels from inactivation. For example, cerebellar granule neurons cultured for 16 days undergo reproducible inactivating inward sodium current and noninactivating outward potassium current upon repeated voltage clamped cycles of 0 mV depolarization (Fig. 5A and Suppl. Table 5). Rapid recovery enables granule neurons to fire continuously when depolarized under current clamp (Fig. 5B and Suppl. Table 5). When 0.5 mM F2A(2-21) peptide was included in a patch pipette, inward transient currents decreased upon repeated depolarization cycles, while outward currents were unaffected (Fig. 5C and Suppl. Table 5), reflecting sodium channel long-term

inactivation. Concomitantly, the peptide-injected cell could not undergo sustained firing at any amplitude of injected current (Fig. 5D and Suppl. Table 5). Peptide injection did not alter the first inward transient current nor the voltage peak amplitude of the first induced action potential (Fig. 5C, D and Suppl. Table 5). A cohort of granule neurons were recorded using pipettes filled with 0, 0.05, 0.1, or 0.5 mM F2A(2-21) peptide, and all neurons were characterized for accumulating loss of inward sodium current and for maximal spike generation. Sodium currents were inhibited in a dose-dependent manner, and there was a strong correlation between sodium channel long-term inactivation and reduction in spike frequency (Fig. 5E and Suppl. Table 5).

A revised transition state model for sodium channels

The empirical data presented in this paper suggests an expanded transition state model for voltage-gated sodium channels (Fig. 6A, B). By analogy to the transitions documented for voltage-gated potassium channels (Long *et al.*, 2005; Pathak *et al.*, 2007), rising voltage allows for widening of the sodium channel's cytoplasmic face, reaching a final conducting open conformation (Fig. 6A). Lesser transitions attained at more negative potentials render the channel competent for inactivation, even without channel opening. The intrinsic fast inactivation particle in the DIII/DIV loop can gain access to the channel pore's cytoplasmic face at more negative potential than can the FHF-associated long-term inactivation particle, and docking of the fast-inactivation particle blocks access of the FHF particle (Fig. 6A). The model reflects several empirical observations: (1) greater depolarization is required to achieve long-term inactivation than is needed for fast inactivation (Fig. 2A,B), (2) somewhat greater depolarization is needed to achieve channel opening than is required for long-term inactivation (Fig. 2A), suggesting potential entrance into long-term inactivation from a closed state as well as the open

state (Fig. 6A), (3) fast inactivation blocks entrance into long-term inactivation (Fig. 2C-H), and (4) long-term inactivation is mediated by an A-type FHF N-terminal particle that is positioned near the channel by FHF core domain interaction with the channel C-terminal tail (Figs. 3, 4). The schematic in Fig. 6A presents one potential model for particle competition, in which the FHF particle binding site lies deep within the cytoplasmic face of the pore and is occluded by fast inactivation. Alternatively, the FHF particle may bind to a regulatory site lying outside the pore that is allosterically obscured by prior fast inactivation.

Independent of precise knowledge of the underlying structural mechanism, the kinetics of FHF-induced sodium channel inactivation can be modeled computationally. The previously described 12-state fast kinetic model for sodium channels posited a series of voltage-dependent rates for transitions through closed states C1 through C5, a final voltage-independent equilibrium between C5 and open state (O), and voltage-independent rate constants for transitions between C1-C5 and O to fast-inactivated states I1 through I6, respectively (Fig. 6B) (Raman & Bean, 2001). Long-term inactivation can be modeled as alternative, mutually exclusive voltage-independent transitions from C3-C5 and O to states L3-L6, respectively, in which the FHF inactivation particle has blocked conduction (Fig. 6B). Appropriate selection of rate constants for state transitions into this 16-state model (see Methods) yields voltage-clamp simulations that approximate the recorded behavior of $Na_v1.6$ in the presence of FHF2A (Fig. 6 C, D). In a simulated 10 msec depolarization to 0 mV, most channels briefly opened followed by entry of approximately one-third of channels into long-term inactivated states L5 and L6, with the remaining channels undergoing fast inactivation (I states). Upon repolarization, the fast-inactivated states I5 and I6 rapidly recovered, while those in L5 and L6 recovered with a time constant on the order of 400 msec (Fig. 6C). Simulations to assay voltage dependence of steady-

state inactivation, long-term inactivation, and activation yielded a $V_{1/2}$ long-term inactivation substantially higher than $V_{1/2}$ for steady-state (fast) inactivation (Fig. 6D), in good accord with the recorded data (Fig. 2A and Table 1).

We modified a previously described computer model of the cerebellar granule cell (D'Angelo *et al.*, 2001; Diwakar *et al.*, 2009) by incorporating sodium channel long-term inactivation states into the model. In a current injection simulation of the granule cell lacking A-type FHF peptide (i.e., transition rates to L states = 0), the neuron could fire continuously at high frequency (Fig. 6E). By contrast, upon modeling the neuron in the presence of A-type FHF peptide, current injection induced a few spikes of declining amplitude followed by failure (Fig. 6F), comparable to our empirical recordings (Fig. 5D,E). The ability of long-term sodium channel inactivation to impair repetitive firing in the model provides evidence that experimental peptide injection into cultured granule cells restricts neuronal excitability specifically through its action of sodium channels.

Discussion

A-type FHFs associate with voltage-gated sodium channels and provide a long-term use-dependent inactivation particle. The FHF-particle can only function at substantial voltage-dependent channel transitions approaching the open state, with ensuing competition between FHF and the channel-intrinsic particles dictating the fraction of channels driven into long-term inactivation. Although the competing particles exert different effects on a sodium channel, they possess curious similarities. Each particle bears and relies upon a cluster of hydrophobic residues flanked by an adjacent cluster of basic residues (West *et al.*, 1992; Eaholtz *et al.*, 1999) (and Figs. 3, 4). While the channel fast inactivation particle is ~8 residues in length, the larger FHF particle (~20 residues) may provide a greater surface for channel interaction underlying this particle's greater stability upon binding.

Several lines of evidence have shown that the fast inactivation particle and the A-type FHF long-term inactivation particle compete for inactivation of sodium channels: (1) Whereas some channels rapidly enter long-term inactivation upon steep depolarization, further entry is inhibited coincident with onset of fast inactivation, (2) weaker depolarization to voltages that favor fast inactivation reduce entry into long-term inactivation upon subsequent further depolarization, (3) by contrast, $Nav1.6_{(A1317Q)}$ channels with leaky fast inactivation continue to accumulate into long-term inactivation during a depolarization phase, and (4) almost all fast-inactivation-defective $Nav1.6_{(F1478Q)}$ channels rapidly enter long-term inactivation in a single depolarization cycle. Competition between inactivation particles may reflect FHF long-term inactivation particle binding deep within the widening channel pore, so as to be inhibited by prior binding of the intrinsic fast inactivation particle (Fig. 6A). Alternatively, fast particle docking may prevent conformational changes that expose an FHF particle's docking site elsewhere on the

channel's cytoplasmic face. Indeed, fast inactivation particle docking has been shown to inhibit conformational changes associated with slow inactivation (Featherstone *et al.*, 1996; Alekov *et al.*, 2001). A related issue is whether FHF-induced long-term inactivation proceeds through a unique structural mechanism or by dramatically accelerating a slow inactivation-type structural change. Clarification of the structural basis for long-term inactivation will require additional functional scanning of the channel surface by site-specific mutagenesis.

Cell perfusion with FHF-derived peptide induces long-term sodium channel inactivation and restricts firing of action potentials in cerebellar granule cells. We speculate that endogenously expressed A-type FHFs underly spike accommodation or arrest of repetitive firing in certain neurons or neuronal subcellular compartments. Consistent with their potential roles as excitation modulators, we have detected endogenously expressed A-type FHFs at axon initial segments of some neurons in the central nervous system (Dover and Goldfarb, unpublished data). Neuronal excitability may be determined by the relative occupancy of sodium channels by A-type vs. B-type FHF isoforms. We also note that the effects of A-type FHFs on excitability are likely to be complex, as their ability to raise the voltage dependence of sodium channel steady-state inactivation is expected to favor neuronal excitability. Additionally, accumulating long-term inactivation of sodium channels mediated by A-type FHFs bears striking physiological resemblance to long-term use-dependent inactivation of dendritic sodium channels in hippocampal neurons responsible for limiting action potential back-propagation from the soma (Jung *et al.*, 1997; Remy *et al.*, 2009). Future experiments are warranted to determine whether dendritic action potentials in some neurons are regulated by A-type FHFs.

Long-term inactivation mediated by A-type FHF requires both its N-terminal inactivation particle and a surface on its β-trefoil core that binds to the channel cytoplasmic tail. The

inactivation particle in isolation can block channels if present at sufficiently high concentration, even if another FHF is docked at the channel tail, as is the case in cerebellar granule neurons (Goldfarb et al., 2007). The superseding effect of FHF N-terminus-derived peptides on long-term inactivation suggests potentially efficacious use of peptides or small molecule mimetics for managing disorders of cellular hyperexcitability in nervous and cardiac systems.

Table and Table Legend

TABLE 1. FHF Protein and Peptide Modulation of Nav1.6 Currents

		No FHF	FHF1A	FHF1B	FHF2A	FHF2B	FHF4A	FHF4B	F2A(2-21) 1mM peptide
LONG TERM INACTIVATION	% Available 40ms after Depolarization Cycle 1 Cycle 2 Cycle 3 # Cells T-test P value	94.3 +/- 2.4 92.4 +/- 4.8 91.4 +/- 4.9 *n=11*	76.4 +/- 3.8 69.7 +/- 1.8 ***64.3 +/- 1.8*** *n=5* ***3 x 10 $^{-10}$***	95.2 +/- 2.8 93.0 +/- 4.8 92.6 +/- 5.0 *n=6*	70.2 +/- 5.2 56.7 +/- 6.7 ***48.8 +/- 7.3*** *n=9* ***8 x 10 $^{-10}$***	95.1 +/- 2.2 94.0 +/- 3.8 93.6 +/- 2.8 *n=10*	58.9 +/- 6.3 47.1 +/- 7.7 ***42.1 +/- 7.2*** *n=5* ***4 x 10 $^{-8}$***	93.6 +/- 5.3 94.6 +/- 7.3 94.6 +/- 6.2 *n=11*	62.0 +/- 8.8 48.1 +/- 9.8 ***40.5 +/- 9.4*** *n=11* ***9 x 10 $^{-11}$***
	Tau Recovery (ms) at -90 mV # Cells at -110 mV # Cells		131 +/- 41 *n=4* N.A.		371 +/- 107 *n=9* 153 +/- 33 *n=5*		206 +/- 67 *n=5* N.A.		323 +/- 14 *n=4* N.A.
	V1/2 (mV) k factor (mV) # Cells		-46.6 +/- 2.7 -4.0 +/- 0.2 *n=4*		-46.7 +/- 5.3 -4.3 +/- 0.4 *n=6*		-47.4 +/- 2.1 -3.3 +/- 0.4 *n=4*		-42.7 +/- 5.0 -6.8 +/- 1.1 *n=6*
STEADY STATE INACTIVATION	V1/2 (mV) k factor (mV) # Cells T-test P value	-79.1 +/- 3.7 -5.5 +/- 0.5 *n=8*	***-66.4 +/- 2.8*** -5.0 +/- 0.2 *n=5* ***3 x 10 $^{-5}$***	-78.0 +/- 2.6 -5.6 +/- 0.3 *n=5*	***-66.3 +/- 4.3*** -5.6 +/- 0.3 *n=8* ***2 x 10 $^{-5}$***	***-71.5 +/- 2.2*** -5.5 +/- 0.5 *n=8* ***3 x 10 $^{-4}$***	***-63.3 +/- 3.3*** -6.1 +/- 0.8 *n=5* ***2 x 10 $^{-5}$***	***-62.3 +/- 4.3*** -6.8 +/- 1.4 *n=8* ***1 x 10 $^{-6}$***	-77.1 +/- 3.2 -5.3 +/- 0.5 *n=7*
ACTIVATION	V1/2 (mV) # Cells	-35.0 +/- 3.3 *n=7*	-40.0 +/- 3.9 *n=5*	-38.3 +/- 1.3 *n=4*	-39.1 +/- 7.0 *n=7*	-36.6 +/- 3.1 *n=6*	-37.6 +/- 4.6 *n=5*	-36.1 +/- 3.7 *n=6*	-34.4 +/- 6.3 *n=7*

Table 1. FHF protein and peptide modulation of $Na_V1.6$ currents. TTX-resistant sodium currents in N2A- $Na_v1.6^{TTXr}$ cells were analyzed after transient transfection with FHF expression plasmids or perfusion with FHF2A-derived N-terminal peptide F2A(2-21). Accumulating long-term inactivation was assayed using four 16 msec 0 mV depolarizations separated by 40 msec –90 mV recovery intervals. Recovery was assayed by varying the duration of a –90 mV recovery interval following three prior depolarization pulses. Voltage dependences for activation, steady state inactivation, and long-term inactivation were analyzed using protocols described in Methods. Values shown as mean +/- standard deviation. Statistical significance by T-tests were determined by comparing values for a given test group to those obtained in absence of FHF plasmid or peptide; highly significant values are highlighted in bold italic. $V_{1/2}$, voltage of half-maximal effect; k, slope factor; N.A, not analyzed. Also see Suppl. Fig. 2 showing lack of TTX-resistant current in parental N2A cells.

Figures and Figure Legends

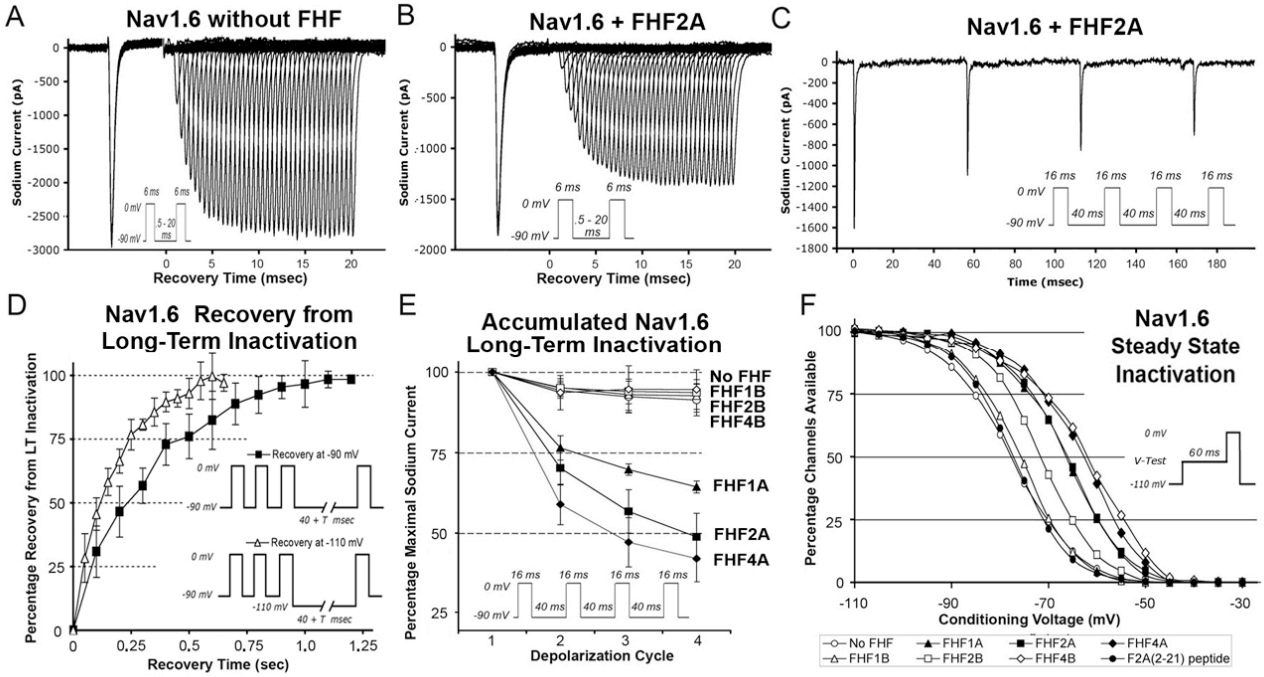

Figure 1. A-type FHFs induce long-term inactivation of $Na_v1.6$.

A, B) FHF2A blocks recovery of sodium channels. TTX-resistant sodium currents in N2A-$Na_v1.6^{TTXr}$ cells with or without transiently expressed FHF2A were recorded during two 6 msec depolarizations with interpulse –90 mV interval varied between 0.5 to 20 msec (see inset). All current traces are shown. Virtually all channels recover in absence of FHF (A), while one-third of channels in FHF2A-expressing cells remain inactivated in this time frame (B). C) Cycle-dependent accumulation of FHF2A-induced long-term inactivation. N2A-$Na_v1.6^{TTXr}$ cell expressing FHF2A was depolarized four times (16 msec each) with 40 msec –90 mV recovery intervals (inset), generating smaller current peaks for each cycle. D) Long-term recovery of $Na_v1.6$ in FHF2A-expressing cells. Cells were depolarized three times to drive a substantial

fraction of channels into long-term inactivation, and long-term recovery was monitored at –90 mV or –110 mV (see insets). The graph isolates the long-term inactivated channel fraction by subtracting out the fast-inactivated channels that had recovered within the first 40 msec. Channels recovered from long-term inactivation faster at the more hyperpolarized voltage. E) All A-type FHFs induce long-term inactivation. Cells were depolarized four times (16 msec each), with 40 msec –90 mV recovery intervals. Graph summarizes data for accumulation of long-term inactivation in cells expressing A- and B- isoforms of FHF1, 2, 4. Only A-type FHFs induce long-term inactivation. F) FHF-induced steady-state inactivation of $Na_v1.6$. N2A-$Na_v1.6^{TTXr}$ cells expressing different FHFs were tested for available sodium channels after 60 msec depolarization to test voltages (see inset). Averaged data for all recorded cells are plotted (see Suppl. Table 1 for standard deviations). FHF4B and all A-type FHFs induce large depolarizing shift in voltage-dependence of inactivation, and FHF2B induces a smaller shift. Injection of F2A(2-21) peptide into untransfected cells had no effect on steady-state inactivation. Also see supporting data in Suppl. Table 1 and Suppl. Fig. 1.

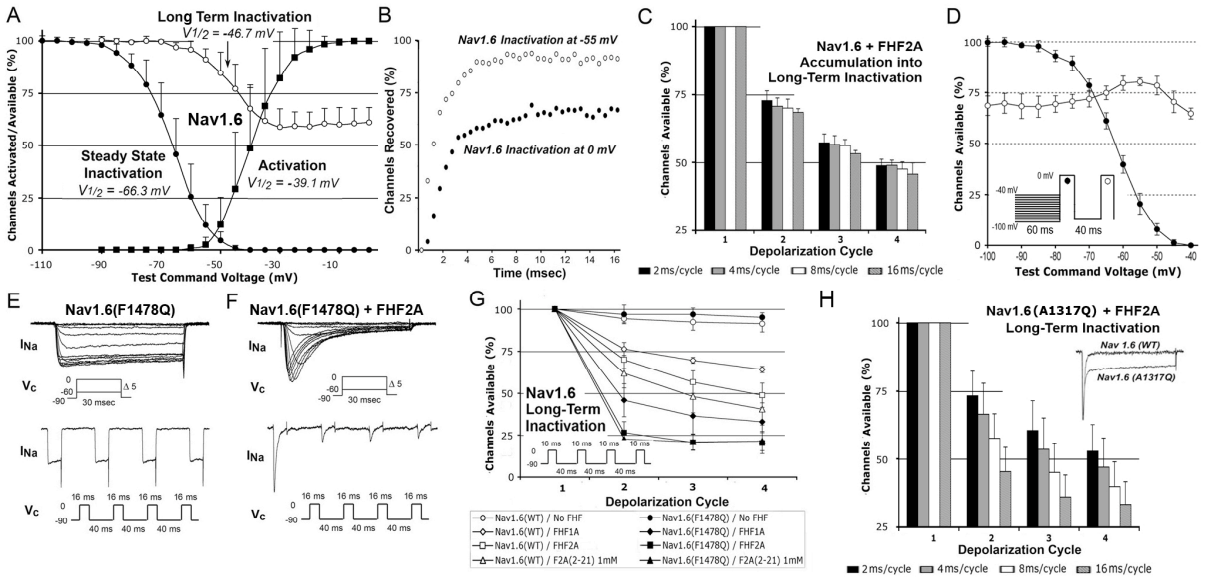

Figure 2. Long-term and fast inactivation are distinct and competing channel states .

A) Long-term inactivation and steady-state inactivation have different voltage thresholds. N2A-$Na_v1.6^{TTXr}$ cells expressing FHF2A were assayed for voltage dependence of activation (n=7), steady-state inactivation (n=8) and long-term inactivation (n=6). Average $V_{1/2}$ for long-term inactivation (-46.7 +/- 5.3 mV) is close to that for activation (-39.1 +/- 7.0 mV) and far more positive than that for steady-state inactivation (-66.3 +/- 4.3 mV). Also see supporting data in Table 1. B) Virtually all steady-state inactivation at –55 mV is fast inactivation. An N2A-$Na_v1.6^{TTXr}$ cell expressing FHF2A was depolarized to either 0 mV or –55 mV followed by recovery (-90 mV) for 0.5-20 msec before measuring current induced by a second depolarization to 0 mV. Long-term inactivation is induced at 0 mV, but steady-state inactivation at –55 mV is almost exclusively fast inactivation. C) Effect of depolarization interval duration on long-term inactivation. N2A-$Na_v1.6^{TTXr}$ cells expressing FHF2A (n=8) were each subjected to four 0 mV depolarization cycles of varying duration (2-16 msec) spaced by 40 msec –90 mV recovery

periods, and available sodium current for each cycle was expressed as percentage of first-cycle current. Long-term inactivation is driven predominantly by the number of depolarization cycles, and not by cycle duration. D) Voltages favoring $Na_v1.6$ fast inactivation inhibit subsequent entry into long-term inactivation. N2A-$Na_v1.6^{TTXr}$ cells expressing FHF2A (n = 4) were clamped to test voltages for 60 msec, followed by two depolarizations to 0 mV separated by a 40 msec recovery period at –90 mV (inset). The current induced in the first 0 mV depolarization (filled circles) reports degree of steady state inactivation, while the second 0 mV depolarization (open circles) reports long-term inactivation. The –50 to –60 mV range, which preferentially induces fast inactivation (panels A, B), partially protects against long-term inactivation upon further depolarization to 0 mV. E, F) FHF2A-induced long-term inactivation of channels lacking intrinsic fast inactivation. N2A cells were transiently transfected with vectors expressing $Na_v1.6_{(F1478Q)}^{TTXr}$ and GFP without (E) or with FHF2A (F). In absence of FHF2A, $Na_v1.6_{(F1478Q)}^{TTXr}$ opens without inactivation (note increased tail current spike upon repolarizations), while FHF2A restores inactivation that is long-term. See supporting data in Suppl. Table 2. G) A-type FHFs induce enhanced long-term inactivation of $Na_v1.6_{(F1478Q)}^{TTXr}$. Accumulating long term inactivation through four 0 mV 16 msec depolarization cycles and –90 mV 40 msec recovery intervals was measured for $Na_v1.6^{TTXr}$ and $Na_v1.6_{(F1478Q)}^{TTXr}$ upon transfection of FHF1A, FHF2A or cell perfusion with F2A(2-21) peptide (see Table 1 and Suppl. Table 2 for # cells analyzed). H) FHF2A induces time-dependent accumulation into long-term inactivation of $Na_v1.6_{(A1317Q)}$ channels. FHF2A-

induced long-term inactivation of $Na_v1.6_{(A1317Q)}^{TTXr}$ channels was measured after four 0 mV depolarization cycles of 2-16 msec separated by 40 msec –90 mV recovery intervals (n = 4). In each depolarization cycle, mutant channels continue to enter the long-term inactivated state during the 16 msec depolarization interval. Scaled sodium current traces for $Na_v1.6^{TTXr}$ and $Na_v1.6_{(A1317Q)}^{TTXr}$ upon depolarization (inset); mutant channel shows enhanced persistent current.

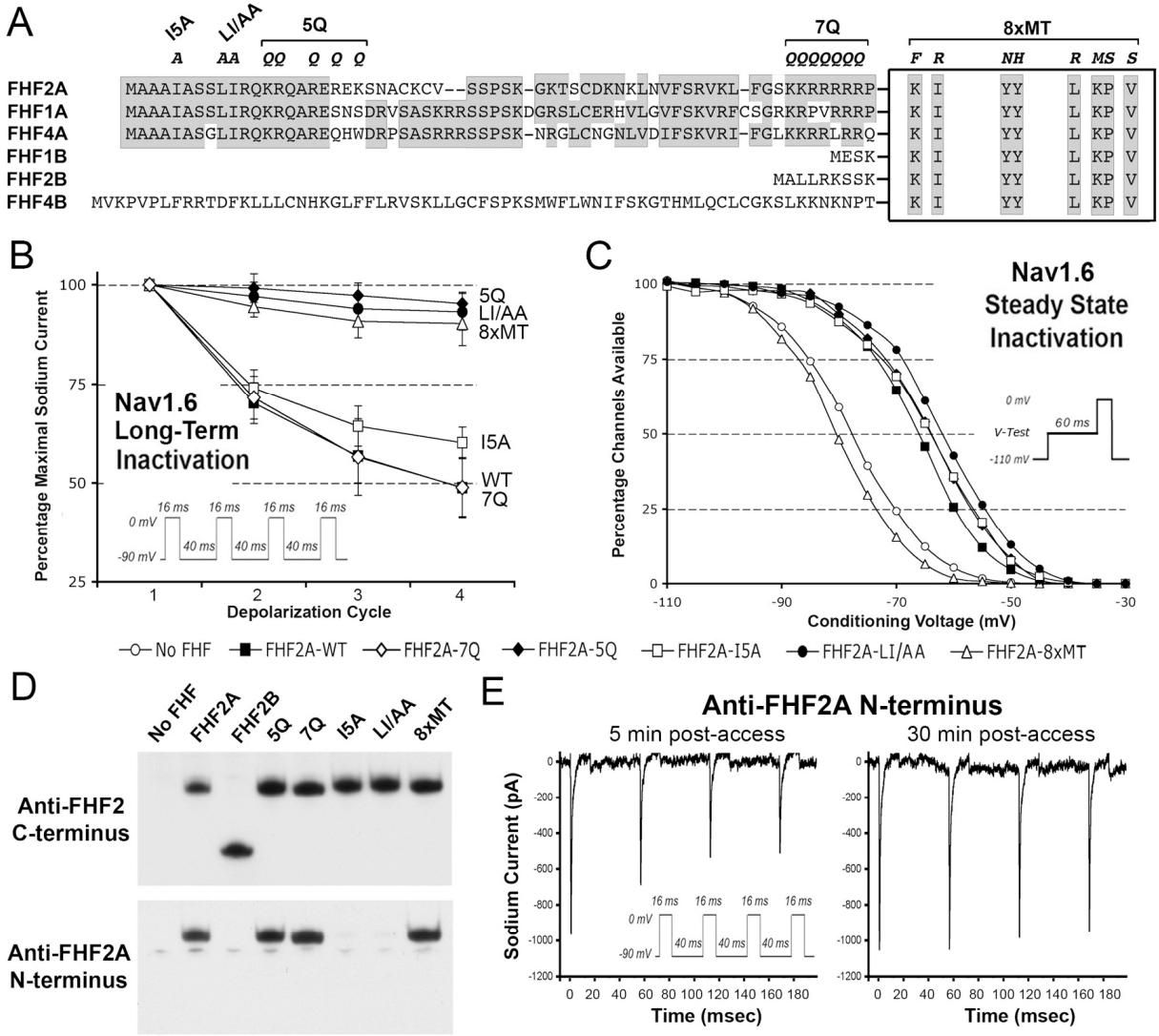

Figure 3. $Na_v1.6$ long-term inactivation requires channel-binding and cytoplasmic effector domains of FHF2A. A) FHF sequence alignment and engineered FHF2A mutations. N-terminal sequences of FHF isoforms are shown attached to the core homology domain for all FHFs (box). Eight core residues required for FHF binding to channel tail (Goetz *et al.*, 2009) are indicated. Sequence similarity is shaded. Individual and combined amino acid substitutions (italicized) and names of mutant FHF2A proteins are marked at the top. B) Accumulating long-term inactivation of $Na_v1.6^{TTX^r}$ mediated by mutant FHF2A proteins. Cells were subjected to

four 0 mV 16 msec depolarizations separated by –90 mV 40 msec recovery intervals. The 7Q mutant was as effective as wild-type FHF2A, I5A mutant had reduced potency, and mutants 8xMT, 5Q, and LI/AA were incapable of inducing long-term inactivation. See Suppl. Table 3 for supporting statistical data. C) Steady-state (fast) inactivation of $Na_v1.6^{TTX^r}$ mediated by mutant FHF2A proteins. Several mutants impaired for long-term inactivation (5Q, LI/AA, I5A) were still able to shift $V_{1/2}$ steady-state inactivation. See Suppl. Table 3 for supporting statistical data. D) Characterization of rabbit polyclonal antibodies reactive to N-terminal FHF2A epitope. Lysates from N2A cells transfected with FHF2 expression vectors were assayed by immunoblotting with antibodies reactive with C-terminus of FHF2 (top). All FHF2 isoforms and mutants were detectable. The blot was then stripped and reprobed with antibodies against the N-terminus of FHF2A (bottom). The epitope for antibodies to the FHF2A N-terminus includes Ile-5, Leu-9, and Ile-10. E) Antibodies to the FHF2A N-terminus block FHF2A-induced $Na_v1.6$ long-term inactivation. Sodium current traces from an N2A-$Na_v1.6^{TTX^r}$ cell expressing FHF2A were recorded 5 and 30 minutes after break-in, using patch pipette solution containing rabbit anti-FHF2A (200 μg/ml). $Na_v1.6$ accumulating long-term channel inactivation is initially detected, but is inhibited following 30-min diffusion of antibodies into the cell. See supporting data in Suppl. Table 3.

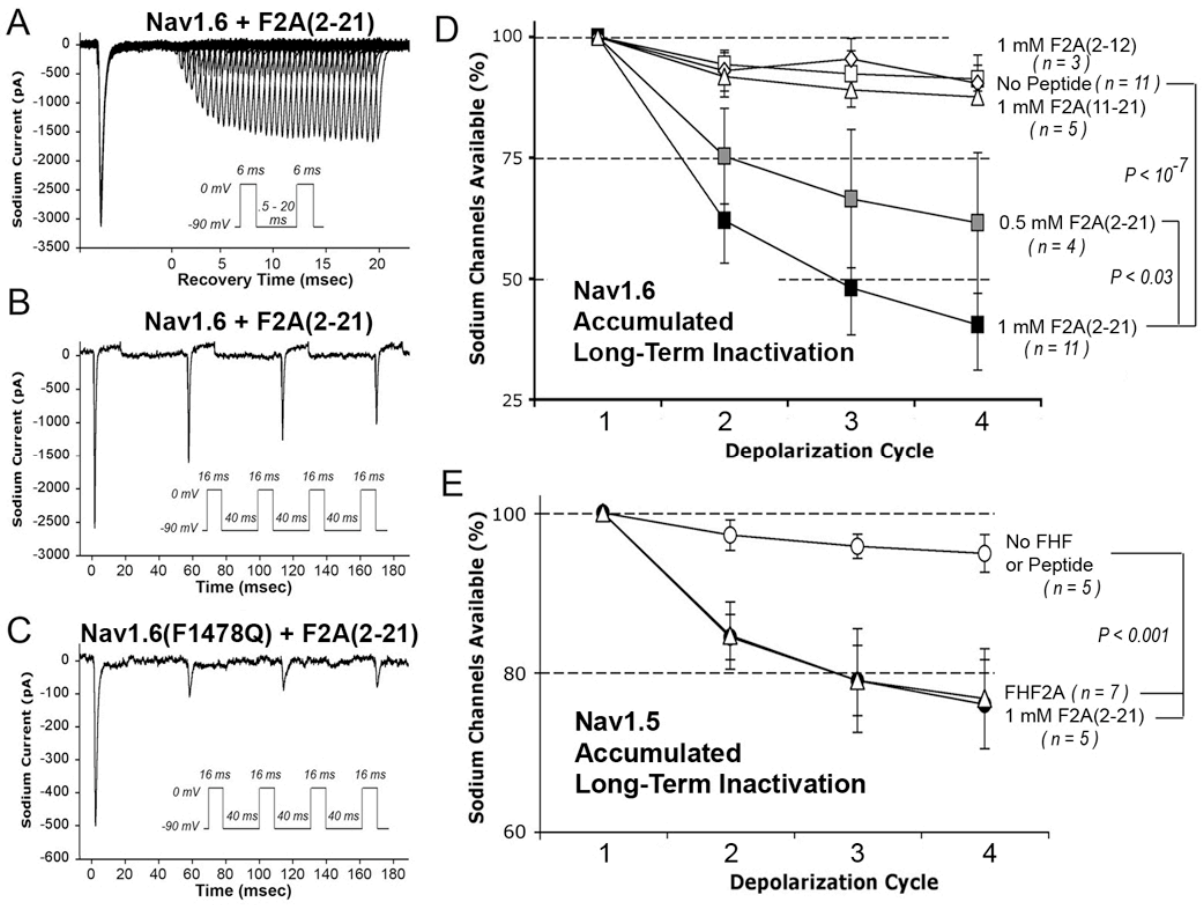

Figure 4. N-terminal FHF2A-derived synthetic peptide acts as a long-term inactivation particle. A, B) Peptide-induced long-term inactivation of $Na_v1.6^{TTXr}$. TTX-resistant sodium current in N2A-$Na_v1.6^{TTXr}$ cells patched with pipettes containing 1 mM peptide corresponding to FHF2A residues 2-21 [F2A(2-21)]. Approximately 40% of channels underwent long-term inactivation after one 0 mV 6 msec depolarization cycle (A) and accumulated to ~60% following three prior 16 msec depolarization cycles separated by –90 mV 40 msec recovery intervals (B). See supporting data in Table 1. C) Enhanced induction of $Na_v1.6_{(F1478Q)}^{TTXr}$ long-term inactivation by F2A(2-21). Cell expressing $Na_v1.6_{(F1478Q)}^{TTXr}$ was patched with pipette

containing 1 mM F2A(2-21) and sodium currents recorded during the four-pulse protocol (as in panel B). One depolarization cycle induced maximum long-term inactivation. See supporting data in Suppl. Table 2. D) Dose dependence and sequence specificity of peptide-induced channel inactivation. N2A-$Na_v1.6^{TTX^r}$ cells were patched with pipettes filled with 0.5 mM F2A(2-21) (n=4), 1 mM F2A(2-21) (n=11), 1 mM F2A(2-12) (n=3), or 1 mM F2A(11-21) (n=5) and subjected to four 16 msec depolarizations spaced by 40 msec –90 mV recovery intervals. F2A(2-21) activity is dose-dependent, and other peptides lack significant effect. See supporting data in Suppl. Table 4. E) Peptide-induced long-term inactivation of $Na_v1.5$. TTX-resistant sodium currents in N2A cells transiently transfected with $Na_v1.5$ vector with or without 1 mM F2A(2-21) or with FHF2A cotransfection. Four 16 msec –30 mV depolarizations were spaced with 40 msec recoveries at –130 mV. Peptide-induced long-term inactivation was comparable to effect of FHF2A transfection.

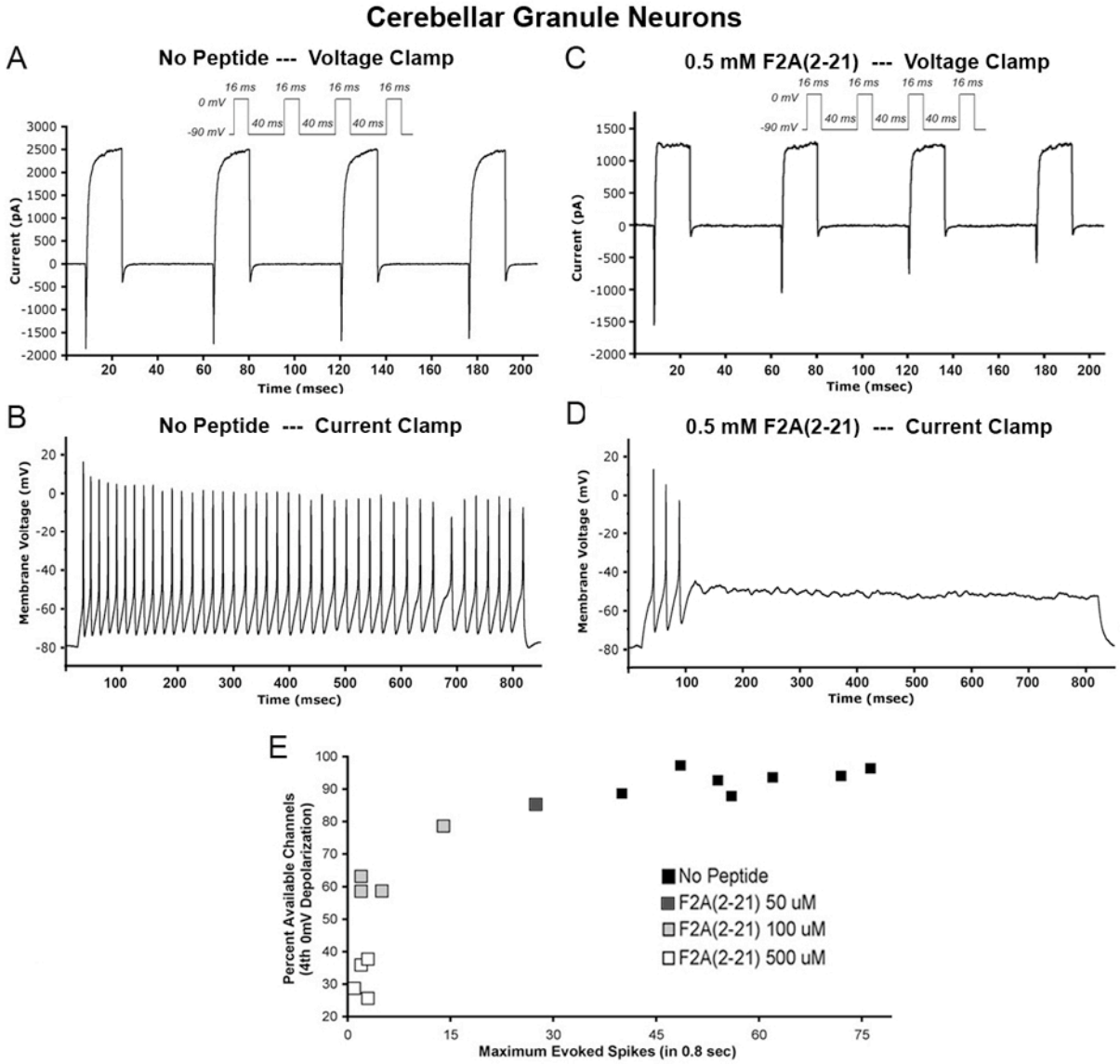

Figure 5. F2A(2-21) peptide modulation of sodium current and excitability of mouse cerebellar granule neurons. Cultured granule neurons (16 days in vitro) were patched with pipette solution with or without F2A(2-21) peptide. A cell patched without peptide (A, B) was subjected four 16 msec 0 mV depolarizations separated by 40 msec –90 mV recovery intervals (A) and current clamped depolarization (B). Inactivating inward current and sustained outward currents were virtually reproduced through four depolarization cycles (A), and current injection

yielded sustained firing (B). Cell patched with 0.5 mM F2A(2-21) (C, D) showed accumulating loss of inward current (C) and generated three spikes of reducing amplitude until failure (D). E) Accumulating inactivation of inward current and loss of spike generation potential. Cells were patched with pipettes containing 0, 0.05, 0.1, or 0.5 mM F2A(2-21) peptide. The graph plots, for each cell, percent accumulated inactivation of inward current vs. maximum spikes generated. Inward current long-term inactivation is peptide dose-dependent, and long-term inactivation correlates with inhibition of spiking.

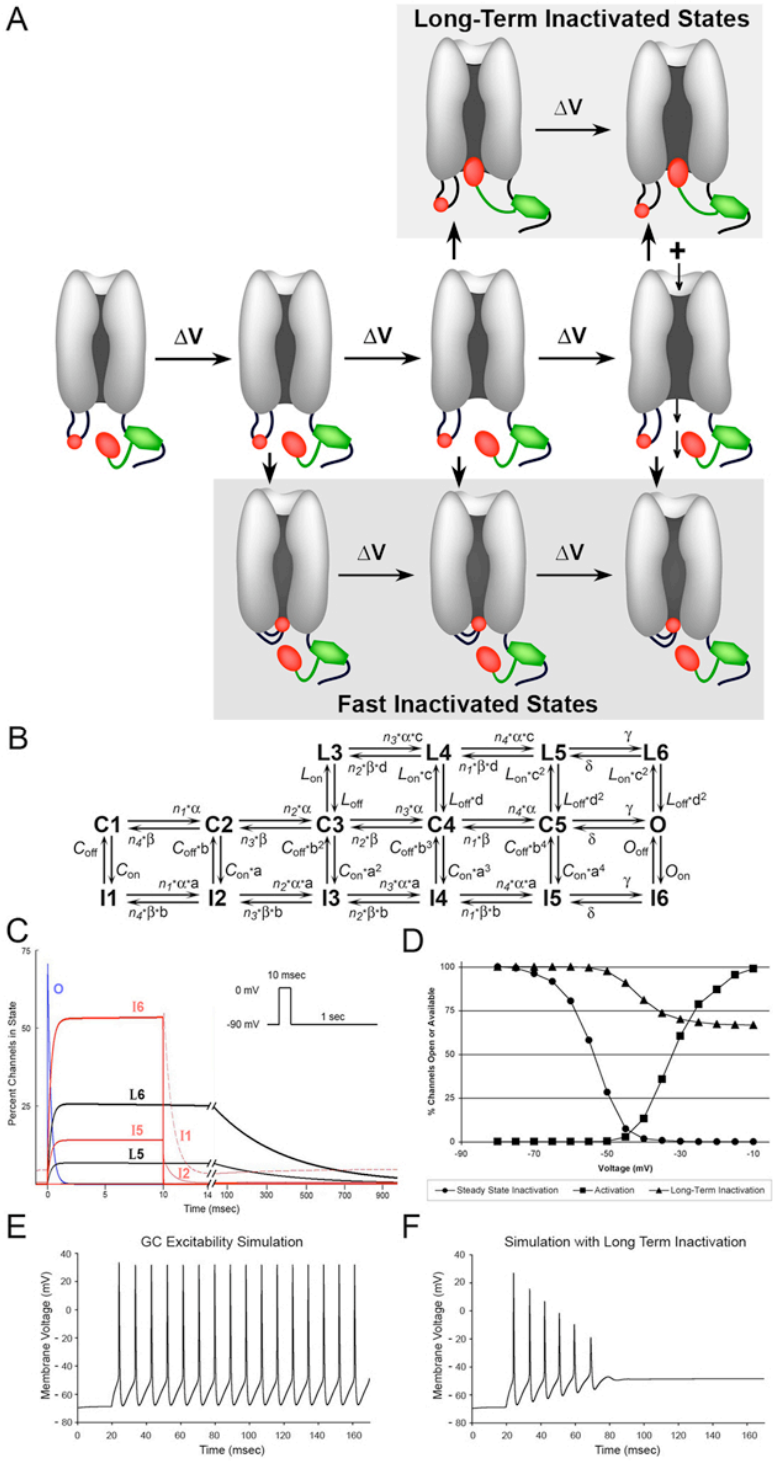

Figure 6. A long-term inactivation model and computer simulation. A) Schematic of voltage-dependent sodium channel transitions. The core domain of FHF (green) is shown tethered to the channel cytoplasmic tail. The channel's intrinsic inactivation particle in the short

cytoplasmic loop (small red oval) and the larger long-term inactivation particle at N-terminus of tethered A-type FHF (larger red oval) compete for access to inactivate the channel at more depolarized voltage-driven transitions near the open state, making long-term inactivation use-dependent. This illustration depicts the two particles competing for docking within the pore. Alternatively, the FHF particle may bind at a channel regulatory site elsewhere that is allosterically obscured by prior fast inactivation (not shown). B) 16-state fast kinetic model of sodium channel bearing tethered A-type FHF. This model adds four states (L3-L6) corresponding to docking of the FHF-derived particle to a previously described Markov model for activation and fast inactivation (Raman & Bean, 2001). Channels in the open state (O) or in closed states approaching the open state (C3-C5) can transit to either fast-inactivated (I) states or long-term inactivated (L) states. C) Simulation of channel state occupancy during 10 msec 0 mV depolarization and 2 sec –90 mV recovery. Open state (O, blue), fast-inactivation states (I1-I6, red), and long-term inactivation states (L5, L6, black) are shown. L_{on} = 0.001 ms^{-1}. Depolarization drives one third of channels into long-term inactivation. See Materials and Methods for all rate constant values. D) Voltage dependence of steady-state inactivation, long-term inactivation, and activation in the simulation of channels with A-type FHF present. $V_{1/2}$ long-term inactivation in simulations approximates that in recordings of $Na_v1.6$ $^{TTX^r}$ cells with FHF2A. E) Current clamp simulation of cerebellar granule neuron during 12 pA current injection (L_{on} = 0). Neuron fires repetitively. F) Simulation of granule neuron with sodium channel long-term inactivation added (L_{on} = 0.001 ms^{-1}). During 12 pA current injection, spikes decrease in amplitude until failure, similar to empirical data in Fig. 5D.

Supplemental Information

"Long-Term Inactivation Particle for Voltage-Gated Sodium Channels"

Katarzyna Dover, Sergio Solinas, Egidio D'Angelo, and Mitchell Goldfarb

Legends to Supplemental Tables and Figures

SUPPLEMENTAL TABLE 1. A-type FHF-induced long-term inactivation of Nav1.5 and endogenous sodium channels in Neuro2A cells

	Nav1.5 LONG TERM INACTIVATION						
	% Available 40ms at -130mV after 16ms Depolarization:				P value	Tau Recovery (ms)	
FHF	Cycle 1	Cycle 2	Cycle 3	# Cells	(vs no FHF)	(at -130 mV)	# Cells
None	97.2 +/- 1.9	95.8 +/- 1.5	94.9 +/- 2.4	5	---	---	---
FHF2A	84.4 +/- 2.8	79.0 +/- 4.4	***76.0 +/- 5.6***	7	***3 x 10 $^{-5}$***	49 +/- 16	3
F2A(2-21) 1 mM	84.6 +/- 4.2	79.0 +/- 6.5	***76.7 +/- 6.3***	5	***0.002***	40 +/- 4	3

	ENDOGENOUS Nav LONG TERM INACTIVATION				
	% Available 40ms at -90mV after 16ms Depolarization:				P value
FHF	Cycle 1	Cycle 2	Cycle 3	# Cells	(vs no FHF)
None	89.8 +/- 6.3	87.1 +/- 8.1	85.2 +/- 7.1	8	---
FHF1A	74.1 +/- 5.4	68.9 +/- 4.0	***64.4 +/- 3.5***	8	***2 x 10 $^{-5}$***
FHF2A	70.0 +/- 7.9	60.9 +/- 9.4	***54.9 +/- 9.8***	9	***3 x 10 $^{-6}$***

Supplemental Table 1. A-type FHF-induced long-term inactivation of $Na_v1.5$ and endogenous sodium channels in N2A cells. Upper box) N2A cells were transiently cotransfected with Nav1.5 and FHF2A cDNA-bearing pIRES-ZsGreen vector or empty vector, and fluorescent cells analyzed for TTX-resistant $Na_v1.5$ currents. Fluorescent cells lacking FHF2A plasmid were also analyzed using pipettes containing 1 mM F2A(2-21) peptide. Cells were subjected to four 16 msec –30 mV depolarizations, with intervening 40 msec –130 mV recovery phases. FHF2A expression or F2A(2-21) injection induced $Na_v1.5$ long-term inactivation. For cells displaying $Na_v1.5$ long-term inactivation, slow recovery rate was assayed by subjecting cells to three –30 mV depolarizations followed by a variable –130 mV recovery phase before a fourth

depolarization. Recovery from long-term inactivation was similar in FHF2A protein and peptide treated cells. Also see related data in Fig. 4E. Lower box) N2A cells were transiently transfected with FHF1A, FHF2A, or empty pIRES-ZsGreen vector, and fluorescent cells were analyzed for sodium currents in the absence of TTX. Cells were subjected to four 16 msec 0 mV depolarizations, with intervening 40 msec –90 mV recovery phases. Both FHF1A and FHF2A induced long-term inactivation of endogenous sodium channels.

SUPPLEMENTAL TABLE 2. A-type FHF-induced long-term inactivation of of mutant Nav1.6 channels

	Nav1.6(F1478Q) LONG TERM INACTIVATION							Nav1.6(F1478Q) STEADY STATE INACTIVATION			Nav1.6(F1478Q) ACTIVATION		
	% Available 40ms at -90mV after 16ms Depolarization:				P value	Tau Recovery (ms)							
FHF	Cycle 1	Cycle 2	Cycle 3	# Cells	(vs no FHF)	(at -90 mV)	# Cells	V1/2 (mV)	k (mV)	# Cells	V1/2 (mV)	k (mV)	# Cells	V1/2 (mV)	k (mV)	# Cells
None	97.6 +/- 5.2	97.0 +/- 3.4	94.7 +/- 2.6	6	---	---	---	---	---	---	---	---	---	N.A.	N.A.	N.A.
FHF1A	45.9 +/- 9.8	36.4 +/- 11.0	***33.0 +/- 11.4***	4	***0.002***	N.A.	N.A.	N.A.	N.A.	N.A.	N.A.	N.A.	N.A.	N.A.	N.A.	N.A.
FHF2A	26.5 +/- 6.5	20.7 +/- 4.9	***20.2 +/- 6.3***	6	***2 x 10 $^{-9}$***	338 +/- 32	5	-34.5 +/- 2.4	3.5 +/- 0.5	4	-39.5 +/- 0.4	3.5 +/- 0.2	3	-31.9 +/- 3.7	3.9 +/- 0.9	4
F2A(2-21) 1 mM	22.6 +/- 3.0	20.9 +/- 4.9	***21.4 +/- 5.8***	4	***7 x 10 $^{-6}$***	N.A.	N.A.	N.A.	N.A.	N.A.	N.A.	N.A.	N.A.	N.A.	N.A.	N.A.

	Nav1.6(A1371Q) LONG TERM INACTIVATION				
	% Available 40ms at -90mV after 16ms Depolarization:				P value
FHF	Cycle 1	Cycle 2	Cycle 3	# Cells	(vs no FHF)
None	92.1 +/- 3.7	89.7 +/- 6.7	88.0 +/- 7.9	3	---
FHF2A	45.4 +/- 8.8	36.1 +/- 8.1	***33.4 +/- 8.3***	4	***5 x 10 $^{-4}$***

SUPPLEMENTAL TABLE 3. Effects of mutations and antibodies on Nav1.6 modulation by FHF2A

	Nav1.6 LONG TERM INACTIVATION										Nav1.6 STEADY STATE INACTIVATION			
	% Available 40ms at -90mV after 16ms Depolarization:				P value	P value	Tau Recovery (ms)							P value
FHF and antibody	Cycle 1	Cycle 2	Cycle 3	# Cells	(vs no FHF)	(vs FHF2A)	(at -90 mV)	# Cells	V1/2 (mV)	k (mV)	# Cells	V1/2 (mV)	k (mV)	# Cells	(vs no FHF)
None	94.3 +/- 2.4	92.4 +/- 4.8	91.4 +/- 4.9	11			---	---	---	---	---	-79.1 +/- 3.7	-5.5 +/- 0.5	8	
FHF2A	70.2 +/- 5.2	56.7 +/- 6.7	***48.8 +/- 7.3***	9	***8 x 10 $^{-10}$***		338 +/- 84	6	-46.7 +/- 5.3	-4.3 +/- 0.4	6	***-66.3 +/- 4.3***	-5.6 +/- 0.3	8	***2 x 10 $^{-5}$***
FHF2A(8xMT)	94.5 +/- 2.6	90.8 +/- 4.2	***90.3 +/- 5.5***	6		***4 x 10 $^{-9}$***	---	---	---	---	---	-80.4 +/- 3.1	-5.8 +/- 0.3	5	
FHF2A(7Q)	71.5 +/- 5.4	56.5 +/- 9.6	***47.7 +/- 7.5***	10	***1 x 10 $^{-12}$***		310 +/- 25	5	-50.8 +/- 1.3	-5.2 +/- 1.3	3	N.A.	N.A.	N.A.	N.A.
FHF2A(5Q)	99.2 +/- 3.6	97.3 +/- 3.2	***95.3 +/- 2.8***	7		***3 x 10 $^{-9}$***	---	---	---	---	---	***-64.2 +/- 5.2***	-5.8 +/- 0.6	7	***7 x 10 $^{-5}$***
FHF2(I5A)	74.0 +/- 4.7	64.3 +/- 5.1	***60.1 +/- 3.9***	9	***5 x 10 $^{-12}$***	***0.001***	151 +/- 42	5	-44.9 +/- 4.6	-3.6 +/- 0.9	4	***-64.7 +/- 6.7***	-5.6 +/- 0.6	7	***0.001***
FHF2A(LI/AA)	97.0 +/- 3.6	94.0 +/- 3.5	***93.2 +/- 4.6***	11		***7 x 10 $^{-10}$***	---	---	---	---	---	***-61.8 +/- 5.0***	-5.8 +/- 0.5	8	***3 x 10 $^{-6}$***
FHF2A + anti-F2ANter	95.8 +/- 5.0	90.7 +/- 2.4	***89.7 +/- 1.8***	5		***3 x 10 $^{-8}$***	---	---	---	---	---	***-67.1 +/- 1.7***	-6.3 +/- 0.2	3	***6 x 10 $^{-6}$***
FHF2A(I5A) + anti-F2ANter	82.1 +/- 4.9	75.9 +/- 6.9	***71.8+/- 7.7***	7	***2 x 10 $^{-4}$***		N.A.	N.A.	N.A.	N.A.	N.A.	N.A.	N.A.	N.A.	N.A.

SUPPLEMENTAL TABLE 4. Long-term inactivation of Nav1.6 by FHF2A-derived peptide injection

	Nav1.6 LONG-TERM INACTIVATION									
	% Available 40ms at -90mV after 16ms Depolarization:				P value	Tau Recovery (ms)				
FHF2A vector or peptide	Cycle 1	Cycle 2	Cycle 3	# Cells	(vs no FHF)	(at -90 mV)	# Cells	V1/2 (mV)	k (mV)	# Cells
None	94.3 +/- 2.4	92.4 +/- 4.8	91.4 +/- 4.9	11		---	---	---	---	---
FHF2A	70.2 +/- 5.2	56.7 +/- 6.7	***48.8 +/- 7.3***	9	***8 x 10 $^{-10}$***	338 +/- 84	6	-46.7 +/- 5.3	-4.3 +/- 0.4	6
F2A(2-21) 0.5mM	75.3 +/- 9.9	66.6 +/- 14.3	***61.5 +/- 14.5***	4	***0.02***	N.A.	N.A.	N.A.	N.A.	N.A.
F2A(2-21) 1 mM	62.0 +/- 8.8	48.1 +/- 9.8	***40.5 +/- 9.4***	11	***9 x 10 $^{-11}$***	323 +/- 14	4	-42.7 +/- 5.0	-6.8 +/- 1.1	6
F2A(2-12) 1 mM	93.0 +/- 4.3	95.4 +/- 4.2	90.5 +/- 3.7	3		---	---	---	---	---
F2A(11-21) 1 mM	92.5 +/- 3.5	90.8 +/- 3.7	88.8 +/- 2.8	5		---	---	---	---	---

SUPPLEMENTAL TABLE 5. A-type FHF-derived peptide induces inward current long-term inactivation and impairs excitability of cerebellar granule neurons

		INWARD CURRENT LONG TERM INACTIVATION				ACTION POTENTIAL PROPERTIES			
		Inward Current 16msec Deploarization							
Peptide Treatment	# Cells	Cycle 1 (pA)	Cycle 4 (pA)	% Available Cycle 4	P value	Peak Voltage (mV)	P Value	Max Spikes in 0.8 sec	P Value
None	7	-1328 +/- 528	-1136 +/- 446	92.9 +/- 3.5	---	9.0 +/- 5.2	---	58.4 +/- 13.0	---
F2A(2-21) 0.1 mM	4	-1469 +/- 699	-936 +/- 391	***64.7 +/- 9.5***	***0.007***	6.5 +/- 10.3	0.67	***5.8 +/- 5.7***	***3 x 10 $^{-5}$***
F2A(2-21) 0.5 mM	4	-1322 +/- 235	-432 +/- 138	***31.9 +/- 5.7***	***3 x 10 $^{-5}$***	5.0 +/- 8.2	0.45	***2.3 +/- 1.0***	***1 x 10 $^{-5}$***

SUPPLEMENTAL TABLE 6. Passive recording properties of N2A-Nav1.6TTX^{r} cells and cultured cerebellar granule neurons

Cell Type	# Cells Measured	Membrane Capacitance (pF)	Leak Resistance (GΩ)	Series Resistance (MΩ)	Series Tau (msec)	Frequency V-Clamp (kHz)
N2A-Nav1.6	10	26.3 +/- 7.4	0.50 +/- 0.23	3.5 +/- 0.9	0.089 +/- 0.025	1.98 +/- 0.82
Granule Neurons	10	4.70 +/- 0.61	0.98 +/- 0.30	14.9 +/- 5.6	0.068 +/- 0.020	2.49 +/- 0.61

Supplemental Table 2. A-type FHF-induced long-term inactivation of mutant $Na_v1.6$ channels.

N2A cells were cotransfected with plasmids expressing mutant $Na_v1.6^{TTXr}$ channels ($Na_v1.6_{(F1478Q)}$ or $Na_v1.6_{(A1317Q)}$) and FHF cDNA-bearing pIRES-ZsGreen vector or empty vector, and fluorescent cells were analyzed for TTX-resistant sodium currents. Fluorescent cells lacking FHF plasmid were also analyzed using pipettes containing 1 mM F2A(2-21) peptide. Induction of channel long-term inactivation was assayed by four 16 msec 0 mV depolarizations with 40 msec –90 mV recovery intervals. Channel long-term recovery was assessed with three 0 mV depolarizations and a subsequent variable duration –90 mV recovery interval preceding another depolarization. Protocols for voltage dependent channel activation, steady state inactivation, and long-term inactivation were also employed (see Methods). Upper box) FHF modulation of inactivation-defective $Na_v1.6_{(F1478Q)}$. FHF1A, FHF2A, and F2A(2-21) peptide each induce long-term inactivation of $Na_v1.6_{(F1478Q)}$, and to an extent much greater than their effects on wild-type $Na_v1.6$ channels (also see Table 1 and Fig. 2). FHF2A-induced $Na_v1.6_{(F1478Q)}$ long-term inactivation has voltage dependence close to that for channel activation, and, furthermore, steady-state inactivation occurs at voltages approaching that for activation, consistent with all inactivation of $Na_v1.6_{(F1478Q)}$ being long-term in nature. Lower box) FHF2A induces greater long-term inactivation of $Na_v1.6_{(A1317Q)}$ than of wild-type $Na_v1.6$ (Table 1), likely due to the unstable docking of the intrinsic fast inactivation particle in the $Na_v1.6_{(A1317Q)}$ pore. Also see related data in Fig. 2H.

Supplemental Table 3. Effects of FHF2A mutations and antibodies on $Na_v1.6$ modulation. N2A-$Na_v1.6^{TTXr}$ cells were transiently transfected with pIRES-ZsGreen plasmids bearing wild-type or mutant FHF2A cDNAs, and fluorescent cells were assayed for $Na_v1.6$ accumulated long-term inactivation and voltage dependence of steady-state inactivation and long-term inactivation, as described in legend to Suppl. Table 2. In some FHF-expressing cells, the patch pipettes contained antibodies specific for the wild-type N-terminus of FHF2A. Some N-terminal substitutions in FHF2A reduced or eliminated $Na_v1.6$ long-term inactivation without impairing modulation of steady-state inactivation, while the (8xMT) substitutions impaired both processes. Antibody perfusion fully blocked long-term inactivation mediated by FHF2A, but not that mediated by mutant FHF2A(I5A). Also see related data in Fig. 3B, C, and E.

Supplemental Table 4. Long-term inactivation of $Na_v1.6$ by FHF2A-derived peptide injection. Long-term inactivation of $Na_v1.6$ in N2A-$Na_v1.6^{TTXr}$ cells following patch pipette perfusion with FHF2A-derived peptides was compared to long-term inactivation induced by FHF2A plasmid transfection. Long-term inactivation accumulation, recovery rate, and voltage dependence was assayed as described in legend to Suppl. Table 2. Long-term inactivation induced by 1 mM F2A(2-21) peptide was comparable to that induced by FHF2A protein, while shorter peptides lacked significant activity. Also see related data in Fig. 4A-D.

Supplemental Table 5. A-type FHF-derived peptide induces inward current long-term inactivation and impairs excitability of cerebellar granule neurons. Cultured cerebellar granule neurons (16 days in vitro) were whole-cell patched with pipettes containing solutions with or

without F2A(2-21) peptide. Each cell was first subjected under voltage clamp to four 16 msec depolarizations at 0 mV separated by 40 msec –90 mV recovery intervals. Peak inward currents on the first and fourth depolarizations are shown, along with the percentage channels still available on the fourth pulse. Each cell was then switched to current clamp, its resting potentials adjusted to –80 mV, and depolarized in 800 msec intervals, using different magnitudes of current application per interval. Action potentials were recorded and analyzed for maximum number of spikes generated among all tested current injections, and for the peak voltage attained by the first spike in any current injection sweep. Peptide induced inward current long-term inactivation in a dose-dependent manner and inhibited repetitive spiking in current clamp. Peptide did not significantly affect initial available sodium channels (first cycle inward current) nor first spike peak amplitude. Also see related data in Fig. 5.

Supplemental Table 6. Passive properties of recorded cells. Passive properties of N2A-Nav1.6$^{TTX^r}$ cells and cerebellar granule neurons were analyzed in the same respective extracellular/pipette solution combinations as used for activated current analyses. Capacitance transient and leak steady-state currents induced by a voltage-clamped 10 mV step were used to calculate membrane capacitance (C_m) and leak resistance (R_{leak}). Curve-fitting of the exponential transient current decay provided the series resistance (R_s) and fast time constant (Tau_{fast}) for membrane charging. For N2A-Nav1.6$^{TTX^r}$ cells, 98 +/- 2% of the membrane capacitance charged with Tau_{fast}; for granule neurons, 85 +/- 8% of capacitance charged with Tau_{fast}. Frequency of voltage clamp was calculated from the formula $fVC = 1/(6.28 * C_m * R_s)$

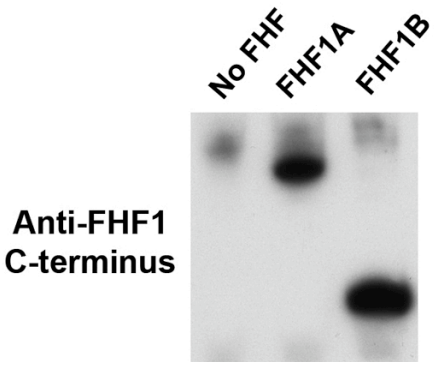

Supplemental Figure 1. Expression of FHF1 isoforms by transfection of N2A cells. N2A cells transfected with pIRES-ZsGreen1 vectors bearing cDNAs for FHF1A, FHF1B, or no FHF were lysed and analyzed by immunoblotting with antibodies against the common C-terminus of FHF1 isoforms. These data control for adequate expression of FHF1B, which failed to elicit any discernable modulation of $Na_v1.6$.

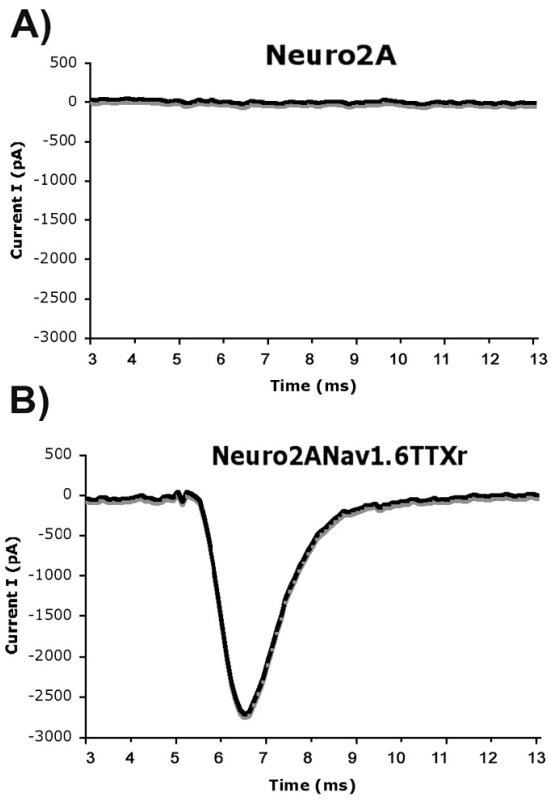

Supplemental Figure 2. Lack of endogenous TTX-resistant sodium current in N2A cells. Sodium current traces following depolarization to 0 mV (at t = 5 msec) in the presence of TTX. A) Parental Neuro2A cell. B) N2A-$Na_v1.6^{TTXr}$ cell. All endogenous sodium channels in N2A cells are TTX-sensitive, making $Na_v1.6$ the only channel carrying TTX-resistant current in N2A-$Na_v1.6^{TTXr}$ cells.

Acknowledgments

We thank Robert Kass (Columbia University) for providing the human $Na_v1.5$ expression vector, David Linden (Johns Hopkins University) for commentary on the manuscript and for suggesting BDNF addition to cerebellar neuron cultures, and Annie Yam Shen and Ivan Anastassov for technical assistance. This work was supported by NIH awards to M.G. (R01-NS39906 and U54-NS40173).

References

ALEKOV, A. K., PETER, W., MITROVIC, N., LEHMANN-HORN, F. & LERCHE, H. (2001). Two mutations in the IV/S4-S5 segment of the human skeletal muscle Na+ channel disrupt fast and enhance slow inactivation. *Neurosci Lett* **306,** 173-176.

CATERALL, W. A. (2000). From ionic currents to molecular mechanisms: the structure and function of voltage-gated sodium channels. *Neuron* **26,** 13-25.

COURTNEY, M. J., AKERMAN, K. E. & COFFEY, E. T. (1997). Neurotrophins protect cultured cerebellar granule neurons against the early phase of cell death by a two-component mechanism. *J Neurosci* **17,** 4201-4211.

D'ANGELO, E., NIEUS, T., MAFFEI, A., ARMANO, S., ROSSI, P., TAGLIETTI, V., FONTANA, A. & NALDI, G. (2001). Theta-frequency bursting and resonance in cerebellar granule cells: experimental evidence and modeling of a slow k+-dependent mechanism. *J Neurosci* **21,** 759-770.

DIWAKAR, S., MAGISTRETTI, J., GOLDFARB, M., NALDI, G. & D'ANGELO, E. (2009). Axonal Na+ channels ensure fast spike activation and back-propagation in cerebellar granule cells. *J Neurophysiol* **101,** 519-532.

EAHOLTZ, G., COLVIN, A., LEONARD, D., TAYLOR, C. & CATTERALL, W. A. (1999). Block of brain sodium channels by peptide mimetics of the isoleucine, phenylalanine, and methionine (IFM) motif from the inactivation gate. *J Gen Physiol* **113,** 279-294.

EAHOLTZ, G., SCHEUER, T. & CATTERALL, W. A. (1994). Restoration of inactivation and block of open sodium channels by an inactivation gate peptide. *Neuron* **12,** 1041-1048.

FEATHERSTONE, D. E., RICHMOND, J. E. & RUBEN, P. C. (1996). Interaction between fast and slow inactivation in Skm1 sodium channels. *Biophys J* **71,** 3098-3109.

FROTTIN, F., MARTINEZ, A., PEYNOT, P., MITRA, S., HOLZ, R. C., GIGLIONE, C. & MEINNEL, T. (2006). The proteomics of N-terminal methionine cleavage. *Mol Cell Proteomics* **5,** 2336-2349.

GOETZ, R., DOVER, K., LAEZZA, F., SHTRAIZENT, N., TCHETCHIK, D., HUANG, X., ELISEENKOVA, A. V., XU, C., NEUBERT, T. A., ORNITZ, D. M., GOLDFARB, M. & MOHAMMADI, M. (2009). Crystal structure of a fibroblast growth factor homologous factor (FHF) defines a conserved surface on FHFs for binding and modulation of voltage-gated sodium channels. *J Biol Chem* **284,** 17883-17896.

GOLDFARB, M. (2005). Fibroblast growth factor homologous factors: evolution, structure, and function. *Cytokine Growth Factor Rev* **16,** 215-220.

GOLDFARB, M., SCHOORLEMMER, J., WILLIAMS, A., DIWAKAR, S., WANG, Q., HUANG, X., GIZA, J., TCHETCHIK, D., KELLEY, K., VEGA, A., MATTHEWS, G., ROSSI, P., ORNITZ, D. M. & D'ANGELO, E. (2007). Fibroblast growth factor homologous factors control neuronal excitability through modulation of voltage-gated sodium channels. *Neuron* **55,** 449-463.

GRIECO, T. M., MALHOTRA, J. D., CHEN, C., ISOM, L. L. & RAMAN, I. M. (2005). Open-channel block by the cytoplasmic tail of sodium channel beta4 as a mechanism for resurgent sodium current. *Neuron* **45,** 233-244.

HARTUNG, H., FELDMAN, B., LOVEC, H., COULIER, F., BIRNBAUM, D. & GOLDFARB, M. (1997). Murine FGF-12 and FGF-13: expression in embryonic nervous system, connective tissue and heart. *Mech Dev* **64,** 31-39.

JUNG, H. Y., MICKUS, T. & SPRUSTON, N. (1997). Prolonged sodium channel inactivation contributes to dendritic action potential attenuation in hippocampal pyramidal neurons. *J Neurosci* **17,** 6639-6646.

LAEZZA, F., LAMPERT, A., KOZEL, M. A., GERBER, B. R., RUSH, A. M., NERBONNE, J. M., WAXMAN, S. G., DIB-HAJJ, S. D. & ORNITZ, D. M. (2009). FGF14 N-terminal splice variants differentially modulate Nav1.2 and Nav1.6-encoded sodium channels. *Mol Cell Neurosci* **42,** 90-101.

LIU, C. J., DIB-HAJJ, S. D., RENGANATHAN, M., CUMMINS, T. R. & WAXMAN, S. G. (2003). Modulation of the cardiac sodium channel Nav1.5 by fibroblast growth factor homologous factor 1B. *J Biol Chem* **278,** 1029-1036.

LONG, S. B., CAMPBELL, E. B. & MACKINNON, R. (2005). Voltage sensor of Kv1.2: structural basis of electromechanical coupling. *Science* **309,** 903-908.

LOU, J. Y., LAEZZA, F., GERBER, B. R., XIAO, M., YAMADA, K. A., HARTMANN, H., CRAIG, A. M., NERBONNE, J. M. & ORNITZ, D. M. (2005). Fibroblast growth factor 14 is an intracellular modulator of voltage-gated sodium channels. *J Physiol* **569,** 179-193.

PATHAK, M. M., YAROV-YAROVOY, V., AGARWAL, G., ROUX, B., BARTH, P., KOHOUT, S., TOMBOLA, F. & ISACOFF, E. Y. (2007). Closing in on the resting state of the shaker k(+) channel. *Neuron* **56,** 124-140.

RAMAN, I. M. & BEAN, B. P. (1997). Resurgent sodium current and action potential formation in dissociated cerebellar Purkinje neurons. *J Neurosci* **17,** 4517-4526.

RAMAN, I. M. & BEAN, B. P. (2001). Inactivation and recovery of sodium currents in cerebellar Purkinje neurons: evidence for two mechanisms. *Biophys J* **80,** 729-737.

REMY, S., CSICSVARI, J. & BECK, H. (2009). Activity-dependent control of neuronal output by local and global dendritic spike attenuation. *Neuron* **61,** 906-916.

RUSH, A. M., WITTMACK, E. K., TYRRELL, L., BLACK, J. A., DIB-HAJJ, S. D. & WAXMAN, S. G. (2006). Differential modulation of sodium channel Na(v)1.6 by two members of the fibroblast growth factor homologous factor 2 subfamily. *Eur J Neurosci* **23,** 2551-2562.

SCHOORLEMMER, J. & GOLDFARB, M. (2001). Fibroblast growth factor homologous factors are intracellular signaling proteins. *Curr Biol* **11,** 793-797.

SHAKKOTTAI, V. G., XIAO, M., XU, L., WONG, M., NERBONNE, J. M., ORNITZ, D. M. & YAMADA, K. A. (2009). FGF14 regulates the intrinsic excitability of cerebellar Purkinje neurons. *Neurobiol Dis* **33,** 81-88.

SMALLWOOD, P. M., MUNOZ-SANJUAN, I., TONG, P., MACKE, J. P., HENDRY, S. H., GILBERT, D. J., COPELAND, N. G., JENKINS, N. A. & NATHANS, J. (1996). Fibroblast growth factor (FGF) homologous factors: new members of the FGF family implicated in nervous system development. *Proc Natl Acad Sci U S A* **93,** 9850-9857.

SMITH, M. R. & GOLDIN, A. L. (1997). Interaction between the sodium channel inactivation linker and domain III S4-S5. *Biophys J* **73,** 1885-1895.

TUCKER, K. & FADOOL, D. A. (2002). Neurotrophin modulation of voltage-gated potassium channels in rat through TrkB receptors is time and sensory experience dependent. *J Physiol* **542,** 413-429.

ULBRICHT, W. (2005). Sodium channel inactivation: molecular determinants and modulation. *Physiol Rev* **85,** 1271-1301.

WANG, Q., MCEWEN, D. G. & ORNITZ, D. M. (2000). Subcellular and developmental expression of alternatively spliced forms of fibroblast growth factor 14. *Mech Dev* **90,** 283-287.

WEST, J. W., PATTON, D. E., SCHEUER, T., WANG, Y., GOLDIN, A. L. & CATTERALL, W. A. (1992). A cluster of hydrophobic amino acid residues required for fast Na+ channel inactivation. *Proc. Natl. Acad. Sci. USA* **89,** 10905-10909.

WITTMACK, E., RUSH, A. M., CRANER, M. J., GOLDFARB, M., WAXMAN, S. G. & DIB-HAJJ, S. D. (2004). Fibroblast growth factor homologous factor 2B: Association with Nav1.6 and selective colocalization at nodes of Ranvier of dorsal root axons. *J Neurosci* **24,** 6765-6775.

CHAPTER VI

Subcellular localization of A-type FHFs

6.1 Introduction

FHF isoforms are not uniformly distributed inside neuronal cells, but rather exhibit preferential localization at distinct neuronal compartments (Goldfarb et al., 2007, Rush et al., 2006; Wittmack et al., 2004). Our best understanding of FHF isoform topology comes from the overexpression studies performed on cultured hippocampal and DRG neurons (Huang, Taweri, Goldfarb, unpublished data). FHF1A and FHF2A expressed as GFP fusion proteins in hippocampal neurons preferentially localized at AIS and the nucleus. In contrast FHF2B-GFP showed no enrichement in those compartments and its expression pattern was uniform throughout the cell. A similar survey performed on myelinated DRG neurons showed preferential accumulation of FHF1A-GFP at the proximal segment (a molecular analogue of AIS) and FHF1B-GFP at distal nodes of Ranvier. This, in conjunction with the electrophysiology data, contributes to the emerging trend: FHFs capable of inducing a strong depolarizing shift in voltage dependence of channel inactivation (A-type FHFs and FHF4B) localize proximally with respect to the cell soma, while small B-type FHFs, having small effect on $v_{1/2}$ of channel inactivation, localize distally. We can further speculate that FHFs role in neuronal physiology is to optimize excitation proximally, and conduction/action potential transmission distally.

A recent discovery of long-term inactivation particle at the N-terminus of all A-type FHFs adds another dimension to the role of this particular group of FHFs in neuronal excitability. In addition to pro-excitatory function, under condition of high frequency stimulation, A-type FHFs contribute to the action potential failure, and therefore are pro-inhibitory.

The objective of this chapter was to re-evaluate previously reported localization studies with the focus on A-type FHFs. Following the development of A-type specific antibody it become possible to detect endogenous A-type FHFs expressed in the mouse brain, cultured hippocampal and cerebellar granule neurons as well as DRG neurons. Our immunofluorescence assays and Western Blot analysis of compartmentalized cerebellar granule neuron cultures aimed to gain insight into the biological function of A-type FHFs at different neuronal compartments.

6.2 Results

6.2.1 Mouse monoclonal antibody raised against a peptide corresponding to amino acid residues 2-21 of FHF2A is suitable for the detection of A isoforms of FHFs

In order to survey tissue distribution of the endogenous A-type FHFs, an A isoform specific antibody was raised against 20 amino acid long peptide corresponding to residues 2-21 of FHF2A. Since all A isoforms of FHFs share a high degree of sequence homology in this region, it was expected that FHF2A (2-21) specific antibody will also recognize the epitopes on related FHFs 1A, 3A and 4A. A mouse monoclonal antibody N235/22.1 IgG2b (also known as anti-A-type FHF antibody) was developed by UC Davis/NIH NeuroMab Facility in the Department of Neurobiology, Physiology and Behavior at University of California at Davis. The initial tests of the antibody's specificity were performed by the research stuff at the facility using the reagents provided by our laboratory. A Western Blot analysis of the cell lysates prepared from cos-1 cells overexpressing FHFs (1A, 2A, 4A, 1B, 2B, 4B) showed specificity of the newly developed antibody for the interaction with A but not B isoforms of FHFs (data not shown). To further characterize anti-A-type FHF antibody, we performed FHF2 pull down assay, followed by A-type FHF Western Blot. Triton lysates were prepared from the cerebellum and the cortex dissected from the WT mouse brains. We took advantage of the previous reports showing lack of FHF2 expression in the murine cerebellum and used cerebellar lysates for establishing of the negative control. A rabbit polyclonal antibody with the specificity for the C-terminal end of the FHF2 was used to immunoprecipitate A and B isoform of FHF2 from both lysates. The eluted material was resolved on 15% polyacrylamide-SDS gel, transferred to PVDF membrane and probed with anti-A-type FHF antibody. As shown in Figure 6.1 A-type FHFs are aboundantly expressed in the cerebellum and the cortex of the WT murine brain. Note the differences in the

level and the expression pattern of A-type FHFs in those two distinct brain regions (left panel, lanes1 and 2). As expected, FHF2A was precipitated only from the cortical lysate and detected in the Western Blot assay by anti-A-type FHF antibody (right panel, lanes 3 and 4). The experiment demonstrates specificity of the tested antibody and its utility for detection of the endogenous A isoform of FHFs in the brain tissue.

6.2.2 Endogenous A-type FHFs co-localize with sodium channels at AIS of hippocampal, cerebellar granule and Purkinje neurons

Newly developed mouse monoclonal anti-A-type FHF antibody was used in profiling the tissue distribution of endogenous A-type FHFs in the wild-type mouse brain. Whole brain saggital cryosections were double labeled with mouse monoclonal anti-PAN sodium channel antibody and mouse monoclonal anti-A-type FHF antibody and corresponding secondary antibodies, conjugated to fluorophores Alexa594 and Alexa488. To facilitate localization of the cell bodies TOPRO was used as a nuclear stain. The confocal examination of the stained cryosections revealed broad distribution of endogenous A-type FHF in the wild-type (WT) mouse brain. To narrow the extent of our survey we focused on two, well characterized brain regions, the cerebellum and the hippocampus. As shown in Figure 6.2 (A-D) and Figure 6.5 (A-H) A-type FHFs were enriched at AIS of hippocampal and cerebellar granule neurons, where they co-localized with sodium channels. The A isoform of FHFs was also aboundant in the soma of Purkinje neurons and positively detected at corresponding AISs (Figure 6.6 (E-H)).

6.2.3 Endogenous A-type FHFs co-localize with sodium channels at AIS, cell surface and can be found at the nucleus of cultured hippocampal neurons

Because of high staining background typical for whole brain slices and the difficulty of navigating in complex brain tissue, more detailed assessment of subcelular distribution of A-type FHFs was carried out in dissociated cultures of rat hippocampal neurons. Rat hippocampal neurons cultured for 12 days were triple labeled for detection of A-type FHFs, PAN sodium channels, and microtubule associated protein 2 (MAP2). The single channel and stacked confocal images of representative hippocampal neurons in culture are presented in Figure 6.2 (E-H), Figure 6.3 (A-H) and Figure 6.4 (A-I). Obtained results further corroborated co-localization of A-type FHFs at AIS. The addition of MAP2 staining, which preferentially labels somatodendritic region of neurons, further facilitated discrimination between axonal and dendritic processes. Because of the lower background, it was possible to demonstrate co-localization of the A-type FHFs and sodium channels on the surface of the hippocampal neurons (Figure 6.3 (H)). Encouraged by this result, attempts were made to search for the presence of A-type FHFs along dendritic processes. Indeed, we obtained comparable levels of detection of sodium channels and A-type FHFs on the surface of the dendrites (Figure 6.4 (G-I)). These preliminary data are consistent with electrophysiology recordings of sodium channel currents present in dendrites of hippocampal neurons, which display long-term inactivation very similar to A-type FHF-induced channel modulation, Additional experiments are needed to conclusively validate the presence of dendritic A-type FHFs.

During examination of different confocal planes, it became clear that endogenous A-type FHFs are also present at the nucleus of hippocampal neurons. This result is of particular

importance, since it suggests some additional function of this subtype of FHFs in neuronal physiology.

6.2.4 Endogenous A-type FHFs are enriched at AIS of cultured cerebellar granule neurons

To further support our initial immunohistochemistry findings, showing preferential localization of A-type FHFs at AIS of cerebellar granule neurons, we performed immunofluorescence experiments on cultured cerebellar granule neurons. Dissociated cerebellar granule neurons were maintained in culture for 14 days and than processed by immunofluorescence for detection of A-type FHFs and PAN sodium channels or A-type FHFs and AIS marker AnkyrinG. As before, TOPRO was used as a nuclear stain in one of the experiments. Data presented in Figure 6.6 are in agreement with our previous reports. Virtually all cultured granule neurons exhibited staining of A-type FHFs at AISs as confirmed by co-locaization with sodium channels and AnkyrinG.

6.2.5 Endogenous A-type FHFs can be detected at the somas of DRG neurons but not at the nodes of Ranvier

As mentioned before, A-type FHFs have broad neuronal tissue distribution and their subcellular localization profiles often overlap those characteristic for sodium channels. Nonetheless, there are examples of neuronal compartments rich in sodium channels and free of A-type FHFs. As illustrated in Figure 6.7 (A-H) cryosections of DRG neurons stained positive for FHF2 at the cell bodies and the sensory nodes of Ranvier. In contrast adjacent DRG cryosection processed with anti-PAN sodium channel and anti-A-type FHF antibodies yield comparable staining of the cell bodies (Figure 6.8 (A-C)) and only sodium channel positive

signals at nodes of Ranvier (Figure 6.8 (D-F)). Taking together, the results of these experiments strongly argue that A isoforms of FHF are not expressed at distal nodes of DRG neurons. The FHF2 positive nodes depicted in the Figure 6.7 (H) refer to the localization of B isoform of FHF2.

6.2.6 A-type FHFs directly interact with sodium channels endogenously expressed in cerebellum and cortex of WT mouse brain

To demonstrate that A-type FHFs not only co-localize but also directly interact with sodium channels, we performed co-immunoprecipitation experiment. WT and FHF1 and FHF4 double mutant (KO) mice were used in preparation of TritonX-100 brain lysates from dissected cerebellum and cortex. A mouse monoclonal anti A-type FHF antibody was used to immunoprecipitate all endogenous A isoforms of FHF. The aliquots of brain lysates used in co-IP experiment, along with the captured immunoprecipitates were resolved on 7.5% and 12.5 % polyacrylamide-SDS gel. Following the transfer to PVDF membrane, blots were cut and processed separately. A mouse monoclonal anti A-type FHF antibody was used to detect A-type FHFs, and a mouse monoclonal anti-PAN sodium channel antibody was used to detect sodium channels. Both blots were additionally probed with the secondary goat anti-mouse HRP conjugated antibody, and immunoreactive proteins were detected on film with ECL reagent. Sodium channels were present in all tested brain lysates (Fig. 6.9, left, upper panel). A-type FHFs were robustly expressed in the cerebral cortex of WT and KO mice (Fig. 6.9, left lower panel, lanes 2 and 4). To the lesser extent A-type FHFs were present in WT cerebellum, and their expression was virtually abolished in the mutant cerebellum (Fig. 6.9, left lower panel, lanes 1 and 3 respectively). As mentioned before, the reduced levels of A-type FHFs in the cerebellum extract was due to the lack of FHF2 expression in that part of the brain, and the fact that in the

KO mice cerebellum the only FHF that could be expressed is FHF3. As presented (left, lower panel, lane 3) the FHF3A signal doesn't exceed the background levels and therefore KO cerebellum lysate was used in co-IP experiment as a negative control. A-type FHF specific antibody efficiently immunoprecipitated A isoform of FHF from WT cerebellum and cortex and KO cortex (right, lower panel, lanes 5, 6, 8). Captured A-type FHFs formed precipitable complexes with sodium channels and the intensity of the sodium channel signals was comparable with the intensity of corresponding A-type FHFs bands (right, upper panel lanes 5, 6, 8). Presented experiment further demonstrates the specificity of the mouse monoclonal anti A-type FHF antibody and its utility in the detection of this particular subtype of FHFs in the native, neuronal tissues. The experimental data greatly substantiates the immunohisto- and the immunocytochemistry findings by demonstrating that A-type FHFs not only co-localize with sodium channels in various cellular compartments but also directly interact with each other.

6.2.7 A-type FHFs accumulate preferentially at proximal but not distal axonal compartments of cerebellar granule neurons

The ultimate goal of A-type FHF subcellular localization studies was to gain insight into the biological function of these FHFs at particular cellular compartments. Because of limitations of the immmunostaining technique, further characterization of FHFs distribution in axonal compartments was conducted using Western blot analysis. In order to determine the ratio of A-type FHFs to sodium channels at proximal and distal regions of the axon, two different axonal preparations were generated. The "total axon prep" containing entire axons of cerebellar granule neurons was prepared by the mechanical separation of axons from cell somas, followed by the differential centrifugation and lysis in the Triton buffer. The "distal axon prep" was obtained

from the compartmentalized cerebellar granule neuron cultures established on filter membranes. The physical dimensions of the filter's pores allow for the maintenance of cell somas at the top portion of the filter, and the growth the axons at filter's bottom. The thickness of the filter membrane further guaranteed that the bottom portion of the filter would contain predominantly axons without AISs. Following 21 days in culture, the distal axons of cerebellar granule neurons were harvested from the bottom portion of the filter membranes, spun down, and lysed in Triton buffer. Aliquots of both axonal preparations were resolved on 7.5% and 12.5% polyacrylamide-SDS gel, transfered to PVDF membrane and probed with antibodies specific for detection of PAN sodium channels and A-type FHFs. Blots with comparable intensity of sodium channel signals in the total and distal axon preps are shown in Figure 6.10 (upper panel, lanes 1 and 2). A-type FHF bands (lower panels, lanes 1 and 2) were far more strongly detected in the total axons compared to distal axons. Therefore, there are reduced amounts of A-type FHFs per sodium channel in the distal portion of the axons (lane 2). Combining the outcome of this experiment with our knowledge of modulatory capabilities of A-type FHFs, we propose, that A-type FHF's function in axonal compartments is to modulate action potential generation proximally, but not action potential propagation distally.

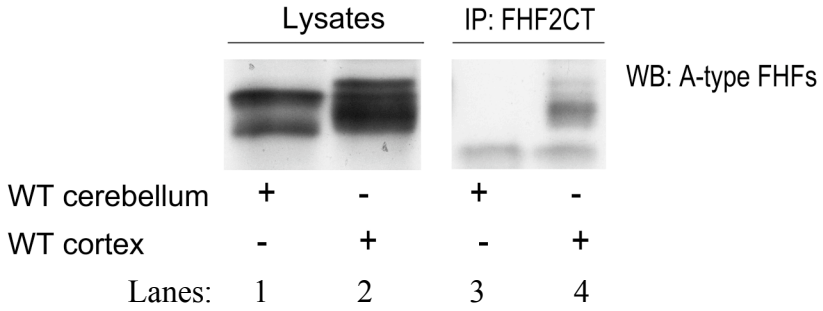

Figure 6.1. A-type FHF specific antibody detects FHF2A in FHF2 pull down assay

Triton X-100 extracts of WT mouse cerebellum and cortex were immunoprecipitated with rabbit polyclonal anti-FHF2 C-terminus antibody. An aliquots of total protein lysates and captured immunoprecipitates were electrophoresed on 15% polyacrylamide-SDS gel, transferred to PVDF membrane and probed with mouse monoclonal anti-A-type FHF antibody. A-type FHF positive bands were detected between 25 and 37 kDa molecular weight markers. Left panel shows positive detection of endogenous A-type FHFs in cerebellum and cortex of the mouse brain. Note differential expression of A-type FHFs in those brain regions. The reduced number of the bands in WT cerebellum confirms the lack of FHF2 expression in the cerebellum. As expected, in the FHF2 pull-down assay, FHF2A was detected in the cortex but not in the cerebellum (negative control). Based on the outcome of this experiment it was concluded that A-type FHF specific antibody from NeuroMab is suitable for the detection of A-type FHFs in the neuronal tissues.

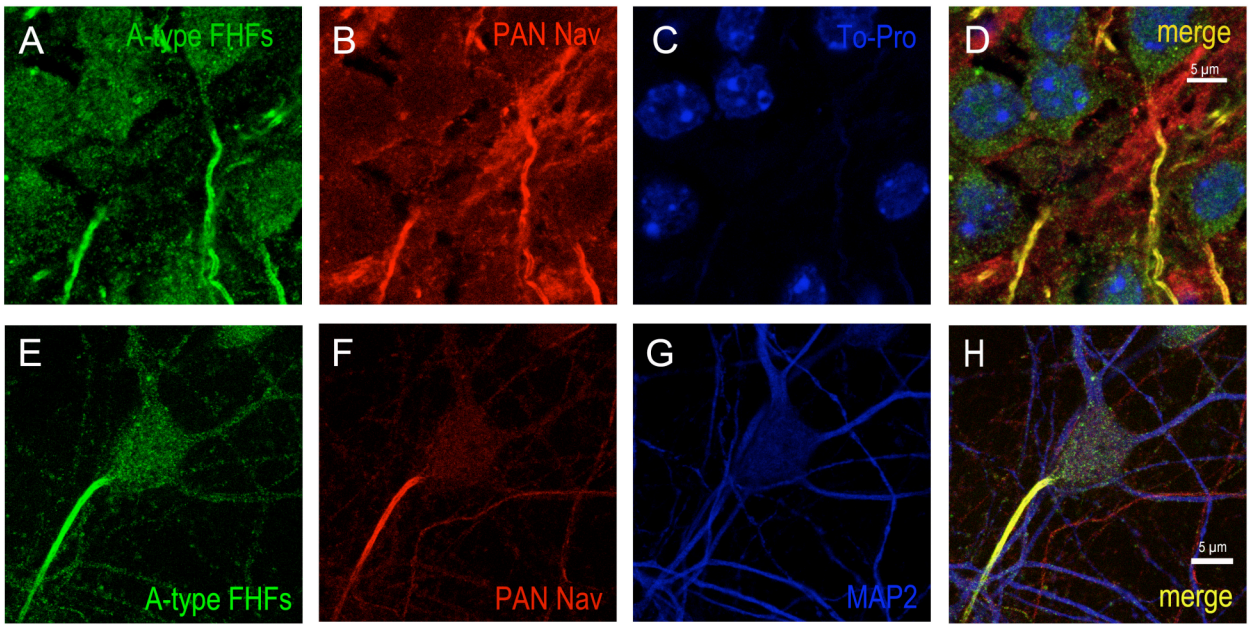

Figure 6.2 Endogenous A-type FHFs are enriched at AIS of hippocampal neurons

20 µm saggital cryosections where prepared from WT adult mouse brain and immunolabeled with antibodies specific for detection of A-type FHFs (panel A, green) and PAN sodium channels (panel B, red). The nuclei were labeled with TOPRO (panel C, blue). The superimposed confocal images revealed co-localization of A-type FHFs with sodium channels at AIS of hippocampal neurons (panel D, yellow). Similar immunostaining experiment was performed on dissociated rat hippocampal neurons cultured on coverslips for 12 days. Confocal images of the representative hippocampal neuron depicting the enrichment of A-type FHFs (green) and sodium channels (red) at AIS are presented in panels E and F respectively. The addition of MAP2 staining (panel G, blue) allowed for discrimination of axons (weak signal) from the dendrites (strong signal). Superimposed images E-G show enrichment and co-localization of A-type FHFs and sodium channels at the axon but not at dendrites of the hippocampal neuron (panel H, yellow).

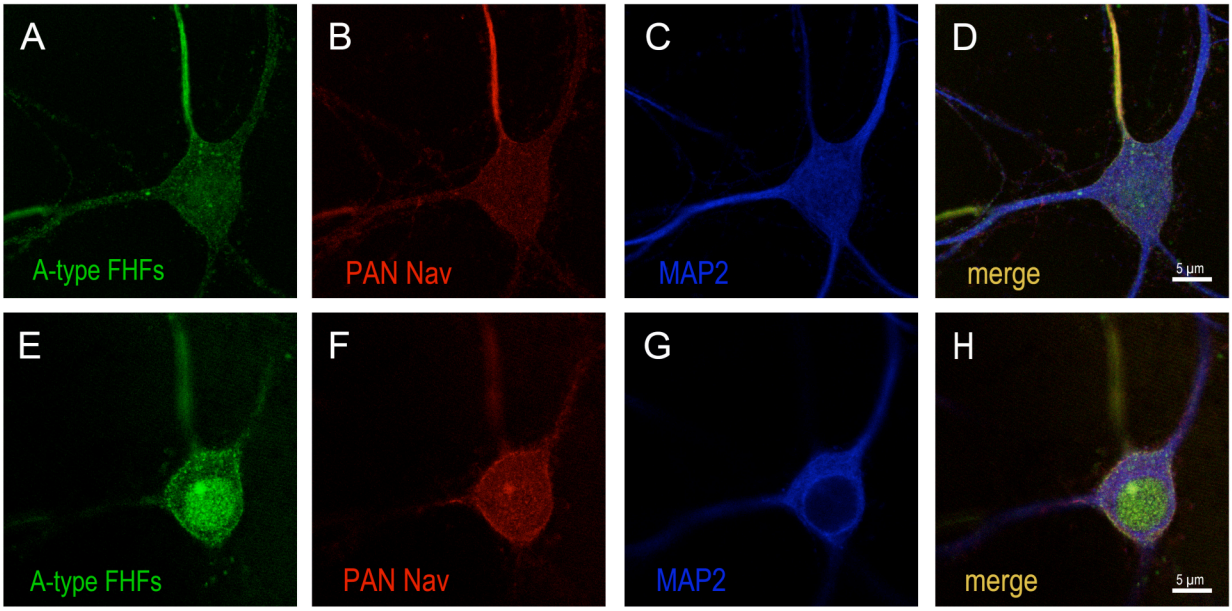

Figure 6.3 Subcellular localization of endogenous A-type FHFs in cultured hippocampal neurons

Rat hippocampal neurons maintained in culture for 12 days were fixed and processed for immunofuorescence with antibodies specific for the detection of A-type FHFs (panels A and E, green), PAN sodium channels (panels B and F, red), and MAP2 (panels C and G, blue). Superimposed confocal images obtained from two different confocal planes show enrichment and co-localization of A-type FHFs and sodium channels at AIS (panel D, yellow), co-localization of A-type FHFs and sodium channels at plasma membrane (panel H, yellow outline of the cell), and the accumulation of A-type FHFs at the nucleus of hippocampal neurons (panel H, green center).

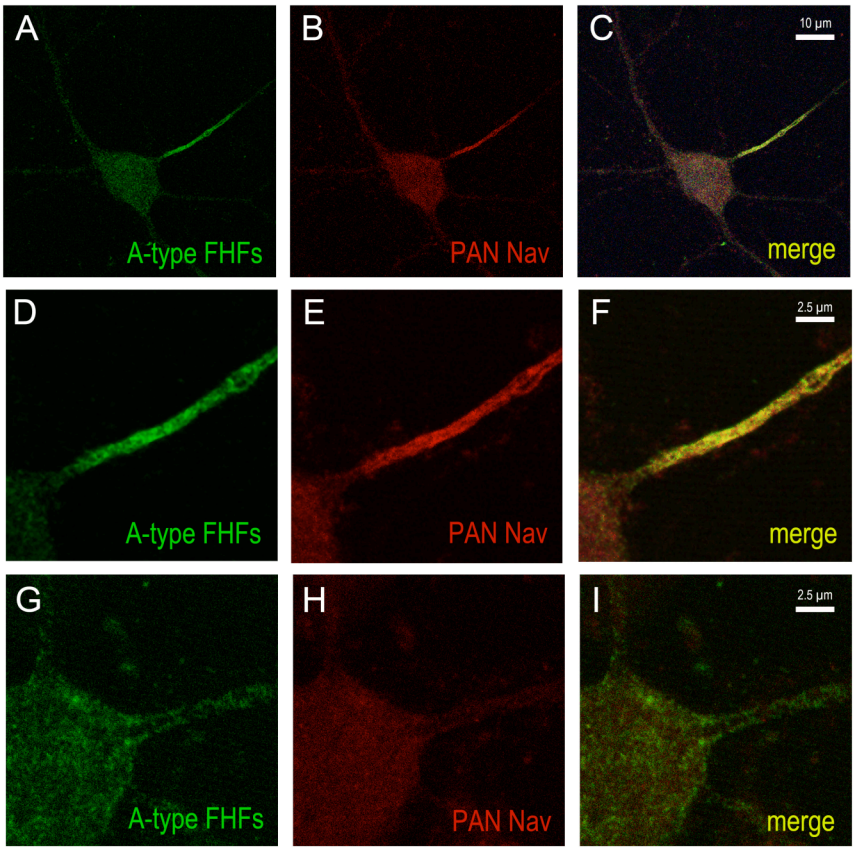

Figure 6.4 Axonal versus dendritic distribution of A-type FHFs in cultured hippocampal neurons.

A-C) Confocal images depict a cultured hippocampal neuron immunolabelled with antibodies specific for A-type FHFs (green) and PAN sodium channels (red). Enlarged, representative images of the axon (panels D-F) and the dendrite (panels G-I) allow for comparison of the subcellular distribution of A-type FHFs in those two distinct cellular compartments. Although, in comparison to the AIS, A-type FHF staining is weak at dendrites of hippocampal neurons, their expression level matches that of sodium channels (compare panel G and H). Also, the outline character of the A-type FHF and PAN sodium channel signals suggests membrane as opposed to the cytoplasmic distribution of both proteins in dendritic compartments.

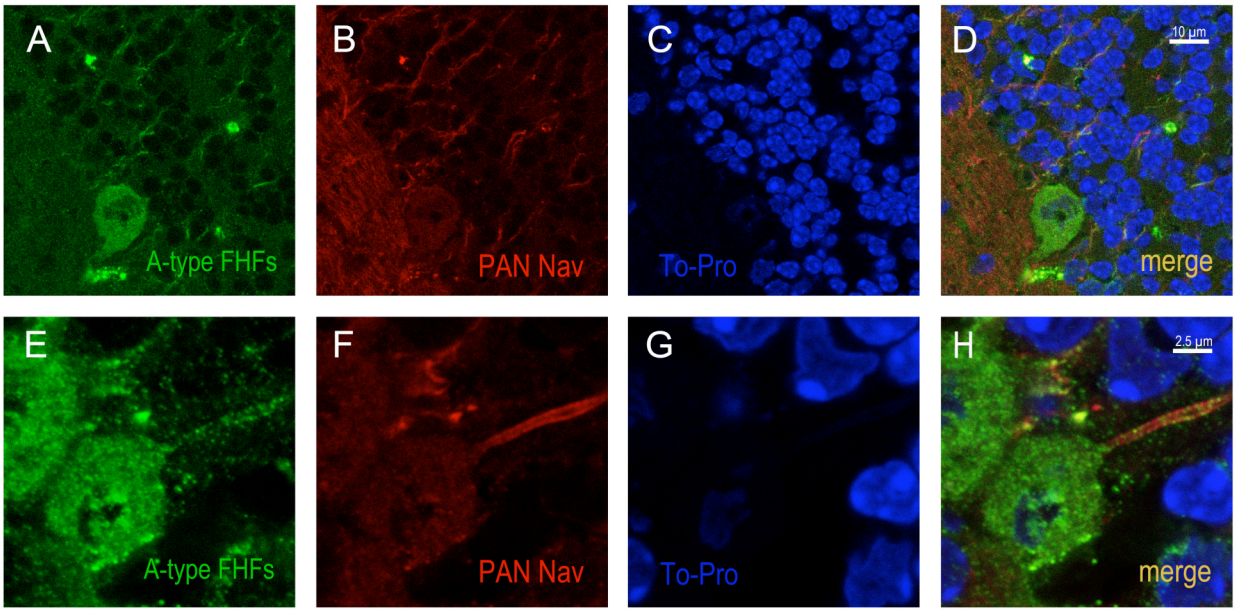

Figure 6.5 Endogenous A-type FHFs co-localize with sodium channels at AISs of cerebellar granule neurons and to the lesser extent with AIS of the Purkinje neurons in the WT mouse brain.

Confocal images of the molecular and the granular layers of the WT mouse cerebellum immunolabelled with anti- A-type FHF antibody (panel A and E, green), anti-PAN sodium channel antibody (panels B and F, red) and the nuclear stain TOPRO (panels C and G, blue). Merged images show an overlapping localization of A-type FHFs and sodium channels at AISs of cerebellar granule neurons and Purkinje neurons (panels D and H, yellow) and the accumulation of A-type FHFs in the cytoplasmic compartments of the Purkinje neurons (panels D and H, green). Note the reduced A-type FHF signals at the AIS of Purkinje neurons suggesting that A-type FHFs are not a dominant isoform of FHF in this particular neuronal compartment.

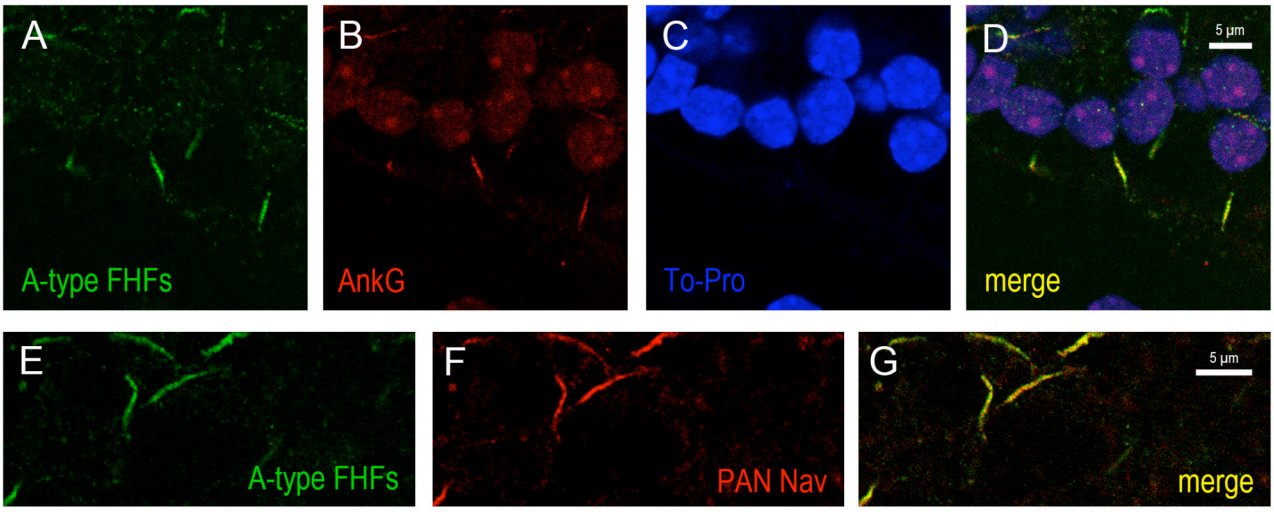

Figure 6.6 Endogenous A-type FHFs co-localize with sodium channels and AnkyrinG at AIS of cultured cerebellar granule neurons

WT mouse cerebellar granule neurons cultured for 14 days were fixed on coverslips and processed for immunofluorescence with antibodies specific for detection of A-type FHFs (panels A and E, green), AnkyrinG (panel B, red) or PAN sodium channels (panel F, red) and counterstained with nuclear marker TOPRO (panel C, blue). Superimposed confocal images clearly ilustrate enrichment and preferential localization of A-type FHFs to AIS of cultured cerebellar granule neurons (panels D and G, yellow).

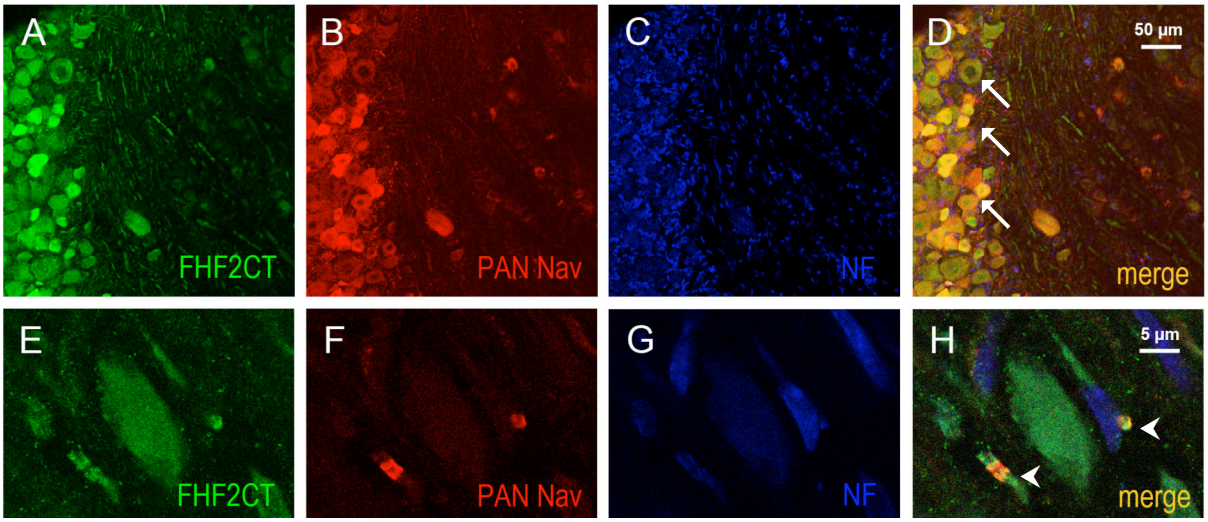

Figure 6.7 Positive detection of FHF2 at cell somas and nodes of Ranvier of DRG neurons. 20 µm cryosections of DRG neurons were prepared from adult WT mice and immunolabeled with antibodies specific for detection of C-terminal end of FHF2 (panel A and E, green), PAN sodium channels (panel B and F, red) and neurofilament (panel C and G, blue). Superimposed confocal images show differential expression of FHF2 in cell somas of DRG neurons and co-localization with sodium channels in cytoplasmic compartments (panel D, yellow). FHF2 was also detected at nodes of Ranvier where it co-localized with sodium channels (panel H, yellow). Inserted full arrows (↖) point at double positive, different diameter DRG cell somas; arrowheads (➤) point at double positive nodes of Ranvier.

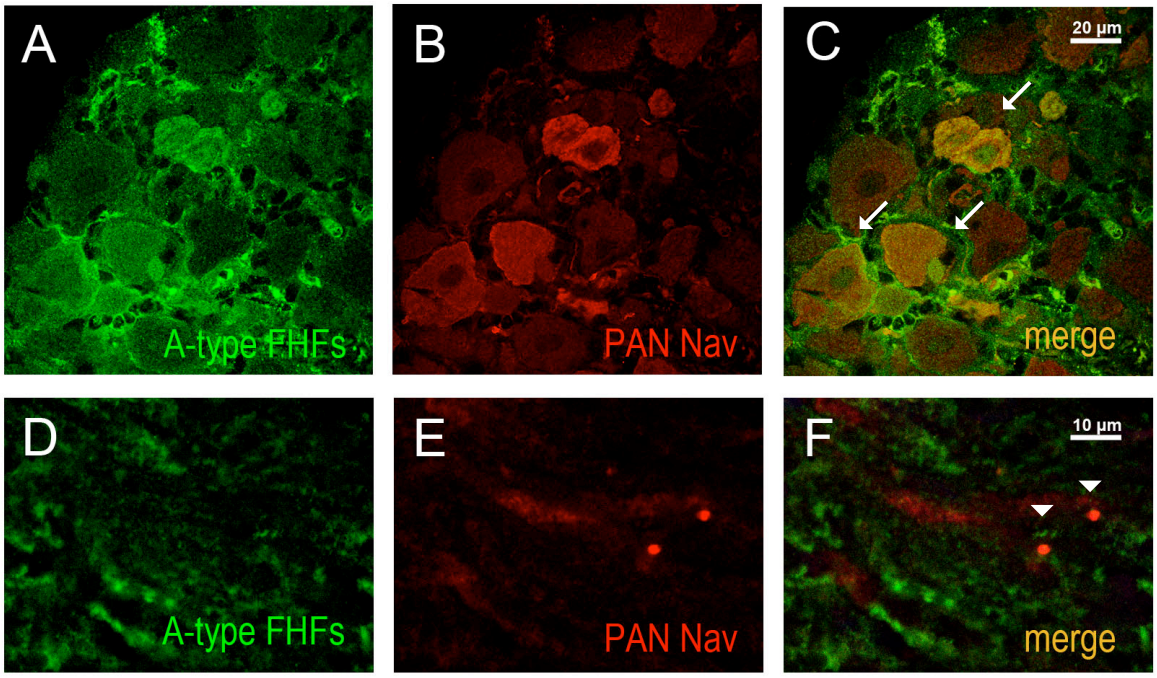

Figure 6.8 A-type FHFs co-localize with sodium channels at cell somas but not at nodes of Ranvier of DRG neurons.

20 µm cryosections of DRG neurons were prepared from adult WT mice and immunolabeled with antibodies specific for detection of A-type FHFs (panel A and D, green) and PAN sodium channels (panel B and E, red). Superimposed confocal images show differential expression of A-type FHFs in cell somas of DRG neurons and co-localization with sodium channels in cytoplasmic compartments (panel C, yellow). Tested anti-A-type FHF antibodies failed to detect A isoform of FHF at nodes of Ranvier (panel F, red), suggesting that the FHF positive node depicted in Fig. 6.7, panel H, represent B isoform of FHF2. The positive immunostaining of A-type FHFs at cell somas eliminates the possibility that the lack of A-type FHF detection at nodes of Ranvier could be due to a staining failure. Inserted arrows (↙) point at double positive DRG cell somas, arrowheads (▾) point at A-type FHF negative nodes of Ranvier.

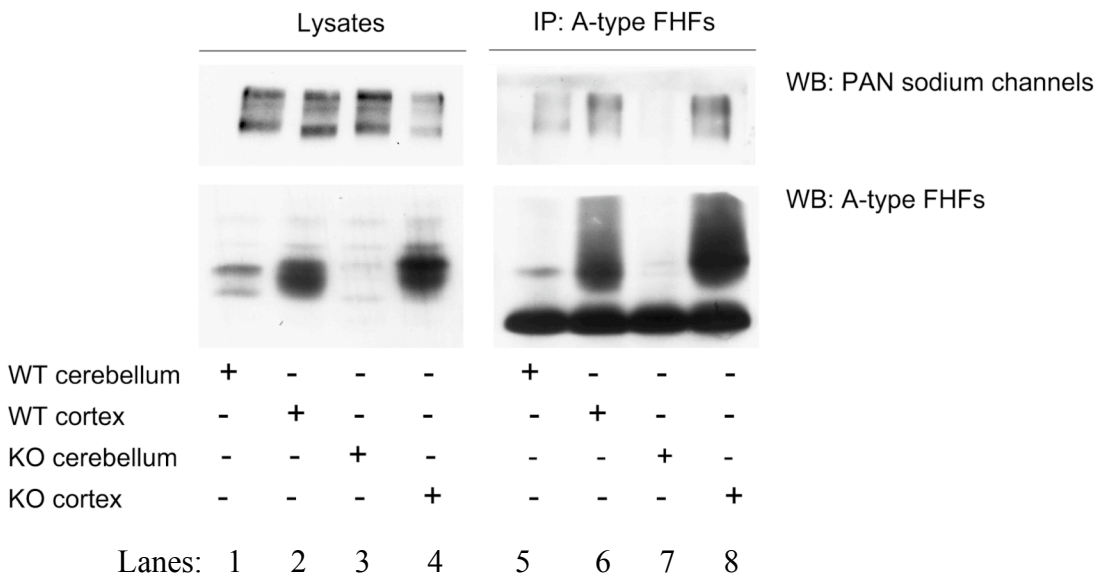

Figure 6.9 A-type FHFs directly interact with sodium channels expressed in mouse brain.

WT and FHF1/FHF4 double knockout mice (KO) were used in preparation of Triton X-100 brain lysates from dissected cerebellum and cerebral cortex. Mouse monoclonal anti-A-type FHF antibody was used to immunoprecipitate endogenous A isoforms of FHFs. The aliquots of brain lysates used in immunoprecipitation reactions along with captured and eluted precipitates were resolved on 7.5% and 12% polyacrylamide-SDS gel. Following transfer to PVDF membrane, blots were cut and processed separately for detection of PAN sodium channels and A-type FHFs. As depicted in both upper panels, sodium channels positive bands migrated above 250 kDa molecular weight marker and A-type FHF positive bands (left and right lower panels) between 25 and 37 kDa markers. Cerebellar lysate prepared from WT mice had diminished amount of A-type FHF due to the lack of the expression of FHF2 in this brain region (lane 1, left, lower panel), and cerebellar lysate prepared from KO mice served as a negative control for this experiment, since the only remaining FHF was FHF3, which was expressed at very low level (lane 3, left, lower panel). Anti A-type FHF antibody was successful in immunoprecipitating A

isoforms of FHFs from WT cerebellum and cerebral cortex and KO cortex (lanes 5, 6 and 8, right lower panel). The captured FHF were associated with sodium channels (lanes 5, 6 and 8, right upper panel). Based on the outcome of this experiment we conclude that A-type FHFs not only co-localize but directly interact with sodium channels at different neuronal compartments.

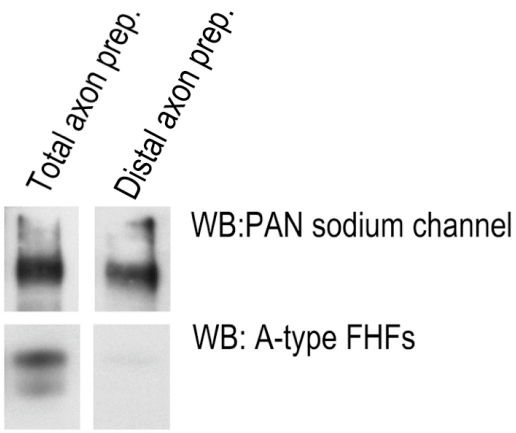

Figure 6.10 The ratio of A-type FHFs to sodium channels is higher at proximal than distal axonal compartments of cultured cerebellar granule neurons.

Triton X-100 lysates containing the entire axons of cerebellar granule neurons (Total axon prep.) and axonal lysates depleted of AISs (Distal axon prep.) were analyzed by Western Blot. Samples containing decreasing amounts of each lysate were resolved on 7.5% and 12.5% polyactrylamide-SDS gel, transferred to PVDF membrane and probed with antibodies specific for detection of PAN sodium channels and A-type FHFs. The lanes of blots showing comparable amounts of sodium channels in both lysates are presented in upper panels. The corresponding lanes on the lower blots show the amount of A-type FHFs in each sample. Sodium channel positive bands were detected above 250 kDa marker and A-type FHF positive bands migrated between 25 and 37 kDa markers. Note diminished amount of A-type FHFs in distal axon prep. (lower, right panel). The experiment demonstrates preferential localization of A-type FHFs to proximal axonal compartments of cerebellar granule neurons and suggests the role of A isoform of FHFs in modulation of cellular excitation but not conduction.

6.3 Discussion

The results presented in this study constitute a comprehensive assessment of A-type FHF distribution in the native neuronal tissues as well as cultured hippocampal and cerebellar granule neurons. Using A-type FHF specific antibody we were able to show the enrichment this particular isoform of FHFs at AIS of hippocampal and cerebellar granule neurons, cell surface of hippocampal neurons, and cell somas of DRG and Purkinje neurons. We also found a reduced amount of A-type FHFs at axons of Purkinje neurons and the lack of this isoform at nodes of Ranvier of DRG neurons. Our data faithfully recapitulated and critically validated earlier findings from in vitro transfection overexpression experiments. An attempt to map A-type FHF distribution in native neuronal tissues was reported previously by Rush et al., 2006. These authors were successful in localization of FHF2A at the cytosolic compartment of DRG neurons but failed to detect A-type FHFs at hippocamus or cerebellum of the rat brain. The reason for this disparity with our data is the type of antibody that was used. The antibody used by Rush et al was raised against an FHF2A-specific epitope approximately 35-50 residues from the N-terminus. Upon testing authors concluded: "While FHF2A anibody has been shown to be specific, it is not robust enough to be used in immunoprecipitation or immunoblot assays from native tissues". The success in immunolabeling of DRG neurons probably stems from the fact that, as indicated by in situ hybridization studies reported by Wittmack et al., 2004, FHF2 is expressed in those neurons at much higher levels than in hippocampus or cerebellum. The alternative explanation is that the FHF2A-specific immunoepitope may be obstructed upon interaction with sodium channels or with other molecules and is therefore not available for antibody detection.

A preferential localization of A isoforms of FHFs at AIS of hippocampal and cerebellar neurons strongly suggests the role of this particular isoform in the regulation of the neuronal excitability. One theory is that A-type FHF occupancy of a subset of AIS sodium channels accounts for action potential spike accommodation or attenuation. Consistent with increased A-type FHFs at AISs of hippocampal neurons compared to cerebellar granule neurons, hippocampal neurons show a greater degree of spike accommodation. The diminished presence of A-type FHFs at distal axons of cerebellar granule neurons and the lack of A-type FHFs at nodes of Ranvier of DRG neurons further suggests that this isoform is not involved in axonal action potential propagation, and that small B-type FHFs are more suitable for that task. Lastly, the preliminary data detecting low levels of sodium channels and A-type FHF in the somatodendritic compartment of hippocampal neurons is consistent with reports demonstrating use dependent inhibition of sodium channels currents recorded in the dendrites of hippocampal neurons (Spruston et al., 1997). To rule out an artifact accounting for the weak observed somatodendritic staining, immunofluorescence analysis with A-type FHF antibody should be repeated to test whether inclusion of competing immunizing peptide during staining abolishes the somatodendritic signal.

One of the less expected results was the identification of A-type FHFs at the nucleus of the cultured hipocampal neurons. Although it has been previously reported (Smallwood et al., 1996 and Wang et al., 2000) that A-type FHFs possess nuclear localization signal in their N-terminal extentions, it was thought that nuclear localization of A-type FHFs was an artificial effect due to the overexpression upon transfection. Here, for the first time we demonstrated that endogenous A-type FHFs can be found in the nuclear compartment of hippocampal neurons. Since the epitope for anti A-type FHF antibody lays within first 21 amino acid residues of the N-

terminal extension we could not determine whether processed fragment or the entire protein was translocated to the nucleus. Also, the fact that the effect was only seen in cultured hippocampal neurons and not in cultured cerebellar granule neurons raises questions whether nuclear localization of A-type FHFs is cell specific or cell stage specific. Further investigation is necessary to provide a biological explanation for nuclear localization of A-type FHFs.

Another finding that needs further investigation was the detection of high-level expression of A-type FHFs at the soma of the Purkinje neurons, combined with the relative attenuated expression of that isoform at AIS. It is possible that the composition of the cytoplasm of these neurons generates high background and the observed result could be an artifact. To address this issue a side-by-side immunohistochemistry staining should be performed on brain cryosections prepared from the WT and FHF1/FHF4 double knockout mice (KO), using anti A-type FHF specific antibody. We would expect that KO Purkinje neurons expressing only FHF3 would have lower somatic levels of A-type FHFs. Including the study of A-type FHF expression in the brain and DRG neurons obtained from the FHF1/FHF4 KO mice would complete the survey of A-type FHF localization in native neuronal tissues.

SUMMARY

In five chapters of this document, I reported several findings implicating FHFs as modulators of voltage gated channels (VGSCs). Using a combination of biochemistry, molecular genetics and whole-cell electrophysiology recordings, a channel-binding surface common to all FHFs was determined. It was shown that this surface is necessary not only for the interaction with C-terminal end of VGSCs but also for the maintenance of FHFs function as channel modulators.

For the first time all major FHF isoforms were studied in a uniform system (Neuroblastoma cell line stably expressing tetrodotoxin resistant version of sodium channel Nav1.6) and evaluated for ability to modulate sodium channel Nav1.6. Based on the outcome of the screen, FHF isoforms were categorized into three functional groups. FHFs with long N-terminal extentions i.e. A-type FHFs and FHF4B having a strong effect on voltage dependence of channel inactivation and smaller B-type FHFs having short N-terminus and modest effect on channel inactivation. In addition, only in the presence of A-type FHFs could a long-term, use-dependent inactivation be observed.

Intrigued by this result, the N-terminal extension of FHF2A, a representative member of A-type FHFs, was studied extensively. Two clusters of positively charged residues were mutated to Q and assayed by whole-cell voltage clamp recordings. It was determined that residues proximal to the core of FHF have an effect on voltage dependence of channel inactivation while residues located in a distal N-terminal end form an inactivation particle, responsible for induction of long-term, use dependent channel inactivation.

The molecular model of long-term, use-dependent channel inactivation was proposed and investigated. According to the model, FHF-derived inactivation particle resembles channel-intrinsic IFM particle. During inactivation both particles exposed to the cytoplasm compete for the ability to inactivate channels. Channels inactivated by IFM particle recover fast (few milliseconds) while channels inactivated by FHF-derived particle recover slower (hundreds of milliseconds). Upon high frequency stimulations channels inactivated by A-type FHFs become unavailable for ion conduction. The accumulation of inactivated channels reduces inward sodium current and leads to suppression of high frequency neuronal firing.

To complete the survey on the biological function of A-type FHFs, the differential localization of that particular isoform was investigated in the central and peripheral nervous system and in cultured neurons. It become apparent that A-type FHFs can be detected at multiple regions of the mouse brain and their overall expression pattern differs from that characteristic for sodium channels. At cellular level, A-type FHFs were detected in the soma and axon initial segment of cerebellar, hippocampal and Purkinje neurons and in the soma of DRG neurons, but not at distal regions of myelinated or unmyelinated axons.

CHAPTER VII

Discussion

7.1 Discussion and future directions

As with every new discovery, new knowledge generates more questions. In this chapter I will address some of them, raised upon accumulating new data on the physiology and cellular localization of different isoforms of FHFs. I will also discuss major results, and point to new directions FHF research could take.

The results described by Goetz at al., 2009 and our data summarized in Chapter III demonstrate the existence of the universal channel-binding surface located within the core of all FHFs. However, as presented by Wittmack et al., 2004, Rush et al., 2006, Goldfarb et al., 2007, Leazza et al., 2009 and by us in Chapter VI, not all FHFs are equally distributed in neuronal compartments, and only FHFs with long N-terminal extensions (FHF4B and A-type FHFs) are enriched at AIS. This raises the possibility that N-terminal extensions of long FHFs contain motifs responsible for sorting/retention of these particular isoforms at the AIS. The search for the molecular determinants, responsible for AIS localization of FHF4 was initiated by Leazza et al., 2009. The deletion of N-terminus of FHF4B abolished localization of the truncated variant of FHF4B to AIS in cultured hippocampal neurons. By further extending deletion and mutagenesis studies it would be possible to map the AIS sorting/retention domain. A good candidate for this study is a centrally located region on N-terminal extension of FHF4B, which contains small groups of highly conserved residues common to FHF4B and A-type FHFs. Beside this region and the cluster or basic residues located close to the core of the protein, FHF4B does not share sequence homology with A-type FHFs. Once identified, AIS sorting/retention motif could be linked to GFP protein and investigated whether, alone, it is sufficient for guidance of tagged GFP

to AIS. Proposed experiments are easy to perform and would yield important insights into differential localization of FHF isoforms and the organization of AIS.

In Chapter V we proposed a molecular model of long-term inactivation of sodium channels by A-type FHFs. Our model strongly relies on voltage driven channel transitions described by Pathak et al., 2007 on the much better studied potassium channels, and on the shared similarities between channel's intrinsic IFM particle and A-type FHF derived long-term inactivation particle. During the course of our investigation we were very successful in replicating findings published by Smith and Goldin et al., 1997, demonstrating that alanine (A) to glutamine (Q) substitution mutation in position 1329 of rat brain sodium channel Nav1.2 affects fast inactivation. The analogous point mutation introduced to the docking site of Nav1.6 channel lowers the affinity of fast inactivation particle for the docking site and allows the long-term inactivation to accumulate in a time dependent manner. Since the magnitude of the long-term inactivation wasn't affected by the A to Q mutation, it has to be determined which residues within the docking site or inner vestibule of the sodium channel are involved in interaction with long-term inactivation particle. Considering the larger molecular surface of the long-term inactivation particle (20 vs. 8 amino acid residues in fast inactivation particle), finding an individual residue critical for direct interaction with the sodium channel might be difficult. Also finding the combination of residues that would cooperatively abolish or destabilize interaction of the sodium channel with the long-term inactivation particle is challenging for two reasons. First, introducing the combination of mutations can interfere with proper channel folding and stability. Second, it is often the case that mutated residues have an effect on other parameters of channel's physiology. Fully aware of those challenges, current experiments performed in our lab aim to localize sites of direct interaction of sodium channels with long-term inactivation particles. The

candidate residues for substitution mutation include highly conservative residues phenylalanine (F) and valine (V) located within S6 subunit of domain IV of sodium channel Nav1.6. As reported by Sunami et al., 2004 the equivalent residues in sodium channel Nav1.4 are exposed to the inner pore of the channel and are involved in the direct interaction with local anaesthetic and antiarrhythmic drugs. Finding the receptor site on the sodium channel for the long-term inactivation particle would strengthen proposed model of channel inactivation in the presence of A-type FHFs and provide valid information for the future development of the particle into a successful drug for treatment of disorders of hyperactivity.

To describe A-type FHF induced inhibition of sodium currents we chose the term "long-term" inactivation over more frequently used term "slow" inactivation. Our choice was not purely aesthetic but intended to convey the message that the described phenomenon differs from classical slow inactivation. Three major factors distinguish long-term inactivation from other types of slow inactivation. First, the newly described process can only be recorded in the presence of A-type FHFs, or A-type FHF derived long-term inactivation particle. Second, the kinetics of long-term inactivation did not fit the parameters characteristic for other types of slow-inactivation. Especially, the onset of the long-term inactivation is much faster, measured on the time scale of milliseconds as opposed to seconds or minutes. Third, in order to accumulate sodium channels into long-term inactivated state, channels have to be cycled through, or near to, the open state (the requirement not necessary for the accumulation of channels into slow inactivation). Since the molecular pathway leading to the development of slow inactivation of channels is still unknown it is difficult to predict whether A-type FHFs enhance existing pathways or act through a separate, slow inactivation-unrelated mechanism. It is also possible that those two processes could occur simultaneously. The results of whole-cell voltage

recordings in the absence of A-type FHFs show accumulation (up to 10%) of channels into inactivated state in the fourth 16 ms depolarization cycle. In the same experiment in the presence of FHF2A sodium channels inactivation reached 50%. Since, in addition to prolonged depolarization, slow inactivation can be induced by high frequency stimulation, the observed minor reduction in sodium channel availability in the absence of A-type FHFs may represent early development of slow inactivation. In the future it would be interesting to further explore these two processes. Experiments can be designed to check whether factors affecting slow inactivation have a similar effect on long-term inactivation. For example, Cheng et al., 2006 reported that substitution mutation involving highly conserved residue asparagine (N), located within S6 segment of domain III, to more hydrophobic alanine (A) increased slow inactivation, while analogous substitution mutation to more hydrophilic aspartate (D), completely abolished it. It would be interesting to see if these mutations have an effect on long-term inactivation. Considering the rapid onset of long-term inactivation we also hypothesize that events such as channel phosphorylation by PKA and PKC, known to affect slow-inactivation (Carr et al., 2003, Chen et al., 2006), are not involved in the development of long-term inactivation. This could be tested by performing whole-cell, voltage clamp recordings on Neuro 2A cells expressing A-type FHFs in the presence of PKA and PKC inhibitors. Being able to differentiate between slow and long-term, use-dependent inactivation would facilitate discerning the biological function of A-type FHFs.

Discovering the long-term inactivating particle was a highlight of my research on FHFs. Because of its selective ability to reduce sodium ion influx into the cell exposed to high frequency stimulation, it holds the promise of being an ideal treatment for disorders of hyperexcitability such as epilepsy or cardiac arrhythmia. Needless to say, there are challenges

that have to be overcome in order to transition this 20 amino acid long particle from the theoretical concept to a medical treatment. In order to exert its function the particle has to be delivered to the affected area at high enough concentration to overcome the lack of tethering to C-terminal end of sodium channel.

The elucidation of the molecular mechanism underlying long-term inactivation of voltage gated sodium channels by A-type FHFs was in the center of my thesis project. In addition to learning much about this process, we also gain some insights into another important function of FHFs, which is modulation of voltage dependence of channel steady-state inactivation. By screening FHF2A mutants, bearing glutamine mutations introduced into two clusters of basic residues within N-terminal extension of FHF2A (5Q, 7Q mutants) we recorded, that 7Q mutant, lost the ability to induce the depolarizing shift in $V_{1/2}$ of inactivation of sodium channel Nav1.6. The fact that 7Q mutant was still capable of inducing long-term inactivation of channels argues against possibility that introduced mutations destabilized FHF2A and abolished its ability to interact with the C-terminal end of the sodium channel. This observation, still preliminary, could be an initial step in a search for the molecular determinants underlying modulation of voltage dependence of channel inactivation by different isoforms of FHF. The data presented in the Chapter IV demonstrate that only A-type FHFs and FHF4B induce strong depolarizing shift in $V_{1/2}$ of inactivation of sodium channel Nav1.6 and several other channel endogenously expressed in Neuro2A cells. Since N-terminal extensions of A-type FHFs and FHF4B don't exhibit substantial sequence homology, the cluster of basic residues located proximally to the core of A-type FHFs and FHF4B seems the only common denominator. By introducing glutamine (Q) mutations into the cluster of basic residues on FHF4B it could be possible to determine the role of these residues in modulation of sodium channel inactivation. If the results obtained for

FHF2A (7Q) mutant could be replicated with FHF4B (5Q) construct, further experiments could include screening charge reversal and charge substitution mutants of FHF2A and FHF4B. Assuming that FHFs tethered to the C-terminal end of voltage gated sodium channels are in proximity of the channel's pore, or are brought to that region during voltage driven conformational rearrangements, the concept of highly positively charged region having an effect on channels behavior should not be dismissed without proper examination. One of the working hypothesis for this study could be that electrostatic repulsion between positively charged residues provided by FHFs and charged residues surrounding IFM particle interfere with docking of the fast inactivation particle and additional voltage driven channel transitions are necessary for the completion of fast inactivation. The elucidation of the molecular mechanism underling FHF's modulatory effect on voltage dependence of sodium channel inactivation is of high importance considering broad distribution of A-type FHFs in neuronal tissues and the fact that missense mutation (F149S) in FHF4B is responsible for human disorders such as spinocerebellar ataxia (SCA27), paroxysmal dyskinesia and mental retardation (Wang et al., 2002, van Swieten et al., 2003, Dalski et al., 2005, Brusse et al., 2006, Wozniak et al., 2007).

The hardest question to address is: What are the biological functions of A-type FHFs? Considering they modulatory capabilities and AIS localization, A-type FHFs govern cellular excitability. By inducing a depolarizing shift in $V_{1/2}$ of inactivation they lower the threshold for action potential generation and promote excitability. On the other hand due to the action of long-term inactivation particle under condition of high frequency stimulation A-type FHFs can limit or completely abolish neuronal firing. Unlike slow inactivation, which can develop upon high frequency or prolong depolarization, the role of A-type FHFs is limited to controlling processes involving high frequency events. This dichotomy in function suggests, that A-type FHFs can

filter trains of action potentials and translate it to burst patterns were the first spike is the strongest following by rapid decline, hence the role in shaping patterns of neuronal firing. Referring to our results from subcellular localization studies, where we documented that A-type FHFs do not localize to nodes of Ranvier of DRG neurons and are depleted at distal axonal compartments of cerebellar granule neurons, we propose, that A-type FHFs are involved in controlling of action potential generation but not action potential propagation. B type FHFs endowed with lesser modulatory capabilities and devoid of long-term inactivation particle seem to be better suited for this task. The localization of A-type FHFs in somato-dendritic compartments has to be further investigated. If confirmed, A-type FHF could be further tested for their influence on action potential back propagation and synaptic integration. One thing is for certain: A-type FHFs are involved in preserving the history of previous activity in the neuron; due to much faster onset than slow inactivation, their role in shaping of cellular plasticity might be more significant than previously suspected.

7.2 Closing remarks

Working on the FHF project was a privilege and an honor. Solving an array of problems, large and small, was exciting and personally satisfying. I had the benefit of working hard with the best, but also the luxury of ample time to use my imagination, to think and wonder. I can assure you, that at times when my hands weren't busy with experiments, my mind was searching for answers. There was hardly a day off from FHFs. I hope your research projects are as dear and rewarding to you, as FHF was to me. Thank you, from the bottom of my heart for your service on this committee.

Sincerely,

Kasia Dover

Bibliography

Balser, J. R., Nuss, H. B., Chiamvimonvat, N., Perez-Garcia, M. T., Marban, E. and Tomaselli, G. F. (1996). External pore residue mediates slow inactivation in mu 1 rat skeletal muscle sodium channels. J Physiol 494, 431–442.

Boiko, T., Rasband, M.N., Levinson, S.R., Caldwell, J.H., Mandel, G., Trimmer, J.S., Matthews, G. (2001). Compact myelin dictates the differential targeting of two sodium channel isoforms in the same axon. Neuron 30, 91–104.

Boiko, T., Van Wart, A., Caldwell, J.H., Levinson, S.R., Trimmer, J.S., Matthews, G. (2003). Functional specialization of the axon initial segment by isoform-specific sodium channel targeting. J. Neurosci. 23, 2306–2313.

Brusse, E., de Koning, I., Maat-Kievit, A., Oostra, B.A., Heutink, P., van Swieten, J.C. (2006). Spinocerebellar ataxia associated with a mutation in the fibroblast growth factor 14 gene (SCA27): a new phenotype. Mov. Disord. 21, 396–401.

Burbidge, S. A., Dale, T. J., Powell, A. J., Whitaker, W. R., Xie, X. M., Romanos, M. A. and Clare, J. J. (2002). Molecular cloning, distribution and functional analysis of the NA(V)1.6. Voltage-gated sodium channel from human brain. Brain Res Mol Brain Res 103, 80–90

Cannon, S. C. (1996). Sodium channel defects in myotonia and periodic paralysis. Annu Rev Neurosci 19, 141–164.

Carle, T., Fournier, E., Sternberg, D., Fontaine, B. and Nacira Tabti (2009). Cold-induced disruption of Na+ channel slow inactivation underlies paralysis in highly thermosensitive paramyotonia. The Journal of Physiology, 587, 1705-1714.

Carr, D.B., Day, M., Cantrell, A.R., Held, J., Scheuer, T., Catterall, W.A. and Surmeier, D.J. (2003). Transmitter modulation of slow, activity-dependent alterations in sodium channel availability endows neurons with a novel form of cellular plasticity. Neuron 39, 793–806.

Catterall, W. A. (2000). From ionic currents to molecular mechanisms: the structure and function of voltage-gated sodium channels. Neuron 26, 13–25.

Catterall, W. A., Goldin, A. L. and Waxman, S. G. (2005). International Union of Pharmacology. XLVII. Nomenclature and structure-function relationships of voltage-gated sodium channels. Pharmacol Rev 57, 397–409.

Chancey, J.H., Shockett, P.E. and O'Reilly, J.P. (2007). Relative resistance to slow inactivation of human cardiac Na+ channel hNav1.5 is reversed by lysine or glutamine substitution at V930 in D2-S6. Am J Physiol Cell Physiol 293, C1895–1905.

Chen, C, Westenbroek, R. E., Xu, X., Edwards, C. A., Sorenson, D. R., Chen, Y., McEwen, D. P., O'Malley H. A., Bharucha, V., Meadows, L. S., Knudsen, G. A., Vilaythong, A., Noebels, J. L., Saunders, T. L., Scheuer, T., Shrager, P., Catterall, W. A and Isom, L. L. (2004). Mice lacking sodium channel beta1 subunits display defects in neuronal excitability, sodium channel expression, and nodal architecture. J Neurosci 24, 4030–4042.

Chen, Y., Yu, F.H., Surmeier, D.J., Scheuer, T. and Catterall, W. A. (2006). Neuromodulation of Na+ channel slow inactivation via cAMP-dependent protein kinase and protein kinase C. Neuron 49, 409–420.

Coulier, F., Pontarotti, P., Roubin, R., Hartung, H., Goldfarb, M., and Birnbaum, D. (1997). Of worms and men: an evolutionary perspective on the fibroblast growth factor (FGF) and FGF receptor families. J Mol Evol. 44, 43-56.

Cronin, N. B., O'Reilly, A., Duclohier, H., Wallace, B. A. (2003). Binding of the anticonvulsant drug lamotrigine and the neurotoxin batrachotoxin to voltage-gated sodium channels induces conformational changes associated with block and steady-state activation. J. Biol. Chem. 278, 10675–1068.

Cummins, T.R., Dib-Hajj, S.D., Herzog, R.I., Waxman, S.G. (2005). Nav1.6 channels generate resurgent sodium currents in spinal sensory neurons. FEBS Lett. 579, 2166–2170.

Dalski A, Atici J, Kreuz FR, Hellenbroich Y, Schwinger E & Zuhlke C (2005). Mutation analysis in the fibroblast growth factor 14 gene: frameshift mutation and polymorphisms in patients with inherited ataxias. Eur J Hum Genet 13, 118–120.

Eaholtz, G., Scheuer, T., and Catterall, W. A. (1994). Restoration of inactivation and block of open sodium channels by an inactivation gate peptide. Neuron 12, 1041-1048.

Eaholtz, G., Zagotta, W. N., and Catterall, W. A. (1998). Kinetic analysis of block of open sodium channels by a peptide containing the isoleucine, phenylalanine, and methionine (IFM) motif from the inactivation gate. J Gen Physiol 111, 75-82.

Eaholtz, G., Colvin, A., Leonard, D., Taylor, C., and Catterall, W. A. (1999). Block of brain sodium channels by peptide mimetics of the isoleucine, phenylalanine, and methionine (IFM) motif from the inactivation gate. J Gen Physiol 113, 279-294.

Fleidervish, I. A., Gutnick, M. J. (1996). Kinetics of slow inactivation of persistent sodium current in layer V neurons of mouse neocortical slices. J. Neurophysiol. 76, 2125-2130.

Fleidervish, I. A., Friedman, A. and Gutnick, M. J. (1996). Slow inactivation of Na+ current and slow cumulative spike adaptation in mouse and guinea-pig neocortical neurones in slices. J. Physiol. (Lond.) 493, 83–97.

Florkiewicz, R. Z., Majack, R. A., Buechler, R. D., Florkiewicz, E. (1995). Quantitative export of FGF-2 occurs through an alternative, energy-dependent, non-ER/Golgi pathway. J Cell Physiol. 162(3), 388–399.

Fournier E., Viala K., Gervais H., Sternberg D., Arzel-Hezode M., Laforet P., Eymard B., Tabti N.,Willer J.C., Vial C. and Fontaine B. (2006). Cold extends electromyography distinction between ion channel mutations causing myotonia. Ann Neurol 60, 356–365.

Goetz, R., Dover, K., Laezza, F., Shtraizent, N., Tchetchik, D., Huang, X., Eliseenkova, A. V., Xu, C., Neubert, T. A., Ornitz, D. M., Goldfarb, M. & Mohammadi, M. (2009). Crystal structure of a fibroblast growth factor homologous factor (FHF) defines a conserved surface on FHFs for binding and modulation of voltage-gated sodium channels. J Biol Chem 284, 17883-17896.

Goldfarb, M. (2005) Fibroblast growth factor homologous factors: evolution, structure, and function. Cytokine Growth Factor Rev. 16, 215-220.

Goldfarb, M., Schoorlemmer, J., Williams, A., Diwakar, S., Wang, Q., Huang, X., Giza, J., Tchetchik, D., Kelley, K., Vega, A., Matthews, G., Rossi, P., Ornitz, D.M., and D'Angelo, E. (2007). Fibroblast growth factor homologous factors control neuronal excitability through modulation of voltage-gated sodium channels. Neuron 55, 449-463.

Goldin, A. L. (2001). Resurgence of sodium channel research. Annu Rev Physiol 63, 871–894.

Goldin, A. L. (2003). Mechanisms of sodium channel inactivation. Curr Opin Neurobiol 13, 284–290.

Groome, J.R., Dice, M.,C., Fujimoto, E., Ruben, P.,C. (2007). Charge immobilization of skeletal muscle Na+ channels: role of residues in the inactivation linker. Biophys J 93(5), 1519-33.

Groome, J. R., Fujimoto, E., Ruben, P. C. (2003). Negative charges in the DIII-DIV linker of human skeletal muscle Na+ channels regulate deactivation gating. J Physiol 548(Pt 1), 85.

Hartung, H., Feldman, B., Lovec, H., Coulier, F., Birnbaum, D. and Goldfarb, M. (1997). Murine FGF-12 and FGF-13: expression in embryonic nervous system, connective tissue and heart. Mech Dev 64, 31–39.

Isom, L.L., Scheuer, T., Brownstein, A.B., Ragsdale, D.S., Murphy, B.J. and Catterall, W.A. (1995). Functional co-expression of the beta 1 and type IIA alpha subunits of sodium channels in a mammalian cell line. J. Biol. Chem. 270, 3306–3312.

Jiang, Y., Lee, A., Chen, J., Ruta, V., Cadene, M., Chait, B.T. and MacKinnon, R. (2003). X-ray structure of a voltage-dependent K+ channel. Nature 423, 33–41.

Jung, H. Y., Mickus, T. and Spruston, N. (1997). Prolonged sodium channel inactivation contributes to dendritic action potential attenuation in hippocampal pyramidal neurons. J Neurosci 17, 6639-6646.

Kontis, K.J., and Goldin, A.L. (1997). Sodium channel inactivation is altered by substitution of voltage sensor positive charges. J. Gen. Physiol. 110, 403–413.

Laezza, F., Lampert, A., Kozel, M. A., Gerber, B. R., Rush, A. M., Nerbonne, J. M., Waxmann, S. G., Dib-Hajj, S. D. and Ornitz, D. M. (2009). FGF14 N-terminal splice variants differentially modulate Nav1.2 and Nav1.6-encoded sodium channels. Mol Cell Neurosci 42, 90-101.

Levin, S.I., Khaliq, Z.M., Aman, T.K., Grieco, T.M., Kearney, J.A., Raman, I.M., Meisler, M.H. (2006). Impaired motor function in mice with cell-specific knockout of sodium channel Scn8a (NaV1.6) in cerebellar purkinje neurons and granule cells. J. Neurophysiol. 96, 785–793.

Liu, C., Dib-Hajj, S. D., and Waxman, S. G. (2001). Fibroblast growth factor homologous factor1B binds to the C terminus of the tetrodotoxin-resistant sodium channel rNav1.9a (NaN). J Biol Chem 276, 18925-18933.

Liu, C. J., Dib-Hajj, S. D., Renganathan, M., Cummins, T. R., and Waxman, S. G. (2003). Modulation of the cardiac sodium channel Nav1.5 by fibroblast growth factor homologous factor1B. J Biol Chem 278, 1029-1036.

Lou, J. Y., Laezza, F., Gerber, B. R., Xiao, M., Yamada, K. A., Hartmann, H., Craig, A. M., Nerbonne, J. M., and Ornitz, D. M. (2005). Fibroblast growth factor 14 is an intracellular modulator of voltage-gated sodium channels. J Physiol 569, 179-193. domain in inactivation of brain and cardiac sodium channels. Proc Natl Acad Sci USA 98, 15348-15353.

McClatchey, A. I., P. Van den Bergh, M. A. Pericak-Vance, W. Raskind, C. Verellen, D. McKenna-Yasek, K. Rao, J. L. Haines, T. Bird, R. H. Brown, Jr., and J. F. Gusella. 1992. Temperature-sensitive mutations in the III-IV cytoplasmic loop region of the skeletal muscle sodium channel gene in paramyotonia congenita. Cell. 68, 769-774.

McCollum, I. J., Vilin, Y. Y., Spackman, E., Fujimoto, E., Ruben, P. C. (2003). Negatively charged residues adjacent to IFM motif in the DIII-DIV linker of hNa(V)1.4 differentially affect slow inactivation. FEBS letters. 552(2-3), 163.

Munoz-Sanjuan, I., Simandl, B.K., Fallon, J.F. and Nathans, J. (1999). Expression of chicken fibroblast growth factor homologous factor (FHF)-1 and of differentially spliced isoforms of FHF-2 during development and involvement of FHF-2 in chicken limb development. Development. 126, 409-21.

Munoz-Sanjuan, I., Smallwood, P.M. and Nathans, J. (2000). Isoform diversity among fibroblast growth factor homologous factors is generated by alternative promoter usage and differential splicing. J Biol Chem. 275, 2589-97.

Motoike, H. K., Liu, H., Glaaser, I. W., Yang, A. S., Tateyama, M., and Kass, R. S. (2004). The Na+ channel inactivation gate is a molecular complex: a novel role of the COOH-terminal domain. J Gen Physiol 123, 155-165.

Ogata, N. and Tatebayashi, H. (1992). Slow inactivation of tetrodotoxin-insensitive Na^+ channels in neurons of rat dorsal root ganglia. J Membr Biol 129, 71–80.

Olsen, S. K., Garbi, M., Zampieri, N., Eliseenkova, A. V., Ornitz, D. M., Goldfarb, M., and Mohammadi, M. (2003). Fibroblast growth factor (FGF) homologous factors share structural but not functional homology to FGFs. J Biol Chem 278, 34226-34236.

O'Reilly, J. P., Wang, S. Y. and Wang, G. K. (2001). Residue-specific effects on slow inactivation at V787 in D2-S6 of Nav1.4 sodium channels. Biophys J 81, 2100–2111.

O'Reilly, A.O., Khambay, B. P. S., Williamson, M. S., Field, L. M., Wallace, B. A., Davies, T. G. E. (2006). Modelling insecticide binding sites in the voltage-gated sodium channel. J. Biochem. 396, 255–263.

Pathak, M. M., Yarov-Yarovoy, V., Agarwal, G., Roux, B., Barth, P., Kohout, S., Tombola, F., and Isacoff, E. Y. (2007). Closing in on the resting state of the shaker k(+) channel. Neuron 56, 124-140.

Pathak, M.M., Kurtz, L., Tombola F. and Isacoff, E. (2005). The cooperative voltage sensor motion that gates a potassium channel. J. Gen. Physiol. 125, 57–69.

Posson, D. J., Selvin, P. R. (2008). Extent of Voltage Sensor Movement during Gating of Shaker K^+ Channels. Neuron 59, 98-109.

Rhodes, T. H., Lossin, C., Vanoye, C. G., Wang, D. W., George A. L. Jr. (2004). Noninactivating voltage-gated sodium channels in severe myoclonic epilepsy of infancy. Proc Natl Acad Sci U S A. 101(30), 11147-52.

Rudy, B. (1978). Slow inactivation of the sodium conductance in squid giant axons. Pronase resistance. J Physiol 283, 1–21.

Ruff, R. L. (1994). Slow Na+ channel inactivation must be disrupted to evoke prolonged depolarization-induced paralysis. Biophys J 66, 542.

Ruff, R. L. (1999). Effects of temperature on slow and fast inactivation of rat skeletal muscle Na+ channels. Am J Physiol Cell Physiol 277, C937–947.

Ruff, R. L. (2008). Slow inactivation: slow but not dull. Neurology 70, 746–747.

Rush, A. M., Wittmack, E. K., Tyrrell, L., Black, J. A., Dib-Hajj, S. D., and Waxman, S. G. (2006). Differential modulation of sodium channel Na(v)1.6 by two members of the fibroblastgrowth factor homologous factor 2 subfamily. Eur J Neurosci 23, 2551-2562.

Schaller, K.L., Caldwell, J.H. (2000). Developmental and regional expression of sodium channel isoform NaCh6 in the rat central nervous system. J. Comp. Neurol. 420, 84–97.

Schoorlemmer, J., and Goldfarb, M. (2001). Fibroblast growth factor homologous factors are intracellular signaling proteins. Curr Biol 11, 793-797.

Schoorlemmer, J. and Goldfarb, M. (2002). Fibroblast growth factor homologous factors and the islet brain-2 scaffold protein regulate activation of a stress-activated protein kinase. J Biol Chem

Shakkottai, V.G., Xiao, M., Xu, L., Wong, M., Nerbonne, J.M., Ornitz, D.M., Yamada, K.A. (2009). FGF14 regulates the intrinsic excitability of cerebellar Purkinje neurons. Neurobiol. Dis. 33, 81–88.

Smallwood, P. M., Munoz-Sanjuan, I., Tong, P., Macke, J.P., Hendry, S.H., Gilbert, D.J., Copeland, N. G., Jenkins, N. A., Nathans, J. (1996). Fibroblast growth factor (FGF) homologous factors: new members of the FGF family implicated in nervous system development. Proc Natl Acad Sci U S A 93, 9850–9857.

Todt, H., Dudley, S.C., Jr., Kyle, J.W., French, R.J., and Fozzard, H.A. (1999). Ultra-slow inactivation in m1 Na+ channels is produced by a structural rearrangement of the outer vestibule. Biophys. J. 76, 1335–1345.

Tomaselli, G. F., N. Chiamvimonvat, H. B. Nuss, J. R. Balser, M. T. Pe´rez-Garcı´a, R. H. Xu, D. W. Orias, P. H. Backx, and E. Marban. (1995). A mutation in the pore of the sodium channel alters gating. Biophys. J. 68, 1814 –1827.

Van Swieten, J. C., Brusse, E., de Graaf, B. M., Krieger, E., van de Graaf, R., de Koning, I., Maat-Kievit, A., Leegwater, P., Dooijes, D., Oostra, B. A., and Heutink, P. (2003). A mutation in the fibroblast growth factor 14 gene is associated with autosomal dominant cerebral ataxia. Am J Hum Genet 72, 191-199.

Vilin, Y. Y., Makita, N., George, A. L. Jr. and Ruben, P. C. (1999). Structural determinants of slow inactivation in humancardiac and skeletal muscle sodium channels. Biophys J 77, 1384–1393.

Verdier, A.S., Mattei, M.G., Lovec, H., Hartung, H., Goldfarb, M., Birnbaum, D., and Coulier, F. (1997). Chromosomal mapping of two novel human FGF genes, FGF11 and FGF12. Genomics. 40, 151-4.

Wang, D. W., Yazawa, K., George, A. L. Jr., and Bennett P. B. (1996). Characterization of human cardiac Na^+ channel mutations in the congenital long QT syndrome. PNAS 93 (23), 13200-13205.

Wang, Q., McEwen, D. G. and Ornitz, D. M. (2000). Subcellular and developmental expression of alternatively spliced forms of fibroblast growth factor 14. Mech Dev 90, 283–287.

Wang, Q., Bardgett, M. E., Wong, M., Wozniak, D. F., Lou, J., McNeil, B. D., Chen, C., Nardi, A., Reid, D. C., Yamada, K. and Ornitz, D. M. (2002). Ataxia and paroxysmal dyskinesia in

mice lacking axonally transported FGF14. Neuron 35, 25–38.

Wang, S. Y. and Wang, G. K. (1997). A mutation in segment I-S6 alters slow inactivation of sodium channels. Biophys J 72, 1633–1640.

West, J. W., Patton, D. E., Scheuer, T., Wang, Y., Goldin, A. L., and Caterall, W. A. (1992). A cluster of hydrophobic amino acid residues required for fast Na+ channel inactivation. Proc Natl Acad Sci USA 89, 10905-10909.

Wittmack, E. K., Rush, A. M., Craner, M. J., Goldfarb, M., Waxman, S. G. and Dib-Hajj, S. D. (2004). Fibroblast growth factor homologous factor 2B: association with $Na_v1.6$ and selective colocalization at nodes of ranvier of dorsal root axons. J Neurosci 24, 6765–6775.

Wozniak, M., Xiao, L., Xu, K.A., Yamada and Ornitz, D.M. (2007). Impaired spatial learning and defective theta burst induced LTP in mice lacking fibroblast growth factor 14, Neurobiol. Dis. 26, 14–26.